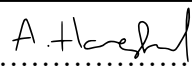




Universitetet  
i Stavanger

FACULTY OF SCIENCE AND TECHNOLOGY

## MASTER'S THESIS

Study programme/specialisation:  Petroleum Engineering/ Reservoir Engineering	Spring / Autumn semester, 2019  Open
Author: Amalie Harestad	 ..... (signature of author)
Supervisor(s): Skule Strand, Tina Puntervold  Co-supervisor: Iván Darío Piñerez Torrijos, Pål Østebø Andersen	
Title of master's thesis:  Effect of Wettability on Waterflooding and Relative Permeability at Medium Water-Wet Conditions.	
Credits (ECTS): 30	
Keywords: Wettability Relative permeability Smart Water Spontaneous imbibition Forced imbibition Carbonate SENDRA simulator	Number of pages: 96  + supplemental material/other: 11  Stavanger, June 15, 2019

## **Acknowledgements**

First and foremost, I would like to express my gratitude to my supervisors Associate Professors Skule Strand and Tina Puntervold. They have both given me professional knowledge and valuable discussion throughout this thesis. I appreciate them for always be available, and ready to help and discuss my results. It has been exciting, interesting and instructive to be a part of their smart water group at the University of Stavanger.

I would also like to thank post-doctoral Iván Darío Piñerez Torrijos, for all the time he spent helping me with laboratory work, and his many advices regarding my thesis.

I would like to thank Pål Østebø Andersen for all the time he spent helping me with SENDRA simulation. He was always available helping me with the simulator and discussing the results.

The work would not have been the same without my fellow laboratory companions; Agnes, Katarina, Erlend and Markus. Thank you for providing a good work environment.

I also acknowledge the national IOR centre for my collaboration.

## **Abstract**

This project contributes with experimental measurement that could increase our understanding on how relative permeability is affected by wettability during an oil recovery process. Wettability has significant attention to the industry and academia, specially linked to enhanced oil recovery (EOR), where diverse mechanisms have been purposed to increase recovery by changing the wetting state of reservoir rocks, as it impacts reserves volumes and flooding performance.

In this study, two carbonate chalk material from Stevns Klint (SK) were cleaned and flooded with a crude oil with an acid number (AN) of 0.34 mgKOH/g, at ambient temperature. AN indicates the amount polar organic components (POC), POC are responsible for wettability alteration to an oil-wet state. The crude oil was displaced with a non-wetting mineral oil (M-OIL) to preserve the wetting. The wettability of the cores after oil flooding were assessed blabalbal. In order to confirm the adsorption effect and wettability, oil recovery tests (spontaneous and forced imbibition) were performed with formation water. Following the forced imbibition test, chromatographic wettability test (CWT) were performed to confirm the wettability of the core. Two strongly water-wet reference cores were used for comparing the results. Strongly water-wet cores were flooded with mineral oil, and recovery test and CWT to confirm the strongly water state. Pressure drop across the cores were logged during the forced imbibition. The pressure drop, oil recovery data and endpoint relative permeabilities was used to simulate the wetting effect on relative permeabilities. Preliminary simulation interpretation with SENDRA was performed.

The study attempts to consider the effect of wettability on waterflooding and relative permeability on chalk cores with different initial wetting states. The results showed that wettability of fractionally-wet cores were altered from very water-wet to medium water-wet, during spontaneous imbibition and chromatographic wettability tests, compared to strongly water-wet reference cores. Results from simulation, showed small differences in relative permeability for all cores.

# Table of contents

Acknowledgements.....	I
Abstract .....	II
List of figures .....	VI
List of tables.....	IX
Nomenclature.....	X
<b>1 Introduction .....</b>	<b>1</b>
1.1 <i>Objectives</i> .....	2
<b>2 Fundamentals of oil recovery .....</b>	<b>3</b>
2.1 <i>Oil recovery mechanisms</i> .....	3
2.1.1 Primary recovery.....	3
2.1.2 Secondary recovery.....	3
2.1.3 Tertiary recovery.....	4
2.2 <i>Waterflooding</i> .....	6
2.2.1 Smart water .....	6
2.3 <i>Displacement forces</i> .....	7
2.3.1 Viscous forces .....	8
2.3.2 Gravity forces .....	9
2.3.3 Capillary forces .....	9
2.3.4 Capillary entry pressure.....	12
<b>3 Fluid flow in porous media .....</b>	<b>13</b>
3.1 <i>Porosity</i> .....	13
3.2 <i>Permeability</i> .....	13
3.3 <i>Mobility ratio</i> .....	14
3.4 <i>Flow regimes</i> .....	15
<b>4 Wettability.....</b>	<b>17</b>
4.1 <i>States of wettability</i> .....	17
4.2 <i>Interfacial tension</i> .....	18
4.3 <i>Wettability measurements methods</i> .....	19
4.3.1 Contact angle measurement .....	19
4.3.2 Amott method .....	21
4.3.3 United states bureau of mines (USBM) method .....	23
4.3.4 Spontaneous imbibition .....	24
4.3.5 Chromatographic wettability test.....	25
4.4 <i>Effect of wettability on core analysis</i> .....	27
4.4.1 Effect of wettability on relative permeability .....	27
4.4.2 Effect of wettability on Capillary pressure .....	30
4.4.3 Effect of wettability on waterflooding .....	31
<b>5 Carbonate reservoirs.....</b>	<b>35</b>
5.1 <i>Carbonate rocks</i> .....	35
5.2 <i>Smart water EOR process in carbonate rocks</i> .....	37

5.3	<i>Wetting in carbonate reservoirs</i> .....	38
<b>6</b>	<b>SENDRA Simulator</b> .....	<b>43</b>
6.1	<i>Laboratory measurements of relative permeability and fluid saturations</i> .....	43
6.2	<i>Relative permeability curves with Corey correlations</i> .....	44
6.3	<i>Two-phase capillary pressure curves with Skjæveland correlations</i> .....	45
<b>7</b>	<b>Experimental work</b> .....	<b>47</b>
7.1	<i>Materials</i> .....	47
7.1.1	Core materials .....	47
7.1.2	Oils.....	49
7.1.3	Brines.....	50
7.1.4	Chemicals.....	51
7.2	<i>Analyses</i> .....	51
7.2.1	pH measurements.....	51
7.2.2	Density measurements .....	52
7.2.3	Viscosity measurements.....	52
7.2.4	Interfacial tension measurements.....	52
7.2.5	Determination of AN and BN.....	53
7.2.6	Ion chromatography .....	53
7.2.7	Scanning electron microscopy (SEM), EDAX.....	54
7.2.8	Data analysis with Sendra .....	54
7.3	<i>Methods</i> .....	54
7.3.1	Initial core preparation.....	54
7.3.2	Oil recovery.....	58
7.3.3	Mild core cleaning.....	60
7.3.4	Chromatographic wettability test.....	60
7.3.5	Determining relative permeability.....	61
<b>8</b>	<b>Results and discussion</b> .....	<b>63</b>
8.1	<i>Chalk core characterization</i> .....	63
8.1.1	Energy dispersive x-ray spectroscopy (EDS).....	63
8.1.2	Effluent pH analysis.....	64
8.2	<i>Oil characteristics</i> .....	65
8.2.1	Preparation of mineral oil (M-OIL).....	65
8.2.2	The effect of AN on IFT.....	66
8.3	<i>Oil recovery from water-wet reference cores</i> .....	67
8.3.1	Forced imbibition.....	67
8.3.2	Spontaneous imbibition .....	69
8.3.3	Spontaneous and forced imbibition for reference core CR2.....	70
8.3.4	Chromatographic wettability test of reference cores.....	71
8.4	<i>Oil recovery and wettability for fractional-wet cores</i> .....	71
8.4.1	Forced imbibition for fractional wet core C2.....	71
8.4.2	Spontaneous imbibition of restored core C2 .....	73
8.4.3	Spontaneous imbibition of core C5.....	74
8.4.4	Spontaneous and forced imbibition of core C5 .....	76
8.4.5	Chromatographic wettability test.....	77
8.5	<i>Comparing oil recoveries with cores with different initial wettability</i> .....	78
8.6	<i>Numerical core analysis</i> .....	82
8.6.1	Methodology .....	82
8.6.2	History match for water-wet cores .....	84
8.6.3	History match for fractionally-wet core.....	88
8.6.4	Relative permeability and capillary pressure curves.....	88
8.6.5	Comparing with other cores.....	92

<b>9</b>	<b>Conclusion and future work .....</b>	<b>95</b>
9.1	<i>Concluations</i> .....	95
9.2	<i>Suggestions for future work</i> .....	95
<b>10</b>	<b>References.....</b>	<b>97</b>
<b>Appendix A: Chemicals .....</b>		<b>103</b>
A.1	<i>Acid number solutions</i> .....	103
A.2	<i>Base number solutions</i> .....	103
<b>Appendix B: Experimental data .....</b>		<b>104</b>
B.1	<i>Spontaneous imbibition data</i> .....	104
B.2	<i>Forced imbibition data</i> .....	106
B.3	<i>pH measurements</i> .....	110
B.3	<i>Chromatography data</i> .....	111
<b>Appendix C: Input parameters in SENDRA .....</b>		<b>113</b>
C1:	<i>Reference cores</i> .....	113
C2:	<i>Fractionally wet core</i> .....	113

## List of figures

<b>Figure 2.1:</b> Illustration of wettability alteration by smart water (smart water IOR group (2019)).	7
<b>Figure 2.2:</b> Curvature of a meniscal surface with two radii, $R_1$ and $R_2$ . Redrawn from Zolotukhin & Ursin (2000).	11
<b>Figure 2.3:</b> Capillary pipe model with two immiscible fluids forming a meniscus. Redrawn from Zolotukhin & Ursin (2000).	11
<b>Figure 3.1:</b> Water saturation as a function of distance between injection and production wells for (a) favorable piston-like displacement and (b) unfavorable displacement. Redrawn from Apostolos et. al (2016).	15
<b>Figure 4.1:</b> Water-wet vs oil-wet system (Green & Willhite, 1998).	18
<b>Figure 4.2:</b> Wettability of an CRB-system. Redrawn from Anderson (1986a).	20
<b>Figure 4.3:</b> Capillary pressure curve for Amott, Amott-Harvey and USBM method. Redrawn from Donaldson & Alam (2008).	22
<b>Figure 4.4:</b> USBM wettability measurement in a water-wet and oil-wet core. Redrawn from Anderson (1986a).	24
<b>Figure 4.5:</b> A sketch of oil recovery from a spontaneous imbibition. The blue curve indicates a steep, rapid recovery, and the yellow curve represent a slower and lower recovery.	24
<b>Figure 4.6:</b> Sketch of adsorption of $\text{SO}_4^{2-}$ onto water-wet, oil-wet and mixed-wet core surfaces (Smart Water IOR group, 2019).	26
<b>Figure 4.7:</b> Relative permeability curves $k_{ro}$ and $k_{rw}$ for (a) water-wet and (b) oil-wet system. Redrawn from Zolotukhin & Ursin (2000).	29
<b>Figure 4.8:</b> Illustration of capillary pressure behavior for (a) water-wet system, (b) mixed-wet system and (c) oil-wet system during drainage and imbibition. Redrawn from Donaldson & Alam (2008).	30
<b>Figure 4.9:</b> Fractional flow curve for very water-wet rock, determination of front saturation, $S_{wf}$ , and average saturation at water breakthrough, $S_{wbt}$ (Craig, 1971).	32
<b>Figure 4.10:</b> Idealized production from three conditions of wettability. Redrawn from Donaldson & Alam (2008).	33
<b>Figure 5.1:</b> SEM picture of chalk showing coccolith rings, pore space and ring fragments.	36
<b>Figure 5.2:</b> Pore size distribution for (a) Stevns Klint chalk by mercury injection. Redrawn after J. Milter (1996). And (b) Valhall reservoir chalk. Redrawn after Webb et al. (2005)	37
<b>Figure 5.3:</b> spontaneous and forced imbibition of formation water (FW) and seawater (SW) into a carbonate core at 110 °C (Smart Water IOR group, 2019)	38
<b>Figure 5.4:</b> Spontaneous imbibition into SK chalk cores saturated with different oil (Standnes & Austad, 2000)	39
<b>Figure 5.5:</b> Oil recovery vs time for three different formation waters at ambient temperature (Smart Water IOR group, 2019).	39
<b>Figure 5.6:</b> Chemical model describing initial wetting in Carbonates (Smart Water IOR group, 2019).	40
<b>Figure 5.7:</b> Zeta potential measurements on 4 wt% chalk suspension in NaCl-brine with $[\text{Ca}^{2+}] = 0.013 \text{ mol/l}$ and varying sulfate concentration, or in NaCl-brine with $[\text{SO}_4^{2-}] = 0.012 \text{ mol/l}$ and varying calcium concentration (Stand et al., 2006).	41
<b>Figure 5.8:</b> Illustration of the suggested chemical mechanism for wettability of carbonate by SW (Zhang et al., 2007)	42
<b>Figure 5.9:</b> Chemical wettability alteration model for carbonates (Smart Water IOR group, 2019).	42
<b>Figure 6.1:</b> Illustration of unsteady-state and steady state methods of measuring two-phase oil and water relative permeability.	43

<b>Figure 6.2:</b> Schematic of bounding curves, capillary pressure, $P_c$ , as a function of water saturation, $S_w$ : (a) primary drainage to establish $S_{wi}$ , (b) Spontaneous imbibition at positive $P_c$ and forced imbibition at negative $P_c$ , (c) secondary drainage and (d) primary imbibition. Redrawn from Skjaeveland et. al (2000).....	46
<b>Figure 7.1:</b> Illustration of viscosity measurements .....	52
<b>Figure 7.2:</b> Du Noüy ring method for IFT measurement (Moradi et al., 2015). .....	53
<b>Figure 7.3:</b> Hassler cell used in experiments.....	55
<b>Figure 7.4:</b> Illustration of vacuum pump set-up for water saturation of core.....	56
<b>Figure 7.5:</b> Illustration of oil flooding set-up .....	57
<b>Figure 7.6:</b> Effluent samples of produced oil during mineral oil flooding.....	58
<b>Figure 7.7:</b> Schematic of experimental stages for cores C2 and C5 .....	58
<b>Figure 7.8:</b> Schematic of spontaneous imbibition procedure .....	59
<b>Figure 7.9:</b> Illustration of the flooding set-up for chromatographic wettability test.....	61
<b>Figure 8.1:</b> Scanning electron microscopy (SEM) picture of the outcrop SK chalk core, magnified 5000x.....	63
<b>Figure 8.2:</b> Example of pH at different PV injected of the water effluent during an viscous force oil recovery test.....	65
<b>Figure 8.3:</b> Viscosity vs percent of Marcol in n-heptane .....	66
<b>Figure 8.4:</b> Acid number dependence of interfacial tension.....	66
<b>Figure 8.5:</b> Oil recovery and pressure drop data vs pore volumes injected during forced imbibition at ambient temperature for left: CR1 (69%OOIP) and right: CR2 (72%OOIP) with two different rates, 1 PV/day and 4 PV/day. DI-water was used as the displacing fluid, and M-OIL was used as the displaced fluid.....	68
<b>Figure 8.6:</b> Oil recovery and pressure drop data vs pore volume injected during forced imbibition at ambient temperature for cores CR1 and CR2 at rate 1PV/day.....	68
<b>Figure 8.7:</b> Oil recovery vs time by spontaneous imbibition of DI-water displacing M-OIL on two water-wet reference restored cores, CR1 and CR2, at ambient temperature. Left: Oil recovery vs time. Right: Oil recovery in a semilog-plot.....	69
<b>Figure 8.8:</b> Oil recovery by spontaneous imbibition and forced imbibition on water-wet reference core, CR2 after second restoration at ambient temperature. ....	70
<b>Figure 8.9:</b> Chromatographic wettability test (CWT) results performed on reference cores at 23 °C. Left: CR1 with a surface area of $A_{water} = 0.301$ . Right: CR2 with a surface area of $A_{water} = 0.263$ .....	71
<b>Figure 8.10:</b> Oil recovery and pressure vs pore volume injected during forced imbibition for fractionally-wet core C2 at ambient temperature and two different rates, 1 PV/day and 4 PV/day. DI-water was used as the displacing fluid, and M-OIL was used as the displaced fluid. The total oil recovery after changing the rate was 71 %OOP. ....	72
<b>Figure 8.11:</b> Forced imbibition process for reference cores (CR1 and CR2) and core C2 at ambient temperature. Oil production is almost the same, but the pressure drop for C2 is lower than for reference cores. ....	73
<b>Figure 8.12:</b> Oil recovery vs time during spontaneous imbibition of core C2 at ambient temperature. DI-water as displacing fluid and M-OIL as the displaced fluid. Total recovery after 6 day was 58 %OOIP. ....	74
<b>Figure 8.13:</b> Oil recovery vs time during spontaneous imbibition of core C5 at ambient temperature. DI-water as displacing fluid and M-OIL as the displaced fluid. Total recovery after 4 day was 37 %OOIP.....	75
<b>Figure 8.14:</b> Comparing oil recovery vs time during spontaneous imbibition of all cores at ambient temperature. ....	76



<b>Figure 8.15:</b> Oil recovery vs times during SI and FI (at two different rates) with DI-water as displacing fluid and M-OIL as displaced fluid at ambient temperature for core C5. The total recovery after high rate was 65%.	76
<b>Figure 8.16:</b> Spontaneous and forced imbibition comparison for core CR2 and C5 at ambient temperature.	77
<b>Figure 8.17:</b> Chromatographic wettability test (CWT) results performed on fractionally-wet cores at 23 °C. Left: C2 with a surface area of $A_{\text{water}} = 0.207$ . Right: C5 with a surface area of $A_{\text{water}} = 0.248$ .	78
<b>Figure 8.18:</b> Comparing oil recovery by SI from core CR2, C4, C5, C6 at ambient temperature. Left: Oil recovery vs time. Right: Oil recovery in a log-plot.	80
<b>Figure 8.19:</b> Comparing oil recovery by SI from core CR1, CR2, C1, C2, C3 at ambient temperature. Left: Oil recovery vs time. Right: Oil recovery in a log-plot.	81
<b>Figure 8.20:</b> Comparing oil recovery (left) and pressure drop (right) vs PV injected for cores CR1, CR2, C1, C2, C3 at ambient temperature.	82
<b>Figure 8.21:</b> History matching of experimental production and pressure drop data of CR1. (a) Automatic history matching with $P_c$ , (b) Manually history matching without $P_c$ and (c) Manually history matching with $P_c$ . Dots plots are the experimental data, and continuous lines are the history matched data.	85
<b>Figure 8.22:</b> History matching of experimental production and pressure drop data of CR1. (a) Automatic history matching with $P_c$ , (b) Manually history matching without $P_c$ and (c) Manually history matching with $P_c$ . Dots plots are the experimental data, and continuous lines are the history matched data.	86
<b>Figure 8.23:</b> History matching of experimental production and pressure drop data of C2. Capillary pressure is negative. Dots plots are the experimental data, and continuous lines are the history matched data.	88
<b>Figure 8.24:</b> Relative permeability and capillary pressure curve for strongly water-wet cores based on manually history matching. (a) Relative permeability for CR1, (b) Relative permeability for CR2, (c) Capillary pressure for CR1 and (d) Capillary pressure for CR2. ...	89
<b>Figure 8.25:</b> Relative permeability and capillary pressure curve for core C2 based on automatic history matching. (a) Relative permeability curve and (c) Capillary pressure curve.	90
<b>Figure 8.26:</b> Fractional flow of water for cores CR1 and CR2 as a function of water saturation.	91
<b>Figure 8.27:</b> Fractional flow of water for core C2, as a function of water saturation.	92
<b>Figure 8.28:</b> Comparison of relative permeability curves and fractional flow curves for cores with different initial wettability.	93
<b>Figure 8.29:</b> Comparison of capillary pressure curve for all cores with different initial wettability. Spontaneous imbibition of the same cores to compare capillary forces.	94

## List of tables

<b>Table 1:</b> Classification of EOR processes (Ahmed, 2010; Taber et al., 1997).....	5
<b>Table 2:</b> EOR process by water based wettability alteration.....	6
<b>Table 3:</b> Core properties .....	48
<b>Table 4:</b> Oil properties.....	50
<b>Table 5:</b> Composition and properties of brines.....	51
<b>Table 6:</b> Pore volumes of cores and injection rates during forced imbibition.....	60
<b>Table 7:</b> End point relative permeabilities with important factors to calculate them.....	62
<b>Table 8:</b> Composition analysis by energy dispersive x-ray spectroscopy of SK chalk. ....	64
<b>Table 9:</b> Reference vaules from reference cores, CR1 and CR2.....	79
<b>Table 10:</b> Comparison of results from cores ( 2 restoration) with varying wettabilities, Case 1 .....	79
<b>Table 11:</b> Comparison of result from cores (1 restoration) with varying wettabilities, Case 2. ....	79
<b>Table 12:</b> Corey and Skjæveland parameters for automatic history matching for cores CR1, CR2 and C2 .....	83
<b>Table 13:</b> Corey and Skjæveland parameters for manually history matching for core CR1 and CR2.....	84
<b>Table 14:</b> Comparing crossover saturation, front saturation and water breakthrough saturation .....	92
<b>Table 15:</b> Chemicals for AN mesurements.....	103
<b>Table 16:</b> Chemicals for BN measurements.....	103
<b>Table 17:</b> SI data, reference core, CR1 .....	104
<b>Table 18:</b> SI data, reference core, CR2.....	104
<b>Table 19:</b> SI data, core C2 .....	105
<b>Table 20:</b> SI data, core C5.....	105
<b>Table 21:</b> FI, reference core CR1 .....	106
<b>Table 22:</b> FI, reference core CR2 .....	107
<b>Table 23:</b> FI core C2.....	108
<b>Table 24:</b> FI core C5.....	109
<b>Table 25:</b> pH measurements from reference core, CR1 .....	110
<b>Table 26:</b> pH measurements from reference core, CR2 .....	110
<b>Table 27:</b> pH measurements from core C2.....	110
<b>Table 28:</b> pH measurements from core C5.....	110
<b>Table 29:</b> Chromatography data for reference core, CR1 .....	111
<b>Table 30:</b> Chromatography data for reference core, CR2 .....	111
<b>Table 31:</b> Chromatography data for core C2.....	112
<b>Table 32:</b> Chromatography data for core C5.....	112
<b>Table 33:</b> Input data for all cores.....	113
<b>Table 34:</b> Input data for CR1 .....	113
<b>Table 35:</b> Input data for CR2 .....	113
<b>Table 36:</b> Input data for C2 .....	113

## Nomenclature

$A$	Cross section area of core [cm <sup>2</sup> ]
$a_o$	Skjæveland exponent for oil
$a_w$	Skjæveland exponent for water
$C_o$	Skjæveland constant for oil [Pa]
$C_w$	Skjæveland constant for water [Pa]
$D$	Diameter of the core [cm]
$DI$	Deionized water
$E$	Overall displacement efficiency
$E_D$	Microscopic displacement efficiency
$E_V$	Macroscopic (volumetric) displacement efficiency
$f_w$	Fractional flow of water
$I_{AH}$	Difference between the two Amott displacement ratios
$I_O$	Displacement-by-oil ratio
$I_{USBM}$	Wettability index (USBM)
$I_W$	Displacement-by-water ratio
$I_W^*_{-SI}$	Wettability index (for SI)
$J(S_w)^*$	Leverett dimensionless entry pressure
$k$	Absolute permeability
$k_{eff,o}$	Effective permeability for oil
$k_{eff,w}$	Effective permeability for water
$k_{ro}$	Oil relative permeability
$k_{rw}$	Water relative permeability
$L$	Length of the core
$M$	Mobility ratio
$m_{dry}$	Weight of dry core [g]
$m_{sat}$	Weight of saturated core [g]
$m_{S_{wi} = 20\%}$	Desired weigh of core [g]
$N_o$	Corey exponent for oil
$N_w$	Corey exponent for water
$P_b$	Bubble point pressure
$P_c$	Capillary pressure [Pa]
$P_{nw}$	Pressure of the nonwetting phase

<i>PV</i>	Pore volume [ml]
<i>P<sub>T</sub></i>	Threshold pressure
<i>P<sub>w</sub></i>	Pressure of the wetting phase
<i>RF</i>	Recovery Factor
<i>S<sub>w</sub></i>	Water saturation
<i>S<sub>wi</sub></i>	Irreducible water saturation
<i>S<sub>or</sub></i>	Residual oil saturation
<i>S<sub>w</sub><sup>*</sup></i>	Normalized water saturation
<i>V<sub>b</sub></i>	Bulk volume [cm <sup>3</sup> ] or [ml]
<i>V<sub>p</sub></i>	Pore volume [cm <sup>3</sup> ] or [ml]

### **Abbreviations**

<i>AN</i>	Acid number [mg KOH/g]
<i>BN</i>	Base number [mg KOH/g]
<i>CBR</i>	Crude oil/ brine/ rock system
<i>EOR</i>	Enhanced oil recovery
<i>EDAX</i>	Energy dispersive x-ray spectroscopy
<i>FI</i>	Forced imbibition
<i>FW</i>	Formation water
<i>IC</i>	Ion chromatography
<i>IFT</i>	Interfacial tension [N/m]
<i>IOR</i>	Improved oil recovery
<i>KOH</i>	Potassium hydroxide
<i>M-OIL</i>	Mineral oil
<i>OOIP</i>	Original oil in place
<i>POC</i>	Polar organic component
<i>SEM</i>	Scanning electron microscopy
<i>SI</i>	Spontaneous imbibition
<i>SK</i>	Stevens Klint
<i>SW</i>	Seawater
<i>SW0T</i>	Synthetic seawater without tracer and sulfate
<i>SW1/2T</i>	Synthetic seawater with equal concentration of tracer and sulfate
<i>USBM</i>	United states bureau of mines

## Symbols

$\phi$	Porosity
$\lambda$	Mobility
$\mu$	Viscosity
$\theta$	Contact angle
$\rho$	Density [g/cm <sup>3</sup> ]
$\sigma$	Interfacial tension

# 1 Introduction

During the past 5 years, the oil price has declined. This drop in oil price has increased the focus regarding cost efficiency in the industry, and improved oil recovery (IOR) from reservoirs has become more important to make projects sustainable. Due to this an increasing interest to find new efficient and more environmental friendly methods has been initiated to increase the oil recovery.

Carbonate reservoir rocks are accounted for approximately 50% of the world's proven oil reserves (Treiber et al., 1972). However, due to natural fractures, low permeability, low water wetness and inhomogeneous rock properties, the oil recovery is quite low (around 30%) (Høgnesen et al., 2005). By altering the wettability towards more water-wet conditions, the capillary forces will increase and as a consequence more oil will be produced during a spontaneous imbibition (Mohammed & Babadagli, 2015).

Seawater has been used as Smart Water to alter the wettability in carbonate rocks (RezaeiDoust et al., 2009). Smart water is an ion-modified brine designed to cause wettability alteration and enhance the oil recovery. An interaction between surface active ions ( $\text{Ca}^{2+}$ ,  $\text{Mg}^{2+}$  and  $\text{SO}_4^{2-}$ ) in the seawater, carbonate surface and the adsorbed carboxylic material from the crude oil can increase the water wetness of the rock, and increase the recovery (Zhang et al., 2007). Seawater injection in the Ekofisk field in the North Sea, is a typically example of successfully Smart Water injection. The reservoir is highly fractured and mixed-wet, which pointed against injection of water. Today, the recovery from the Ekofisk field is estimated to reach 50-55% of original oil in place (OOIP), compared to 18% in the beginning (Punternvold & Austad, 2008; Torsaeter, 1984).

During a smart water injection, the reservoir will preferably experience a wettability alteration from oil-wet/ mixed-wet/slightly water-wet conditions towards strongly water-wet conditions. Laboratory results have shown, by spontaneous imbibition tests, that capillary forces are an important recovery mechanism in low permeable, heterogeneous and fractured carbonate material (Fathi et al., 2011). Reservoir simulations require relative permeability data to predict fluid flow in the reservoir and needs two sets of relative permeability data to capture the change in wettability; one for the initial wettability, and one for the final wetting established at the end

of smart water injection. The focus of this work is therefore to investigate the influence of wettability on relative permeability curves and oil recovery.

## 1.1 Objectives

The main objective of this study is to understand the effect of small changes in wettability on relative permeability curves and waterflooding. Two reference outcrop SK chalk cores with a wettability of strongly water-wet were used, including two cores which were fractionally-wet. All chalk cores were restored and established with the same initial water saturation,  $S_{wi} = 20\%$ . The fractionally-wet cores were flooded with a crude oil with acid number,  $AN=0.34$  mgKOH/g. A mineral oil displaced the crude oil, leaving the polar organic components (POC) adsorbed onto rock surface, preserving a constant wettability state during the core flood. Reference cores were flooded with mineral oil, with no surface active components. A simulator was used to model relative permeability curves based on the experimental work. Results were compared with other cores with different initial wettability (Radenkovic, 2019; Wathne, 2019). For this purpose these objectives were evaluated:

- Oil recovery experiments (both spontaneous and forced imbibition) at constant wetting are performed on chalk cores with different initial wettability. How will acid number and IFT affect the oil recovery?
- Wettability was determined by Amott wettability index, modified Amott wettability index, and the fraction of water-wet surface area is also determined by the chromatographic wettability test are done, to confirm the wettability from oil recovery experiments.
- SENDRA is used to develop relative permeability data from the unsteady state oil recovery experiment to verify the influence of wettability on modelled relative permeability.
- Capillary forces will not be the main driving force during the oil production in a simulator. Low mobility for water at water-wet systems is the main forces for later water breakthrough and increased oil recovery. Wettability alteration in simulator is represented at changed relative permeability curves. Small changes was observed in relative permeability curves. Can these relative permeability curves represent the wettability alteration in a reservoir, or must realistic capillary forces be present in the model?

## **2 Fundamentals of oil recovery**

There are many factors affecting the oil recovery from a reservoir field. Oil recovery mechanisms use natural energy present in the reservoir and supplements to maintain reservoir pressure to “drive” more oil through wells to the surface. Oil recovery is also an equivalent to displacement efficiency and if the overall displacement efficiency is high, the recovery will also be high. Oil recovery mechanisms and displacement forces are described in the following sections.

### **2.1 Oil recovery mechanisms**

Oil recovery methods is traditionally divided into three phases: primary, secondary and tertiary recovery, also known as enhanced oil recovery (EOR) (Ahmed, 2010). These three stages describes the production in a chronological sense. However, today these recovery stages are not necessarily operated in this specific order. Pressure maintain typically starts early in the process. To avoid two phase or three phase flow, water or gas is injected to maintain reservoir pressure above  $P_b$  (bubble point pressure) (Bavière, 1991; Green & Willhite, 1998).

#### **2.1.1 Primary recovery**

The initial production stage, primary recovery, describes the production of hydrocarbons that naturally rise to the surface. It takes advantage of the natural energy present in the reservoir, without supplements like gas or water injections (Ahmed, 2010). Basically, there are six essentially driving mechanisms that contribute in the primary stage, which are: Solution-gas drive, gas-cap drive, natural water drive, fluid and rock expansion, gravity drainage and combination drive (Green & Willhite, 1998). Primary recovery is relatively inefficient process and in most cases the result will end up with a low overall oil recovery, normally around 12-15% of the original oil in place (OOIP) (Herrera & Pinder, 2012).

#### **2.1.2 Secondary recovery**

To maintain reservoir pressure and produce more oil, after primary recovery, water and/or immiscible gas are injected into the reservoir. This process is called secondary recovery, and aims to displace oil towards the production wells. Secondary recovery usually follows primary recovery, but it can also be implemented directly with primary recovery (Ahmed, 2010; Lake, 1989).



Water and/or gas flooding are injected into wells while producing from the surrounding wells. Gas injection is also used to maintain the gas cap pressure even if oil displacement is not required (Alagorni et al., 2015). By secondary recovery methods, another additional 15-20% of OOIP may be produced. However, the recovery factor from the reservoir will not be maxed alone with secondary recovery. There are three main factors for this, and they are: heterogeneity, problems related to well siting and spacing and unfavorable mobility ratio between the displaced and displacing fluid. These three factors results in low macroscopic sweep efficiency. When the secondary phase becomes insufficient the tertiary recovery takes place (Green & Willhite, 1998; Zolotukhin & Ursin, 2000).

### **2.1.3 Tertiary recovery**

Tertiary recovery, also known as Enhanced Oil Recovery (EOR), is the additional recovery following what could be recovered by primary and secondary methods. EORs are combined methods used to increase the ultimate total oil recovery by injecting suitable fluids that are not commonly present in the reservoir. Typically, fluids like chemicals, solvents, oxidizers and heat carriers are injected, to induce new mechanisms for producing the remaining oil in the reservoir (Green & Willhite, 1998). This is the purpose of using an EOR process. EOR processes can be divided into five categories: Chemicals, miscible, immiscible gas drives, thermal and other processes (Abdelgawad & Mahmoud, 2014; Ahmed, 2010). Classification of the processes are listed in table 1.

**Table 1:** Classification of EOR processes (Ahmed, 2010; Taber et al., 1997)

Chemical	Polymer Surfactant Alkaline Micellar Emulsion
Miscible	Slug Process Enriched Gas Drive Vaporizing Gas Drive CO <sub>2</sub> Miscible N <sub>2</sub> Miscible Alcohol
Immiscible gas drives	CO <sub>2</sub> Flue Gas Inert Gas
Thermal	Hot Water In-Situ Combustion Steam Electrical heating
Alternative	Microbial Enhanced Oil Recovery Foam Water Alternating Gas Low Salinity Water Injection

Wettability alteration has, recently, been suggested as a new EOR mechanism, due to its effect on capillary forces and microscopic sweep efficiency. Wettability alteration is a process of making the reservoir rocks more water-wet (Mohammed & Babadagli, 2015). If capillary forces in a core are low, wettability alteration can take place during the flood, thus increase the microscopic sweep. Wettability can be altered by injecting water with different compositions compared to the initial formation water which can disturb the original chemical equilibrium of the crude oil/brine/rock system. Injection of water similar to formation water is characterized as secondary method, since the chemical equilibrium will be little affected. For more than 20 years, several laboratory studies has been conducted on different CBR-systems. Today, one can say that modified water flooding is the most cost efficient and environmental EOR method (Austad, 2013). Table 2 shows methods for wettability alteration.

**Table 2:** EOR process by water based wettability alteration

Wettability Alteration	Smart Water
	Seawater/modified seawater (in Carbonates)
	Low Salinity Water (in Sandstones)
	Cationic surfactants (in Carbonates) Anionic surfactants (in Sandstones)

## 2.2 Waterflooding

At first, waterflooding was adopted for pressure maintenance in the reservoir after primary depletion and to displace oil by taking advantages of viscous forces (Austad, 2013). Since then it has become the most universally accepted improved oil recovery (IOR) technique. The waterflooding technique has been tested successfully over a broad range of reservoirs and reservoir conditions (Morrow & Buckley, 2011; Wade, 1971). To consider if a reservoir is suitable for waterflooding, some reservoir characteristics must be studied. In addition to good execution, knowledge of the reservoir must be considered. Parameters that affect the performance of waterflooding in a reservoir are linked to reservoir geometry, fluid properties, reservoir depth, lithology and rock properties, and fluid saturation (Ahmed, 2010).

Waterflooding becomes an EOR method when the composition of the injected water differs from the composition of formation water. In a standard waterflooding process, where formation water is injected to the reservoir, the wettability of the reservoir rock will not change significantly. In this case, the waterflooding process is a secondary recovery method and not an EOR method. But, by modifying compositions in the injected water, wettability of the rock can be affected and altered. This increase the oil recovery, and waterflooding, where the water composition has been manipulated, becomes an EOR method (Anderson, 1986b; Morrow, 1990). By understanding the water chemistry and chemical interactions with the rock and crude oil, the oil recovery can be improved significantly (Austad, 2013).

### 2.2.1 Smart water

Smart water is one of several EOR processes that have evolved during the recent years. A chemical equilibrium between crude oil, brine and rock (CBR) system has been established during millions of years. Then, the distribution of oil and formation brine in the porous system is linked to the contact between the rock surface, oil and brine. This distribution is fixed at given saturations of oil and water (Austad, 2013). The main idea of smart water is to alter the initial

wetting condition by injecting water with modified compositions. The purpose of adjusting the ion composition is to change the equilibrium of the initial CBR system which will modify the wetting conditions, and hence increase oil recovery. This change in wetting properties in the CBR system has a favorable effect on the capillary pressure and relative permeability of oil and water (RezaeiDoust et al., 2009). Oil is more mobile and can easily be displaced from the porous rock, as illustrated in Figure 2.1. This smart water technique is more environmental friendly and economical, with no expensive chemicals are added. There are also no problems with injection. It is preferential to flood with the smartest water from the beginning of the water flooding process (Austad, 2013). To conduct smart water, it is essential to understand the initial wetting of the system, and factors influencing it. This will be discussed later in section 5.2.

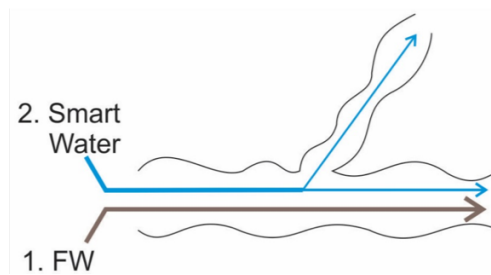


**Figure 2.1:** Illustration of wettability alteration by smart water (smart water IOR group (2019)).

### 2.3 Displacement forces

Many forces act on the fluid movement in a reservoir, and the most important displacement forces within oil production are gravity, viscous and capillary forces. In an oil reservoir the amount of produced oil are determined by interaction of these forces (Mohammed & Babadagli, 2015). During an EOR process, the overall displacement can be viewed from different scales. The overall displacement efficiency ( $E$ ) is defined as the product of microscopic and macroscopic (volumetric) displacement efficiencies, as shown in Equation 2.1 (Morrow, 1979):

$$E = E_D E_V \quad (2.1)$$

Where:

- $E$  Global displacement efficiency (oil recovery by process/oil in place at the beginning of the process)
- $E_D$  Microscopic displacement efficiency expressed as fraction
- $E_V$  Macroscopic (volumetric) displacement efficiency expressed as fraction

Microscopic displacement efficiency,  $E_D$ , gives information of the moveable oil at pore scale, and reflects the magnitude of the residual oil saturation,  $S_{or}$ , where the displaced fluid is in contact with the displacing fluid. The macroscopic displacement efficiency,  $E_V$ , measures the effectiveness of the displacing fluid when it comes in contact with the reservoir in volumetric sense.  $E_D$  is related to the rock wettability state, while  $E_V$  is mostly related to the mobilization of the displacing fluid. Since both  $E_D$  and  $E_V$  are expressed as fraction, it is convenient that both is close to 1. This is to obtain a high displacement efficiency, and hence increase the oil recovery (Green & Willhite, 1998).

The main purpose of EOR processes is to extract more crude oil from the oil field that cannot be extracted from primary and secondary processes, i.e. lower the  $S_{or}$ . By reducing  $S_{or}$ , the displacement efficiency at the microscopic level will increase. EOR processes that will affect  $S_{or}$  and microscopic sweep efficiency are IFT, oil viscosity and wettability alteration (Ahmed, 2010; Green & Willhite, 1998).  $E_D$  is described in Equation 2.2:

$$E_D = \frac{S_{oi} - S_{or}}{S_{oi}} \quad (2.2)$$

Where:

$S_{oi}$  = Initial oil saturation

$S_{or}$  = Residual oil saturation

Macroscopic displacement efficiency is equally important, and it is affected by geological heterogeneity, mobilities and densities between the displacing and displaced fluids and rock characteristics. There are also factors that can make unfavorable displacement efficiencies, and some of them are large differences in densities and low mobility ratios, and geology of the reservoir that is non-favorable. These factors can lead to fingering effects, under- or overriding of the displaced fluid (Green & Willhite, 1998).

### 2.3.1 Viscous forces

Through a porous medium, viscous forces are reflected in the magnitude of the pressure drop that occurs as a result of fluid flow through the matrix. The easiest way used to calculate the viscous force is to assume laminar flow through the system, consider the medium as a bundle

of parallel capillary tubes. Pressure drop through a single tube is given by Poiseuille's law and is shown by the Equation 2.3 (Green & Willhite, 1998):

$$\Delta P = -\frac{8\mu L \bar{v}}{r^2 g_c} \quad (2.3)$$

Where

$\Delta P$	pressure drop across the capillary tube [Pa]
$\mu$	viscosity [Pa.s]
$L$	length of the capillary tube [m]
$\bar{v}$	average flow velocity in the capillary tube [m/s]
$r$	radius of the capillary tube [m]
$g_c$	conversion factor

### 2.3.2 Gravity forces

The main driving force for gravity forces are determined by the density of the fluids. Droplets of oil within a pore space is influenced by gravity forces (Lake, 1989). In a multiphase system where there are large differences in densities of the fluids, gravity forces play a significant role. The pressure difference between oil and water due to gravity is shown in the Equation 2.4:

$$\Delta P_g = \Delta \rho g H \quad (2.4)$$

Where

$\Delta P_g$	pressure difference between oil and water due to gravity [Pa]
$\Delta \rho$	density difference between oil and water [kg/m <sup>3</sup> ]
$g$	gravity acceleration, 9.81 [m <sup>2</sup> /s]
$H$	height of the liquid column [m]

### 2.3.3 Capillary forces

Capillary forces are the most dominant driving forces in fluid flow in porous media and govern the distribution of fluids within an oil reservoir. The forces depend on interfacial tension (IFT) between water and oil, the radius ( $r$ ) of the pores and the wettability represented as contact angle ( $\theta$ ) (Mohammed & Babadagli, 2015). Capillary forces can act both against and in favor of oil recovery. In fractured reservoirs, the forces can be an important mechanism of oil

production (Lake, 1989; Lee, 2010). In a non-fractured reservoir, strong capillary forces during waterflooding can induce trapped oil and cause a high residual oil saturation (Anderson, 1987b; Lee, 2010). When two immiscible fluids are in contact with each other, the strong adhesive force to the wetting phase causes the interface between these two fluids to curve. A meniscus develop and it is convex towards the wetting phase. The pressure difference between the wetting and non-wetting fluid is called capillary pressure,  $P_c$  (Donaldson & Alam, 2008; Zolotukhin & Ursin, 2000):

$$P_c = p_{nw} - p_w \quad (2.5)$$

Where:

- $P_c$  Capillary pressure [Pa]
- $p_{nw}$  Pressure of the non-wetting phase at interface [Pa]
- $p_w$  Pressure of the wetting phase at interface [Pa]

When two immiscible fluids are in contact with each other, the interface will normally be curved as a meniscus, and the curvature of the meniscal surface can be characterized by two radii (shown in Figure 2.2). The pressure difference between these two fluids are the reason for the curvature, and the interface will be convex towards the fluid with greater internal pressure (the wetting fluid). The Equation 2.6 shows the Laplace equation (Zolotukhin & Ursin, 2000):

$$P_c = \sigma \left( \frac{1}{R_1} + \frac{1}{R_2} \right) \quad (2.6)$$

Where

- $\sigma$  interfacial tension between the non-wetting and wetting fluid [N/m]
- $R_1, R_2$  principal radii of the interface curvature

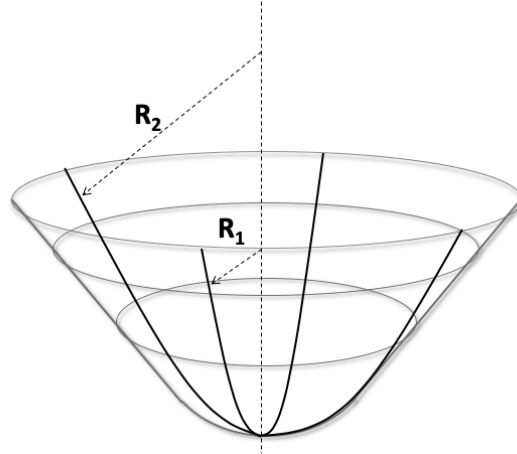


**Figure 2.2:** Curvature of a meniscal surface with two radii,  $R_1$  and  $R_2$ . Redrawn from Zolotukhin & Ursin (2000).

For a spherical oil droplet equal to pore size,  $R_1$  and  $R_2$  becomes equal and hence  $\Delta p = 2\sigma/r$ . Below, Figure 2.3 and capillary pressure equation (Equation 2.7), showing a cylindrical pore throat filled with oil and water, where water is the wetting fluid.

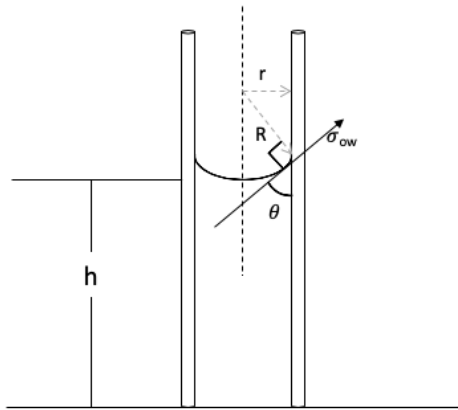


**Figure 2.3:** Capillary pipe model with two immiscible fluids forming a meniscus. Redrawn from Zolotukhin & Ursin (2000).

$$P_c = \frac{2\sigma_{ow}\cos\theta}{r} \quad (2.7)$$

Where:

- $\sigma_{ow}$  Interfacial tension (IFT) between the non-wetting and wetting fluid [N/m]
- $r$  Radius of the cylindrical pore channel



- $\theta$  Contact angle; defined as the angle between tangent to the oil-water surface in the triple point solid-water-oil, measured through the water phase and the cylindrical wall.

The phase that preferentially wets the capillary tube will always be the phase with lowest pressure. Capillary pressure can be both positive and negative, and the sign expresses which phase that has lowest pressure. (Green & Willhite, 1998). In cores with the same pore size distribution, the capillary forces increases with increasing water wetness. Larger changes in interfacial tension between oil and water ( $\sigma_{ow}$ ) could also have significant effect on capillary pressure.

### 2.3.4 Capillary entry pressure

Pressure continuity at no-flow condition requires capillary pressure to be constant. It also requires that the interface curvature between oil and water must be constant within the pore space (Chukwudeme et al., 2014). In 1941 Leverett proposed a J-function to calculate the capillary entry pressure. J-function is the saturation-dependent dimensionless capillary pressure (Leverett, 1941). Spontaneous imbibition can be an important mechanism, and the effectiveness of it is linked to the wettability of the system. In case of an oil-wet scenario, the imbibing fluid must overcome the entry pressure of the rock (Ahmed, 2010; Fanchi, 2018). During flooding, a discontinuity in capillary forces, at the inlet and outlet, can distort the fluid production. In a two-phase flow, when both phases are producing, the outlet  $P_c$  will be zero, even though inside the core, the two phases have different pressures. This is called the capillary end effects (Rapoport & Leas, 1953). The calculation of capillary entry pressure is shown in Equation 2.8:

$$P_c = \sigma \sqrt{\frac{\phi}{k}} J^* \quad (2.8)$$

Where:

- $P_c$  Capillary pressure (Pa)
- $\sigma$  Interfacial tension (IFT) (N/m)
- $\phi$  Porosity
- $k$  Permeability ( $m^2$ )
- $J^*$  Leverett dimensionless entry pressure ( $J^* \approx 0.25$  for a complete water-wet system)

### 3 Fluid flow in porous media

Knowledge of the physical properties of a given rock, the interaction between the fluids in the system and flow behavior of the fluids in the system is essential in understanding and evaluating the performance of a reservoir and its fluids.

#### 3.1 Porosity

Porosity of the rock is the measure of the void space of the rock total volume, unoccupied by the rock grains and mineral cement. On the other hand, porosity is the ratio of the pore volume to the total (bulk) volume of the rock, between 0 and 1 in fraction. Porosity can be determined mathematically, and the relationship is shown in Equation 3.1:

$$\phi = \frac{V_p}{V_b} \quad (3.1)$$

Where:

$\phi$	Porosity
$V_p$	Pore volume
$V_b$	Bulk volume

During past geological eras, sediments were deposited and rocks were formed. Due to excessive cementation, some of the pore volume developed into isolated void spaces. Many of the void spaces are interconnected, while some are completely isolated. This leads to two different types of porosity (Ahmed, 2010; Lake, 1989; Zolotukhin & Ursin, 2000):

- Absolute porosity is defined as the ratio of the *total* void space in the rock with respect to the bulk volume.
- Effective porosity is the ratio of the *interconnected* void space in the rock with respect to the bulk volume. The interconnected pore volume is the recoverable hydrocarbon, so the effective porosity is used in all reservoir engineering calculations.

#### 3.2 Permeability

The property of a porous media that measures the capability and ability of transmitting fluids through the interconnected pores in the formation is called permeability. Permeability of the rock is a very important rock property because it controls the flow rate and movement of the reservoir fluids in the formation. Fluid flow through a porous media is a significant aspect to

recover oil from reservoirs. Darcy (1856) proposed a relationship of fluid flow through an unfractured reservoir, and it is described by Equation 3.2 (Ahmed, 2010; Zolotukhin & Ursin, 2000).

In the laboratory, permeability is measured by flooding a fluid with known viscosity through the core with known diameter and length. The pressure drop is measured at a constant rate across the core. Darcy's law can be described as:

$$q = -\frac{kA}{\mu} \frac{dp}{dx} \quad (3.2)$$

Where:

$q$	Flow rate [m <sup>3</sup> /s]
$k$	Permeability [m <sup>2</sup> ]
$A$	Cross section of flow [m <sup>2</sup> ]
$\mu$	Fluid viscosity [Pa.s]
$\frac{dP}{dx}$	Pressure gradient [Pa/m]

### 3.3 Mobility ratio

The mobility of any fluid,  $\lambda$ , is defined as the ratio of the effective permeability of flowing phase to viscosity of the fluid and is a strong function of the fluid saturation. In a reservoir system where two fluid phases coexist, when waterflooding in oil reservoir as an example, the wettability and viscosity of the system drive the overall efficiency. In calculations involving a displacement process, the mobility ratio is a useful concept. The mobility ratio,  $M$ , is defined as the mobility of the displacing fluid to the mobility of the displaced fluid, and is estimated in Equation 3.3 (Ahmed, 2010; Green & Willhite, 1998):

$$M = \frac{\lambda_D}{\lambda_d} = \frac{\lambda_w}{\lambda_o} = \frac{\left(\frac{k_{rw}}{\mu_w}\right)_{Sor}}{\left(\frac{k_{ro}}{\mu_o}\right)_{Swi}} \quad (3.3)$$

Where:

$M$	mobility ratio
$\lambda_D$	mobility of the displacing fluid (m <sup>2</sup> /Pa.s)

$\lambda_d$	mobility of the displaced fluid ( $\text{m}^2/\text{Pa}\cdot\text{s}$ )
$\lambda_w$	mobility of water ( $\text{m}^2/\text{Pa}\cdot\text{s}$ )
$\lambda_o$	mobility of oil ( $\text{m}^2/\text{Pa}\cdot\text{s}$ )
$k_{rw}$	relative permeability of water ( $\text{m}^2$ )
$\mu_w$	water viscosity ( $\text{Pa}\cdot\text{s}$ )

During a displacement process, a mobility ratio greater than 1 ( $M > 1$ ) is considered unfavorable, while mobility ratio less than 1 ( $M < 1$ ) is considered favorable (Fanchi, 2010). When the mobility ratio is favorable, the displacement is called “piston-like displacement”. In this case there is a sharp interface between oil and water. Oil is flowing in presence of connate water in front, while water in presence of residual oil is flowing behind. In the case of a unfavorable mobility ratio, water flows faster than oil which leads to an early breakthrough of water and reduces the volumetric displacement efficiency due to gravity segregation (Apostolos et al., 2016; Bavière, 1991). Figure 3.1 shows the difference in favorable and unfavorable mobility ratios:

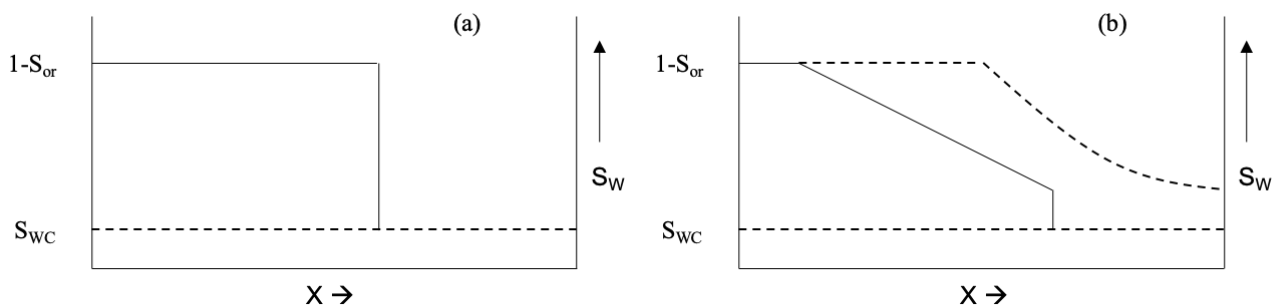


**Figure 3.1:** Water saturation as a function of distance between injection and production wells for (a) favorable piston-like displacement and (b) unfavorable displacement. Redrawn from Apostolos et. al (2016).

### 3.4 Flow regimes

Flow regimes describes fluid flow behavior and are related with different boundary conditions, and can be identified by the rate of change in pressure with time. There are basically three types of flow regimes: steady state, pseudo-steady state and unsteady state (Ahmed, 2010; Fanchi, 2010).

The steady state flow represents a condition that exists when the pressure at every location in the reservoir remains constant. During a steady state flow, two phase are injected simultaneously into the core at constant rate and pressure. Using Darcy's law to determine the effective permeability for each phase at a given saturation (Apostolos et al., 2016). Equation 3.4 states that the rate of change in pressure, P, with respect to time, t, at any location, i, is zero:

$$\left(\frac{\partial P}{\partial t}\right)_i = 0 \quad (3.4)$$

The pseudo-steady state flow is when pressure changes at a constant rate. Pressure at different locations in the reservoir is declining linearly as a function of time. The system with pseudo-steady state flow acts like a closed system, and therefore there are not any fluid movement across boundaries (Ahmed, 2010). As follows, Equation 3.5 states that the rate of change in pressure with respect to time at every position is constant:

$$\left(\frac{\partial P}{\partial t}\right)_i = \text{constant} \quad (3.5)$$

The unsteady state flow, also called transient flow, is the flow regime where pressure changes as a function of time. During a unsteady state flow, only one fluid is injected into the core at a constant. There are no restrictions on fluid movement, and saturation equilibrium will not be reached (Apostolos et al., 2016). The pressure derivative is essentially function of both position, i, and time, t:

$$\left(\frac{\partial P}{\partial t}\right) = f(i, t) \quad (3.6)$$

## 4 Wettability

The definition of wettability is “ the tendency of a fluid to spread on, or adhere to a solid in the presence of other immiscible fluids” (Craig, 1971). Throughout the years, laboratory experiments and understanding of wettability have confirmed that rock wettability affects the displacement of oil. By making wrong assumptions about the reservoir wettability, can lead to irreversible reservoir damage. The limitation of the definition of wettability does not take into account the interaction of the three phases in a crude oil/brine/rock system, as each phase has many components that can affect the wetting (Drummond & Israelachvili, 2002).

In addition to this, it is important to obtain an adequate physical description of the rock, which includes porosity, permeability and pore size distribution. Also the chemical composition of brines and oil are of high importance because when interacting with the rock they establish the wetting conditions of the system (Anderson, 1986b). The wetting properties of a crude oil/brine/rock (CBR) system strongly influences the two-phase fluid flow in the porous medium. The properties dictates capillary pressure and relative permeability. Studies have been done by Jadhunandan and Morrow (1995), showing that optimum recovery during waterflooding are with slightly water-wet systems (Jadhunandan & Morrow, 1995).

### 4.1 States of wettability

In a crude oil/brine/rock system (CRB), wettability is classified by four main states: water-wet, fractionally-wet, mixed-wet and oil-wet (Donaldson & Alam, 2008). A reservoir rock is considered water-wet, when water occupies smaller pores and water exists as a film covering the surface in larger pores. Oil droplets are lodged in larger pores, resting on the water film. Water exist as a continuous phase throughout the whole porous rock. At irreducible water saturation ( $S_{wi}$ ), water occupies smaller pores, and oil saturation is high enough to exist as the continuous phase through the larger pores of the rock. During a waterflooding process water saturation increases, and some of the oil is pushed out of the system and the rest of the oil will be trapped as droplets completely surrounded by water and become discontinuous.

When a CBR-system is heterogeneous wetted and the surface can be both water-wet and oil-wet it is characterized as fractionally-wet (Brown & Fatt, 1956). The preferential wetting is randomly distributed throughout the rock (Donaldson & Alam, 2008). This term must not be mistaken with another heterogeneous term introduced by Salathiel (1973): mixed-wet. It is a

condition where the fine pores are preferentially water-wet, and the larger pores are oil-wet and oil is in contact with the pore walls which form a continuous path throughout the rock. This way water can displace oil from the larger pores and capillary forces will hold little or no oil in the smaller pores. This explains why mixed wettability is characterized by such a low  $S_{or}$ . (Salathiel, 1973). Both fractionally-wet and mixed-wet are characterized as the term neutral-wettability. Natural-wet only implies that the rock is heterogeneous wetted and half of the rock is water-wet and the other half is oil-wet, and does not categorize the type of wettability condition.

In an oil-wet system, the position of water and oil in the rock is reversed. Oil will be in the smaller pores, and also exists as a film on the rock surface. Water droplets will be present in the middle of the larger pores. When a waterflooding process begins, water will flow through the larger pores, but avoiding smaller pores, while the oil will remain covering the rock surface (Anderson, 1986b; Donaldson & Alam, 2008). Figure 4.1 illustrates a water-wet and an oil-wet system.

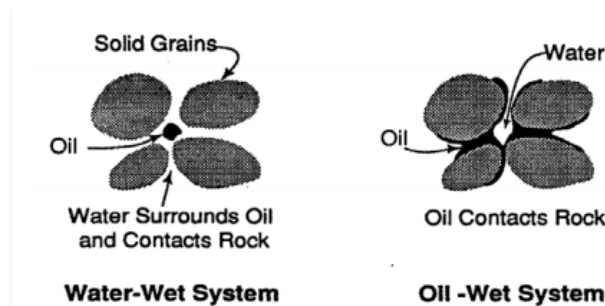


**Figure 4.1:** Water-wet vs oil-wet system (Green & Willhite, 1998)

## 4.2 Interfacial tension

Interfacial tension (IFT) is surface energy related to the interface between two immiscible fluids that coexist in a porous media. Two fluids are immiscible when the molecules of each fluid are strongly attracted to the molecules of their own kind. The area of their contact surface is minimized and the interfacial tension is positive ( $\sigma > 0$ ). The magnitude of the interfacial tension represents the required energy or work to keep the two fluids apart in an equilibrium. In the case where stronger intermolecular attraction within a fluid phase, one need greater work to bring the molecules to the surface (Donaldson & Alam, 2008; Zolotukhin & Ursin, 2000). This

results in greater interfacial tension. The work required to create a new surface area is expressed in Equation 4.1:

$$W = \sigma dA \quad (4.1)$$

Where:

$W$  Energy applied to surface [Nm]

$dA$  New surface area [m<sup>2</sup>]

$\sigma$  Interfacial tension [N/m]

### 4.3 Wettability measurements methods

There are several methods used to evaluate the wetting of a system, both qualitative and quantitative. Quantitative methods that are described below are contact angle measurements, Amott (imbibition and forced displacement), the USBM method and chromatographic wettability test (Donaldson & Alam, 2008). The qualitative methods includes measurements of the imbibition rates, microscope examination, flotation, glass slide method, relative permeability curves, capillary pressure curves, capillarimetric methods, displacement capillary pressure, permeability/saturation relationships, reservoir logs, nuclear magnetic resonance and dye adsorption (Anderson, 1986a).

When measuring wettability, one must ensure that the method used does not change the wetting condition of the surface during the measurement procedure. The minerals of the rock and hence also the pores have various surface characteristics, including also chemical properties that can influence the wettability. Crude oil with acidic and basic material can also be of influence (Hopkins, 2016). Today, no single accepted method is used, but the most generally used is the quantitative methods. Contact angle measures the wettability of a specific area, while Amott and USBM measures the average wettability of the core (Anderson, 1986a). In the following sections describes some of the quantitative methods.

#### 4.3.1 Contact angle measurement

The rock prefers either water or oil on the flow properties during a waterflood. The surface energies in a rock/brine/oil system may be written by Young's Equation 4.2 (Craig, 1971). Only



the oil-water interfacial tension and contact angle can be determined in the laboratory. The oil-solid and water-solid interfacial tension cannot be measured directly.

$$\cos\theta = \frac{\sigma_{os} - \sigma_{ws}}{\sigma_{ow}} \quad (4.2)$$

Where:

- $\theta$  contact angle of the water/oil/solid contact line (usually measured through the water phase)
- $\sigma_{ow}$  interfacial tension between oil and water
- $\sigma_{os}$  interfacial tension between oil and solid
- $\sigma_{ws}$  interfacial tension between water and solid

Figure 4.2 illustrates the surface energies in the CRB-system:

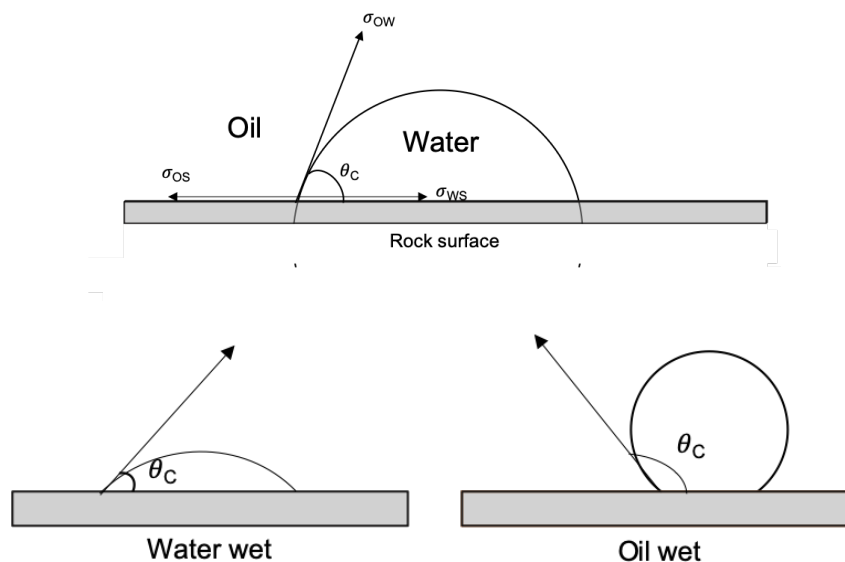


**Figure 4.2:** Wettability of an CRB-system. Redrawn from Anderson (1986a).

The contact angle test is the most beneficial wettability measurement method when only water and oil (and no other components that can alter the wettability) are present and cores with smooth surfaces are used. The method shows the equilibrium between the interfacial tensions of the two fluids towards each other and towards the solid, and indicates how well a liquid phase spread over a surface. There are many methods for measuring the contact angle and the most generally method used in the petroleum industry is the sessile drop method, which measures contact angle directly (Anderson, 1986b). As seen in Figure 4.2, when contact angle is smaller than  $90^\circ$  the surface is preferentially water-wet. Water occupies the smaller pores and

is the spreading fluid on the rock surface. If the contact angle is greater than 90° the rock is considered oil-wet, where oil is the spreading fluid and occupies the smaller pores. When contact angle is equal to 90°, the rock is intermediate or neutrally wet (Craig, 1971).

### 4.3.2 Amott method

In the Amott method both spontaneous imbibition and forced displacement are combined to measure the average wettability of the core (Amott, 1959). The principle behind this method is that the wetting fluid will imbibe spontaneously into the core and displace the non-wetting one. The ratio of spontaneous to forced imbibition is used to reduce the influence of other factors, like viscosity, relative permeability and initial saturation of the matrix (Anderson, 1986a).

The results of the Amott test is the “displacement-by-water ratio”,  $I_w$ , and the “displacement-by-oil ratio”,  $I_o$ . These two ratios are shown in Equations 4.3 and 4.4:

$$I_w = \frac{\Delta S_{WS}}{\Delta S_{WS} + \Delta S_{WF}} \quad (4.3)$$

$$I_o = \frac{\Delta S_{OS}}{\Delta S_{OS} + \Delta S_{OF}} \quad (4.4)$$

Where:

$\Delta S_{WS}$  saturation change during spontaneous imbibition of water

$\Delta S_{WF}$  saturation change during forced imbibition of water

$\Delta S_{OS}$  saturation change during spontaneous imbibition of oil

$\Delta S_{OF}$  saturation change during forced imbibition of oil

Cores that are strongly water-wet, will show  $I_w$  approaching 1 and  $I_o$  approaching zero. The opposite results are given for a strongly oil-wet case. For natural wet, both ratios are zero (Amott, 1959).

Equation 4.4 shows a modification of the Amott test method, called the Amott-Harvey method. It is a method which is most commonly used, and results in the Amott-Harvey relative displacement index,  $I_{AH}$ , which represents the difference between the two Amott displacement ratios (Anderson, 1986a):

$$I_{AH} = I_O - I_W \quad (4.5)$$

The Amott-Harvey index ranges from -1 to +1, where -1 represents completely oil-wet system and +1 represents a completely water-wet system. The index range is extended by characterizing  $-1 < I_{AH} < -0.3$  for oil-wet systems,  $-0.3 < I_{AH} < 0.3$  for an intermediate-wet system and  $0.3 < I_{AH} < 1$  for a water-wet system (Cuiec, 1984). Amott methods are time-consuming, and is not sensitive to neutral wettability (Anderson, 1986a). They do not state clear differences between different degrees of strong water wetness (Ma et al., 1999; Morrow, 1990).

Figure 4.3 shows a capillary pressure curve. The Amott-Harvey test-cycle is divided into five segments, which are all illustrated in figure 4.3 (Donaldson & Alam, 2008):

1. The core is initially filled with water, then drainage of water by oil to establish water saturation,  $S_{wi}$  (oil drive)
2. Spontaneous imbibition of water
3. Forced displacement of oil by water to  $S_{or}$  (water drive)
4. Spontaneous imbibition of oil
5. Forced displacement of water by oil to  $S_{wi}$  (final drive)

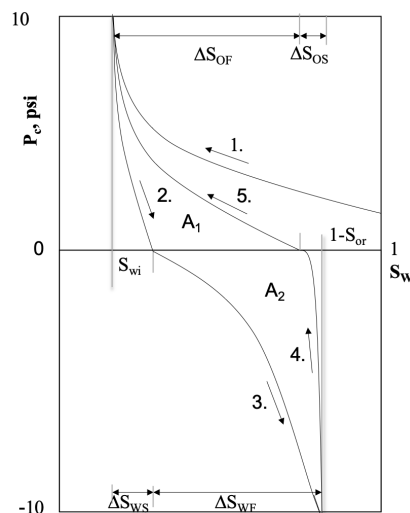


**Figure 4.3:** Capillary pressure curve for Amott, Amott-Harvey and USBM method. Redrawn from Donaldson & Alam (2008).

### 4.3.3 United states bureau of mines (USBM) method

The USBM method is similar to the Amott method, which also measures the average wettability of the rock. This method have both advantages and disadvantages, and the advantage is that it is time efficient and sensitive close to neural wettability, where Amott method is not. The core samples need to spin in a centrifuge, so the method can only measure plug-size samples which is one of the disadvantages (Anderson, 1986a). The USBM method measure the area in the two regions of capillary pressure curves produced during forced drainage and imbibition process, when one fluid displaces another fluid (see Figure 4.4) (Donaldson et al., 1969). The work required for the wetting fluid to displace the non-wetting fluid from the core is less than the work required for the non-wetting fluid to displace the wetting one, due to favorable change in the free-energy. The required work is found to be proportional to the area under capillary pressure curve. In Figure 4.4, one can see that if a core is water-wet, the area under the water-drive capillary pressure curves, when water displaces the oil, is smaller compared to the area under the capillary pressure curve when oil displaces water (Anderson, 1986a).

To calculate the wettability index ( $I_{USBM}$ ) the ratio of the areas under the two capillary pressure curves ( $A_1$  and  $A_2$ ) is used (shown in Figures 4.3 and 4.4), and is defined as:

$$I_{USBM} = \log \left( \frac{A_1}{A_2} \right) \quad (4.6)$$

Where

- $A_1$  the area between the forced drainage curve and the saturation axis
- $A_2$  the area between the forced imbibition curve at the saturation axis

The core is water-wet, when  $I_{USBM}$  is greater than zero. When  $I_{USBM}$  is less than zero, the core is oil-wet. The core is neutrally wet, when  $I_{USBM}$  has values close to zero (Anderson, 1986a).

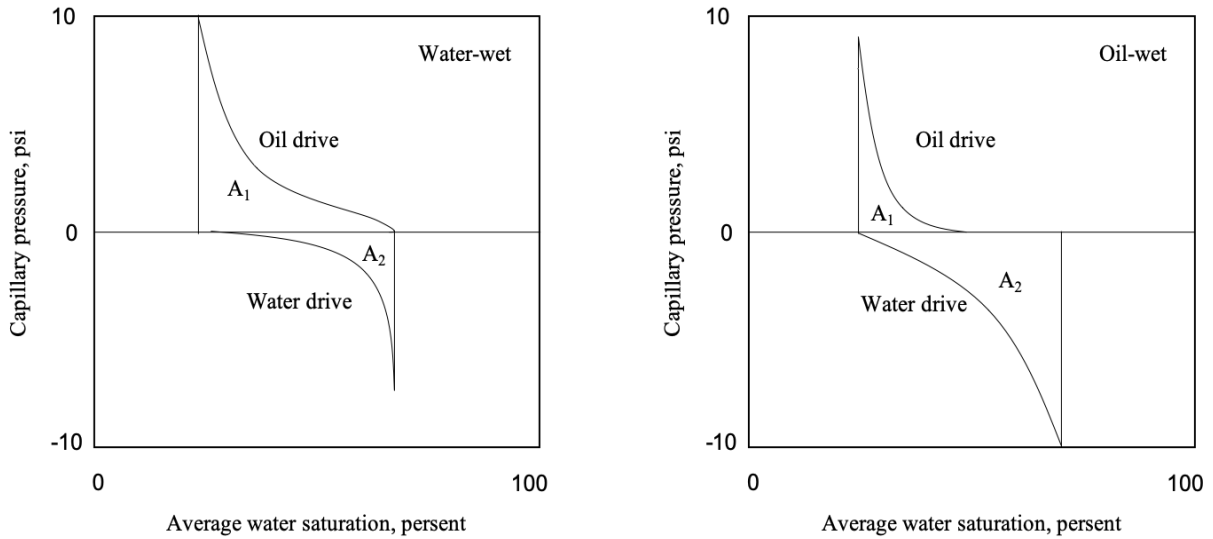


**Figure 4.4:** USBM wettability measurement in a water-wet and oil-wet core. Redrawn from Anderson (1986a).

#### 4.3.4 Spontaneous imbibition

Spontaneous imbibition (SI) is the process where the wetting fluid is dragged into the porous media by capillary forces in centimeter scale, and SI is therefore directly related to the capillary pressure. For a fractured reservoir, spontaneous imbibition is particularly important to oil recovery (Morrow & Mason, 2001). When water spontaneously imbibe into the pores and displace the oil, both rate and total recovery of the oil is measured (Morrow, 1979). Figure 4.5 shows a sketch of results from a spontaneous imbibition showing total recovery vs time:

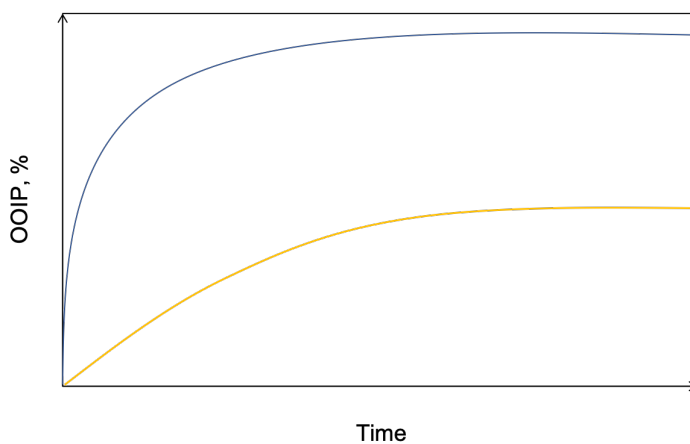


**Figure 4.5:** A sketch of oil recovery from a spontaneous imbibition. The blue curve indicates a steep, rapid recovery, and the yellow curve represent a slower and lower recovery.

The form of the imbibition curve is important, and characterization of wettability of a core by spontaneous imbibition is made by comparing to a reference core that have close to perfect wetting conditions (Morrow & Mason, 2001). Figure 4.4 shows an illustration of two cases of spontaneous imbibition. The steeper blue curve represents a more piston-like displacement and a higher ultimate recovery, than the slower yellow curve. The blue one indicates a more water-wet system.

A new simplification of the wetting index,  $I_w^*$ , which is only based on SI experiments. The degree of water-wetness can be quantified by a modified Amott water index ( $I_{w-SI}^*$ ) using a strongly water-wet core as a reference core (Torrijos et al., 2019). This is shown in Equation 4.3:

$$I_{W-SI}^* = \frac{SI_c}{SI_{WWC}} \quad (4.7)$$

Where:

$SI_{WWC}$  the oil recovery (%OOIP) by spontaneous imbibition from the reference (strongly water-wet) core

$SI_c$  the oil recovery (%OOIP) by spontaneous imbibition from the assessed core

The degree of water-wetness,  $I_{w-SI}^*$ , approaches 1 for a water-wet core and 0 for a fractionally/neutral wet core. This wettability index is applicable when the  $S_{wi}$  for both cores are identically.

#### 4.3.5 Chromatographic wettability test

In 2006, Strand et.al developed a new wettability test, the chromatographic wettability test for carbonates (Strand et al., 2006). The main principle behind the test is that it analyzes the reactivity on the rock surface, by measuring the amount water-wet carbonate surface. It is performed at  $S_{or}$  at room temperature, using a core flooding set up. The method is based on chromatographic separation between two water-soluble ions, with different affinities. The component with affinity towards the water-wet areas of the core is  $SO_4^{2-}$ , which is the ion that will adsorb onto the water-wet carbonate surface. Thiocyanate,  $SCN^-$ , is a tracer with no affinity towards the carbonate surface. In Figure 4.6 one can see the adsorption process to the surface for different wettabilities.

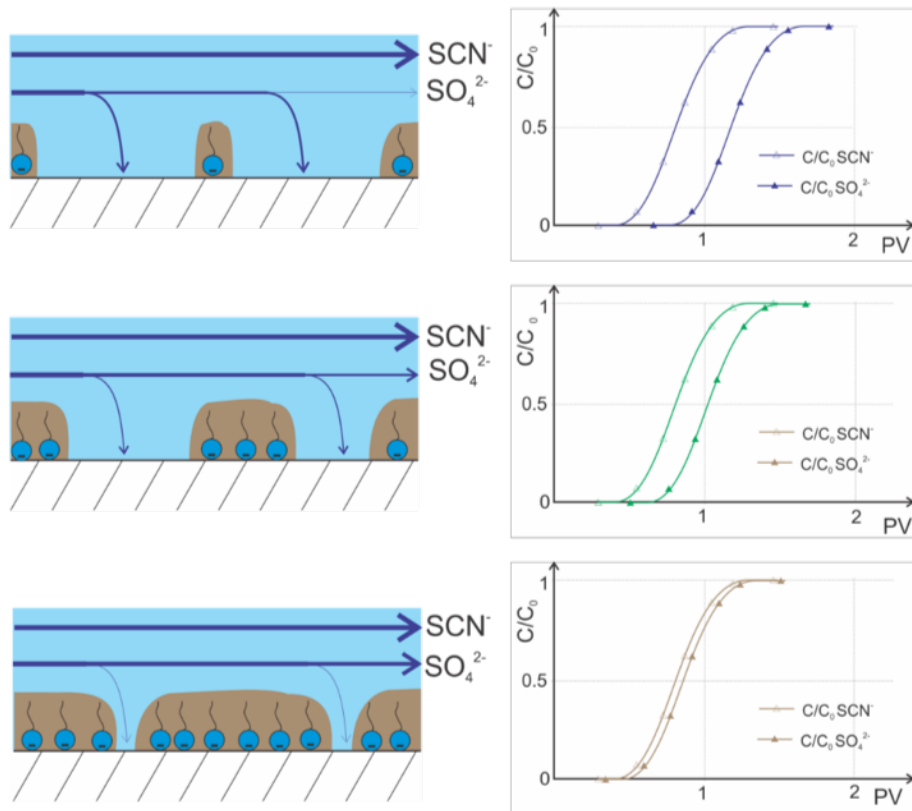


**Figure 4.6:** Sketch of adsorption of  $\text{SO}_4^{2-}$  onto water-wet, oil-wet and mixed-wet core surfaces (Smart Water IOR group, 2019)

During a core flooding, with brine containing  $\text{SO}_4^{2-}$  and  $\text{SCN}^-$ , effluent of the produced water is collected. The ion chromatography (IC) measures the concentrations of samples, where both anions and cations are analyzed. As  $\text{SO}_4^{2-}$  adsorbs onto the rock surface, during the chromatographic analysis of the effluent anions, the sulfate concentration will appear to be delayed compared to the thiocyanate concentration. The area between these two curves are proportional to the water-wet spots on the rock surface in contact with water during the core flooding. The separation only takes place at the water-wet areas of the surface (see Figure 4.6). The wettability index (WI) is defined as:

$$WI = \frac{A_{\text{wett}}}{A_{\text{heptane}}} \quad (4.8)$$

Where

$A_{\text{wett}}$  area between the thiocyanate and sulfate curves

$A_{\text{heptane}}$  area of a reference (completely water-wet) containing 100 % heptane

The wettability index is a ratio and varies from zero to 1. The areas are calculated using the trapezoidal method of numerical integration. Zero is oil-wet, 0.5 is neutral wet and 1 is completely water-wet. The advantages of the chromatographic wettability test is that the method is time-efficient and has good sensitivity near neutral wetting conditions (Strand et al., 2006).

#### 4.4 Effect of wettability on core analysis

Changes in rock wettability affects capillary pressure, waterflood behavior and relative permeability. Wettability controls location, flow and distributions of fluids in a porous medium, along with  $S_{wi}$  and  $S_{or}$ . To predict the behavior of a reservoir rock, the most accurate measurements are done on an native/non restored core (Anderson, 1987). In next sections effect of wettability on relative permeability, capillary pressure and waterflooding are described.

##### 4.4.1 Effect of wettability on relative permeability

In a two-phase flow in porous media, the relative permeability of a phase is a dimensionless measure of the effective permeability of that phase. Relative permeability is the ratio of the effective permeability of that phase to the absolute permeability. Absolute permeability is the measure of the capacity of the medium to transmit fluids. If two fluids are present in the core, the permeabilities of each fluid as a function of saturation and wetting characteristics of the rock, are called effective permeabilities ( $k_w$  and  $k_o$ ) (Ahmed, 2010; Lake, 1989). When oil and water is present in a rock at the same time, the relative permeability of each phase is expressed in Equation 4.9:

$$k_{ro} = \frac{k_o}{k}; k_{rw} = \frac{k_w}{k} \quad (4.9)$$

Where:

- $k_{ro}$  relative permeability of oil
- $k_{rw}$  relative permeability of water
- $k$  absolute permeability
- $k_o$  effective permeability of oil for a given oil saturation
- $k_w$  effective permeability of water for a given water saturation



Relative permeability of a given fluid is a strong function of the fluid's saturation. Additional relative permeability and saturation is also a function of rock properties and wettability (Lake, 1989). Relative permeability of a fluid decreases as the saturation of that fluid decreases. As soon as relative permeability reaches zero, the fluid cannot longer flow, and saturation cannot be lowered more at this point. This saturation is called residual saturation ( $S_{wi}$  or  $S_{or}$ ) (Anderson, 1987). During a waterflood in a core filled with oil, the oil relative permeability decreases as water relative permeability increases as a function of water saturation (Donaldson & Alam, 2008).

Other important factors on the relative permeability curve (see Figure 4.7) are the endpoint relative permeabilities. These relative permeabilities for one phase are constant at the other phase's residual saturation and are measures of the wettability. Relative permeability of a fluid in strongly wetted systems is generally higher when the fluid is in the non-wetting phase, i.e. water relative permeability is higher in an oil-wet system compared to a water-wet system (Lake, 1989). This is because the non-wetting fluid is located in the center of the pores and travels more easily, and at low non-wetting phase saturation the non-wetting fluid will become trapped as discontinuous droplets in the larger pores. On the other hand the wetting fluid tend to travel through smaller, less permeable pores and give lower relative permeability.

At low wetting phase saturations, the non-wetting phase relative permeability approaches 1, i.e. effective permeability will be close to absolute permeability of the rock. This demonstrate that the wetting phase does not greatly restrict the flow of the non-wetting phase (Craig, 1971; Lake, 1989). The crossover saturation (COS), where relative permeabilities are equal to each other, are even more a relevant indicator of wettability of the porous material. The reason may be that it is less sensitive to the values of residual saturations (Zolotukhin & Ursin, 2000). A rule of thumb proposed by Craig (1971) is when the crossover saturation is more than 50 % water saturation ( $S_w > 0.5$ ) it is water-wet, and when the crossover saturation is less than 50 % water saturation ( $S_w < 0.5$ ) it is oil-wet.

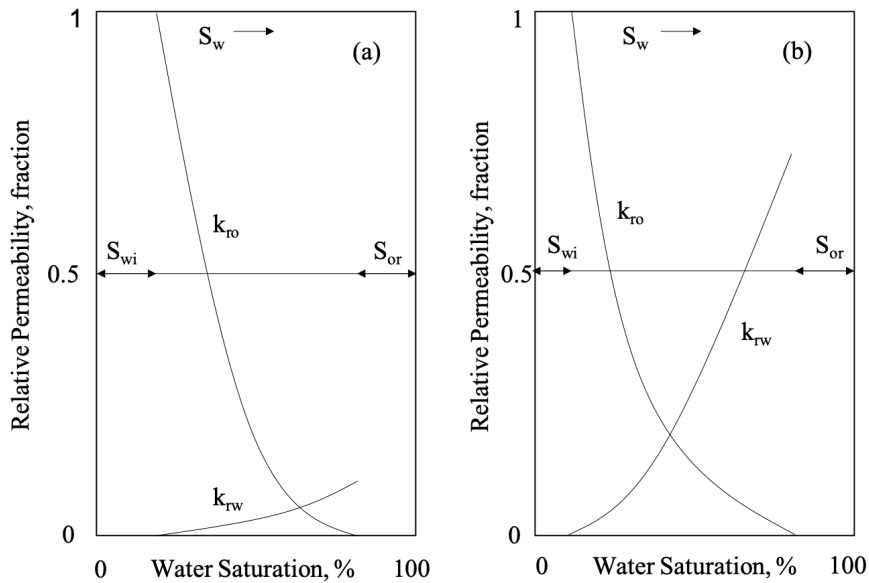


**Figure 4.7:** Relative permeability curves  $k_{ro}$  and  $k_{rw}$  for (a) water-wet and (b) oil-wet system. Redrawn from Zolotukhin & Ursin (2000).

For a water-wet core (Figure 4.7a), water will be present in the small cavities and at the grain surface, whereas oil will be in the larger pores. During a waterflood, both oil and water will flow, and the high oil relative permeability will decrease as oil saturation decreases. Water will imbibe into the core forcing oil to move to larger pores, where oil easiest can be displaced. Water relative permeability will increase as water saturation increases. Water saturation will increase first in the smaller pore spaces, due to wetting forces (capillary forces). When displacement moves from smaller to larger pores, water will occupy pores that formerly was filled with oil. Some of the oil-filled pores can become trapped, because driving pressure is not sufficient to overcome the capillary entry pressure. Eventually, oil stops flowing when all continuous flow paths are filled with water. Due to oil trapped in large pores, the final  $k_{rw}$  is lower than  $k_{ro}$  (Anderson, 1987).

For an oil-wet core (Figure 4.7b), the rock prefers to be in contact with the oil. Location of water and oil are reversed from the water-wet case. Oil will be present in small pores and at the rock surface. Water will be located in the centers of the larger pores. In some oil-wet reservoirs,  $S_{wi}$  appears to be droplets in the centers of the pore spaces (Raza et al., 1968). In the beginning of a waterflood, water will flow through the centers of the larger pores, forming continuous channels or fingers through. Waterflooding in a strongly oil-wet rock is less efficient than for a water-wet rock. Oil is flowing more poorly (than for a water-wet case), and remaining oil will be in the smaller pores, on rock surface and trapped oil surrounded by water in larger pores.

#### 4.4.2 Effect of wettability on Capillary pressure

As discussed in section 4.4, wettability is an important factor in remaining oil saturation and in relative permeability curves, but also in capillary pressure (Anderson, 1986a; Anderson, 1987a). Below, Figure 4.8 shows capillary pressure curves of the capillary behavior of a water-wet, mixed-wet and an oil-wet system:

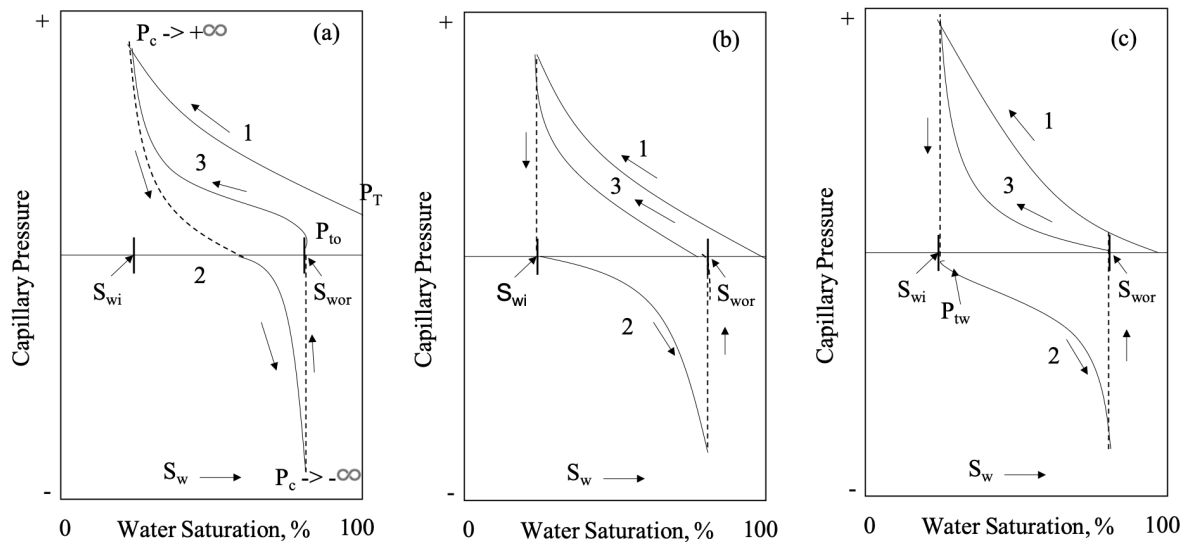


**Figure 4.8:** Illustration of capillary pressure behavior for (a) water-wet system, (b) mixed-wet system and (c) oil-wet system during drainage and imbibition. Redrawn from Donaldson & Alam (2008).

Figure 4.8a shows the capillary pressure behavior for a water-wet system. Segment 1 is for primary drainage process, and corresponds to the initial displacement when a water-wet core comes in contact with oil and water saturation starts to reduce. Before oil will enter the water-wet core, a threshold pressure ( $P_T$ ) is required, and when  $P_T$  is exceeded, oil enters the core and displace water to  $S_{wi}$ . When the core reaches  $S_{wi}$  and the capillary pressure curve is almost vertical, water starts to imbibe spontaneously into the core and water will displace the oil (segment 2). When the spontaneous imbibition reaches a limiting value ( $P_c = 0$ ), pressure must be applied to force water into the core and displace oil to a practical residual oil saturation ( $S_{wor}$ ), and capillary pressure approaches a negative infinite value. A new threshold pressure ( $P_{to}$ ) at  $S_{wor}$ , before oil enter the core displacing water (Donaldson & Alam, 2008).

Figure 4.8b shows the capillary pressure behavior for a natural wetted system. In this case no threshold pressure is needed. Some oil may imbibe into the core at  $P_c = 0$ , after which pressure

is required for injection of oil to displace water to  $S_{wi}$ . At  $S_{wi}$ , small amounts of water will spontaneously imbibe into the core until  $P_c = 0$ . Oil will then be displaced down to  $S_{wor}$ , and then water pressure increase. The capillary pressure is negative because the water injection pressure is greater than the oil pressure ( $P_c = P_o - P_w < 0$ ) (Donaldson & Alam, 2008).

Figure 4.8c shows the capillary pressure behavior for an oil-wet system. The core is initially saturated with water, and when oil comes in contact with the core, it will spontaneously displace the water down to  $S_{wi}$ . At this point, water will not spontaneously imbibe into the core. A threshold pressure ( $P_{tw}$ ) needs to overcome the forces of water. After exceeding  $P_{tw}$ , oil will be displaced to  $S_{woc}$ . If the core at this point is in contact with oil, the oil will spontaneously imbibe into the core (Donaldson & Alam, 2008).

#### 4.4.3 Effect of wettability on waterflooding

Waterfloods in water-wet and oil-wet systems have long been known to behave very differently. For water-wet systems waterflooding is recognized to be more efficient than for oil-wet system (Anderson, 1987b). The recovery by waterflooding is controlled by oil and water relative permeabilities and viscosities of water and oil. The effect of relative permeabilities and viscosities on waterflooding can be demonstrated by fractional flow equation assuming horizontal flow, is shown in Equation 4.10 (Craig, 1971):

$$f_w(S_w) = \frac{1}{1 + \frac{\mu_w}{\mu_o} \frac{k_{ro}}{k_{rw}}} \quad (4.10)$$

Where:

- $f_w$  Fractional flow of water
- $S_w$  Water saturation
- $\mu_w, \mu_o$  Oil and water viscosities [cp]
- $k_{ro}, k_{rw}$  Oil and water relative permeabilities

Fractional flow of water at a given saturation increases when water/oil viscosity ratio decreases. This decrease in viscosity ratio will result in earlier breakthrough and lower oil production. Similar are the effects for increased oil/water relative permeability ratio. Relative permeabilities are functions of water saturation, pore geometry, wettability and fluid distribution (Anderson,

1987b; Craig, 1971). In Figure 4.9, a typical fractional flow curve for strongly water-wet rock which is generally concave up is illustrated:

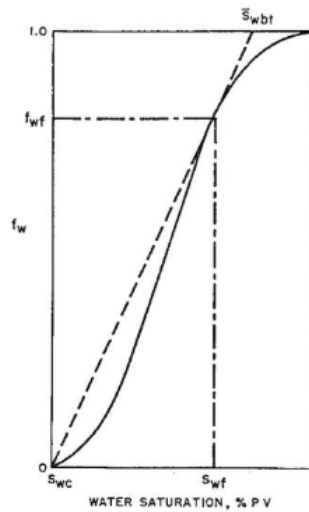


**Figure 4.9:** Fractional flow curve for very water-wet rock, determination of front saturation,  $S_{wf}$ , and average saturation at water breakthrough,  $\bar{S}_{wbt}$  (Craig, 1971).

The tangent point in the curve defines the front saturation,  $S_{wf}$ , and the fractional flow of water at the flood front,  $f_{wf}$ . The point where the tangent meets  $f_w=1$ , is the average water saturation at breakthrough. At water breakthrough, the oil recovery factor can be calculated as:

$$RF = \frac{\bar{S}_{wbt} - S_{wi}}{1 - S_{wi}} \quad (4.11)$$

Where:

- $RF$  Recovery factor
- $\bar{S}_{wbt}$  Average water saturation at breakthrough
- $S_{wi}$  Irreducible water saturation

Before water breakthrough, the oil recovery equals to water injected. At breakthrough, where  $S_{wbt} = S_{wf}$ , the front reaches production well. Water production at this point increases from zero to  $f_{bt} = 1$ . After breakthrough, both oil and water will be produced (Craig, 1971; Kootiani & Samsuri, 2012). As mentioned before, the efficiency of the waterflood depends on mobility ratio of water and oil. Lower ratio gives more efficient displacement, and the fractional flow shifts to right. In extreme cases where the ratio is very low, front saturation is equal to average

water breakthrough. In this case at water breakthrough, oil left in the reservoir is only the immobile oil, i.e. residual oil (Apostolos et al., 2016).

Oil recovery during waterflooding is a function of wettability, pore geometry, fluid distribution, saturation, saturation history and oil/water viscosity ratio. Wettability controls the flow and spatial distribution of fluids in a porous rock during waterflooding. Figure 4.10 shows production from water-wet, neutral-wet and oil-wet systems.

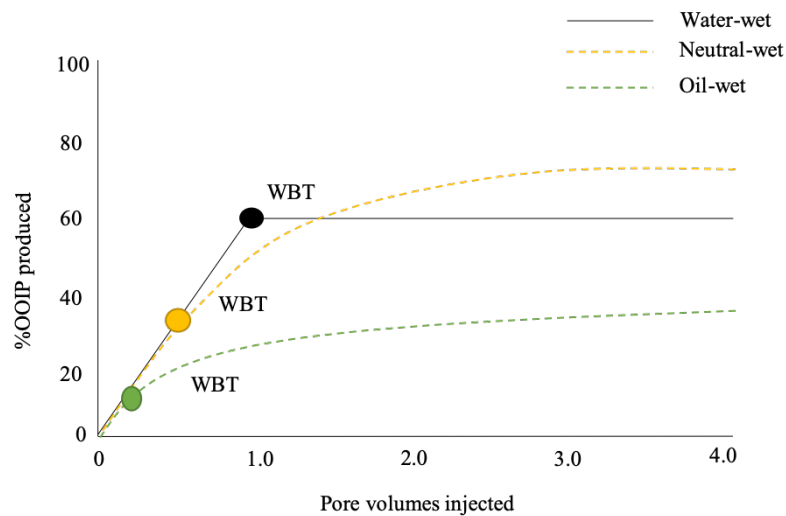


**Figure 4.10:** Idealized production from three conditions of wettability. Redrawn from Donaldson & Alam (2008).

As discussed in section 4.4, wettability has a strong effect on relative permeability. When a core becomes more oil-wet, the relative permeability of water increases and decreases for oil. This leads to better flow of water, causing earlier water breakthrough and less efficient production. As mentioned before, a water-wet core initially at  $S_{wi}$ , water will occupy the cavities and forming a water film on the rock surface, while oil will be in the larger pores. This fluid distribution is the most energetically favorable. Oil that are located in small pores, would be displaced into the center of the larger pores by spontaneous imbibition due to lowering the energy of the system (Raza et al., 1968). There are three different oil saturations important for waterflooding; breakthrough saturation, economical saturation and true residual saturation (Anderson, 1987b).

In Figure 4.10, one can see the difference in recovery for water-wet, neutral-wet and oil-wet, assuming each has the same water/oil viscosity ratio. During waterflooding in a water-wet

system, with moderate viscosity ratio, almost all recoverable oil are produced before water breakthrough. After water breakthrough, the viscosity ratio increases, and small additional amount of oil is produced after the breakthrough and the rest is immobile oil. During waterflooding in an oil-wet system, at moderate viscosity ratio, water breakthrough occurs earlier, and most of the oil is recovered after water breakthrough. Waterflooding is less efficient in oil-wet cases, due to larger amount of injected water is required to recover the same amount of oil as for water-wet systems. In a water-wet system, with moderate viscosity ratio, the breakthrough, economical and true residual saturation are essentially equal, while in an oil-wet system the breakthrough saturation is relatively high and true residual saturation is lower than economical (practical) saturation (Anderson, 1987b). Neutral-wet systems exhibits an earlier water breakthrough than water due to water advancing ahead of the main production front. The production continuous at increasing viscosity ratios to a practical oil saturation which is lower than for water-wet systems (Donaldson & Alam, 2008).

## 5 Carbonate reservoirs

In a carbonate reservoir, the majority of reservoir rocks are mineral carbonates, like calcium carbonate ( $\text{CaCO}_3$ ) and magnesium carbonate ( $\text{MgCO}_3$ ). Of world's proven petroleum reserves approximately 50 % are contained in carbonate reservoirs (Speight, 2017). Nearly all carbonate reservoirs are fractured to some amount, and are characterized by heterogeneous porosity and permeability (Ahr, 2008a, 2008b; Jardine & Wilshart, 1982). Permeability is rather low, in the range of 1-10 mD. Due to natural fractures, low permeability, low water wetness and inhomogeneous rock properties in carbonate reservoirs, the oil recovery factor is quite low, well below 30% in OOIP (Austad, 2013; Høgnesen et al., 2005).

### 5.1 Carbonate rocks

Carbonates are sedimentary rocks composed of anionic complexes of  $\text{CO}_3^{2-}$ , along with divalent metallic cations (2+) like calcium, magnesium, iron, manganese, zinc, barium, strontium and copper, together with other less common elements (Ahr, 2008a). As ancient rocks, carbonates occur naturally as sediments in shallow, tropical and temperate oceans, either by precipitation out of seawater or biological extraction of calcium carbonate from seawater. The distribution of the dispositional texture is sediments composed of particles with different sizes, shapes, chemical compositions and pore-size distribution, along with other properties (Lucia, 1999). Sedimentary rocks can be divided into clastic and non-clastic rock. Clastic material is when particles are derived from fragmentation, and non-clastic material is when the rock mainly consist of not broken (intact) sediments, like chemical or biogenetic deposits (Zolotukhin & Ursin, 2000).

The most common carbonate rocks are composed of calcite ( $\text{CaCO}_3$ ) and/or dolomite ( $\text{CaMg}(\text{CO}_3)_2$ ). Limestone contains mainly or entirely of the mineral calcite, detrital or crystalline, while dolomite or dolostone composed mainly of the mineral dolomite (Mazzullo et al., 1996; Zolotukhin & Ursin, 2000). Carbonates and sandstones are both sedimentary rocks, but differ in many aspects. There are two main differences between those two sedimentary rocks: the site of sediment production and the greater chemical reactivity of carbonate minerals (Ehrenberg & Nadeau, 2005). Sandstones is a result of transported and eroded detritus, while carbonates are formed from remains of plants and animals (Mousavi et al., 2012).



Chalk is classified as a limestone and is a non-clastic sedimentary rock, which are of bioclastic origin. It is composed of a very small skeletal part of pelagic coccolithophorid algae, called coccoliths (Zolotukhin & Ursin, 2000). These algae have a ring structure with 3-15  $\mu\text{m}$  in diameter (Punternold, 2008). Figure 5.1 shows a scanning electron microscopy (SEM) image clearly showing the ring structure, intact and non-intact. Chalk, compared to other carbonates, is characterized with high porosity, which is seen as the black spaces in the figure. The microscopic size of the constituents causes low permeability (Milter, 1996).

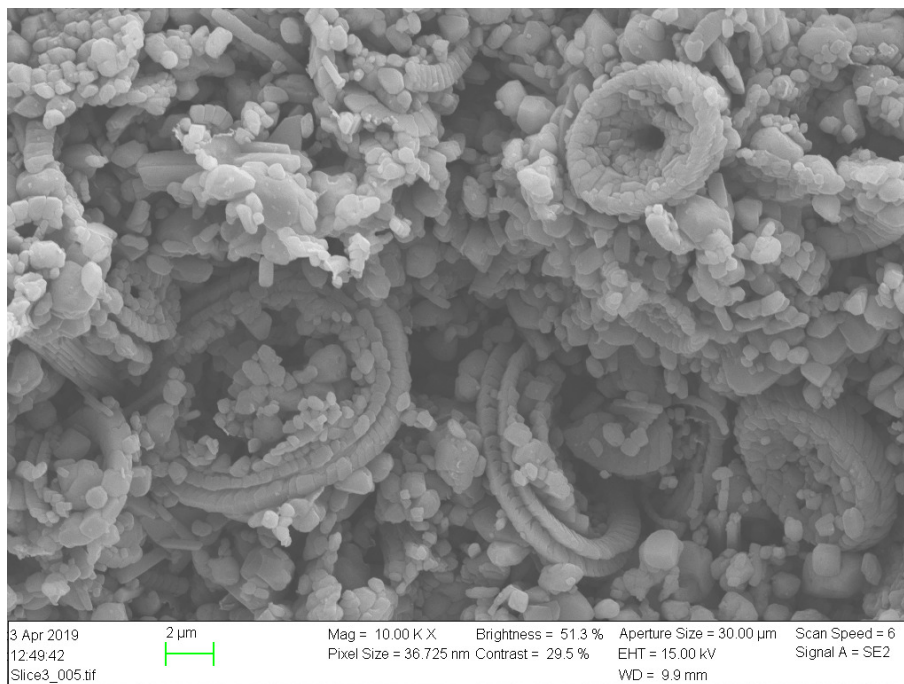


**Figure 5.1:** SEM picture of chalk showing coccolith rings, pore space and ring fragments

Milter (1996) studied the pore size distribution in SK chalk with mercury injection, and his results are presented in Figure 5.2a. The figure indicates that the pore size varies from 100 nm as the smallest ones to 1000 nm as the largest ones. Main pore diameter is around 500 nm. This indicates that SK chalk has a heterogeneous pore size distribution (Milter, 1996). The pore size distribution in SK chalk can be compared to the reservoir chalk in Valhall field, shown in Figure 5.2b. Valhall chalk also have heterogeneous pore size distribution (Webb et al., 2005).

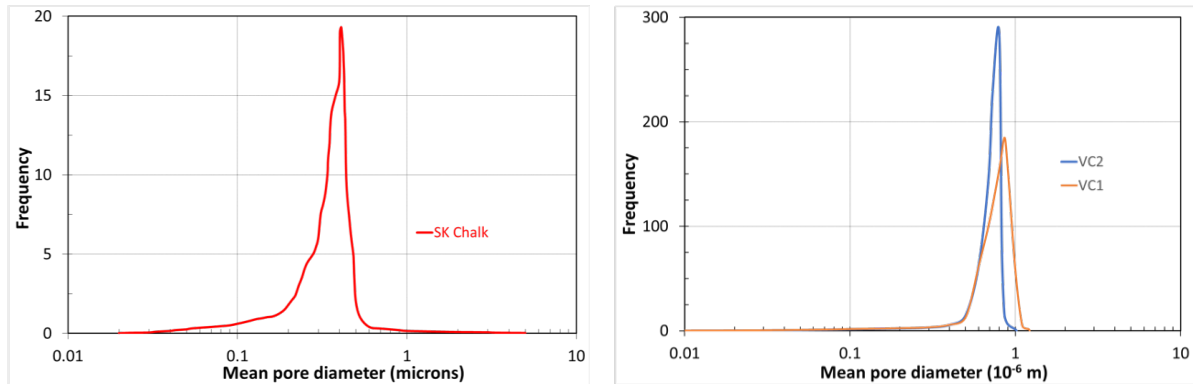


**Figure 5.2:** Pore size distribution for (a) Stevns Klint chalk by mercury injection. Redrawn after J. Milner (1996). And (b) Valhall reservoir chalk. Redrawn after Webb et al. (2005)

## 5.2 Smart water EOR process in carbonate rocks

In carbonate reservoirs, due to unfavorable wetting properties and heterogeneous characteristic, it is challenging to use an EOR method. Injection of chemical can be both expensive and not good for the environment. Oil recovery in carbonate rocks are strongly affected by reservoir wettability, dictated by chemical interactions between polar components present in the crude oil, formation water ions and rock surface mineralogy. Often, the initially reservoir wettability in carbonates are not always optimum for recovery by water flooding. Another complexity of waterflooding in carbonates are the large permeability contrast between matrix and high permeability layers and fractures.

As mentioned before, the idea of smart water is to modify the wetting conditions by injection a fluid with different composition compared to the initial formation water. In Ekofisk field, as an example, seawater as smart water for carbonates has been injected with great success. The goal by using smart water is to disturb the established equilibrium of the CBR-system and a new equilibrium is established and alter wettability is altered towards a more water-wet system, increasing capillary forces and promoting spontaneous imbibition (Austad, 2013). This will increase the recovery and it is cheaper and more environmental friendly than other chemicals. Smart water has minor changes in IFT, but alter the wettability and increases the microscopic sweep (Fathi et al., 2010; Fathi et al., 2012). Figure 5.3 shows recovery after spontaneous imbibition with formation water, forced imbibition of formation water and forced imbibition with seawater. Seawater or modified seawater is often used as smart water in carbonates and is more efficient at higher temperatures.

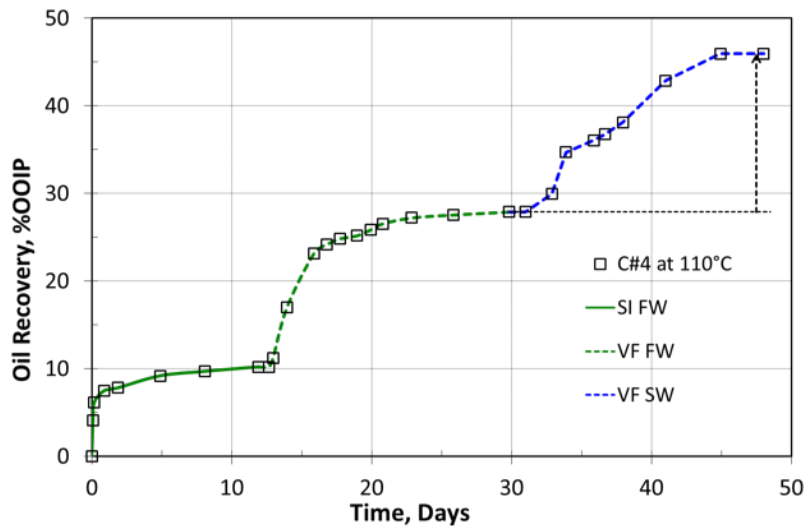


**Figure 5.3:** spontaneous and forced imbibition of formation water (FW) and seawater (SW) into a carbonate core at 110 °C (Smart Water IOR group, 2019)

### 5.3 Wetting in carbonate reservoirs

Wettability of a CBR-system is determined by brine composition, crude oil,  $S_{wi}$  and the aging temperature (Jadhunandan & Morrow, 1995). In carbonate reservoirs the formation water may be of high salinity, usually rich in  $Ca^{2+}$ . Oil recovery from carbonates are usually low due to low permeability, natural fracture, low water wetness and heterogeneous rock properties (Austad, 2013). At reservoir conditions, carbonate surface is positively charged, and the carboxylic ( $-COO^-$ ) acid in crude oil (determined as acid number, AN) is the main wetting component for the CBR-system of a carbonate rock. The AN is in unit mg KOH/g crude oil quantify these polar organic components (POC). Naturally, clean chalk is water-wet, but crude oil may break the water film lying onto the rock. The surface active components of the crude oil can adsorb onto the rock surface proving to a more oil-wet surface (Høghesen et al., 2005). The negatively charged carboxylic group ( $-COO^-$ ) and the positively charged sites on carbonate surface creates a strong bond, and the large molecules will cover the carbonate surface. Reservoir temperature also affects the wettability and chemical composition of crude oil due to decarboxylation processes at high temperature, which decreases the AN of the crude oil (Shimoyama & Johns, 1972). The effect of AN in crude oil on initial wetting of SK chalk is illustrated in Figure 5.4. The figure show spontaneous imbibition of six equally restored SK cores with  $S_{wi} = 0$ . Water wetness and oil recovery increases with increasing reservoir temperature and decreasing AN (Rao, 1999; Standnes & Austad, 2000).

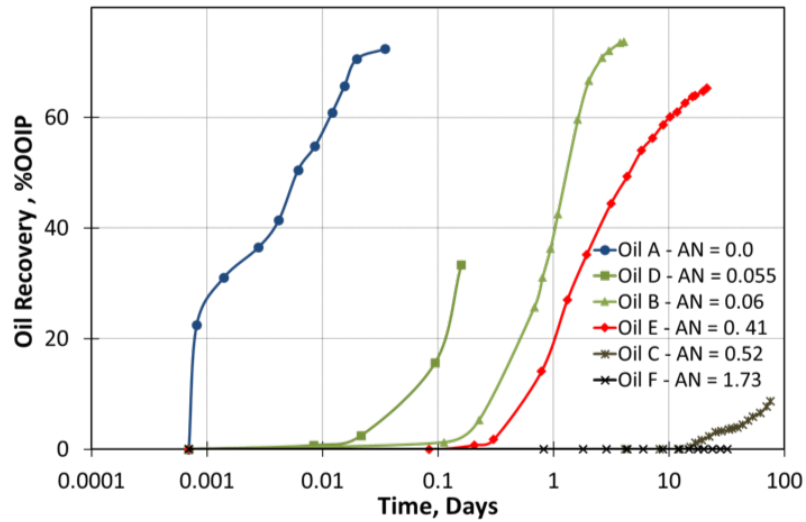
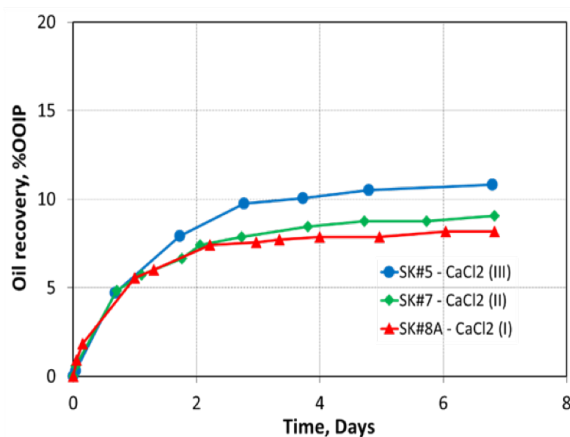


**Figure 5.4:** Spontaneous imbibition into SK chalk cores saturated with different oil (Standnes & Austad, 2000)

The established initial wetting properties of a reservoir are related to the CBR-system, and the wetting can be affected by the composition of the formation water. Sulfate,  $\text{SO}_4^{2-}$ , is the most active ion conserving wetting properties in carbonates. The amount of  $\text{SO}_4^{2-}$  present in the formation water can be usually low due to high concentration of  $\text{Ca}^{2+}$  which precipitate to anhydrite,  $\text{CaSO}_4$ . The presence of sulfate in the formation water will increase the water wetness of the system (Shariatpanahi et al., 2011). In Figure 5.5, the effect of formation water on initial wetting in chalk is demonstrated. With increasing of  $\text{Ca}^{2+}$  concentration at constant salinity, the water wetness of the core will decrease and adsorption of acidic components will increase. Increasing concentration of  $\text{Ca}^{2+}$  results in lower oil recovery.



Ions	CaCl <sub>2</sub> (I) mM	CaCl <sub>2</sub> (II) mM	CaCl <sub>2</sub> (III) mM
Mg <sup>2+</sup>	0	0	0
Ca <sup>2+</sup>	566	283	46
Na <sup>+</sup>	0	538	987
TDS, g/l	62.83	62.83	62.83
IS, mole/l	1.698	1.387	1.126

**Figure 5.5:** Oil recovery vs time for three different formation waters at ambient temperature (Smart Water IOR group, 2019).

In Figure 5.6 the effect of  $\text{Ca}^{2+}$  concentration and salinity of formation water is illustrated. Both formation water composition and salinity influences the adsorption of negatively charged carboxylic group ( $-\text{COO}^-$ ) of the crude oil. With increasing double layer of  $\text{Ca}^{2+}$  concentration on the rock, the adsorption of crude oil will increase. The highest adsorption, though, happens when using DI-water as formation water, where there are no salts ions are presence in the formation water. The lack of ionic double layer on chalk surface makes it easier for the carboxylic anchor molecules to break the water film (Shariatpanahi et al., 2016).

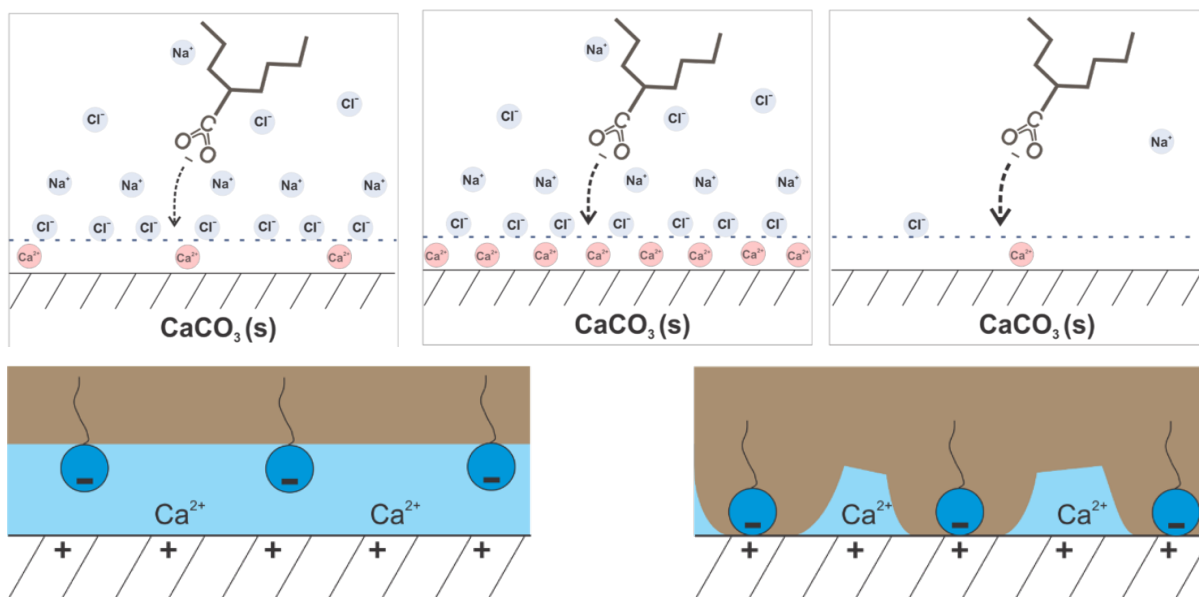


**Figure 5.6:** Chemical model describing initial wetting in Carbonates (Smart Water IOR group, 2019).

Toward the chalk surface there are three reactive ions in the seawater, and these act as potential determining ions since they can change the surface charge of  $\text{CaCO}_3$ . The ions are  $\text{Ca}^{2+}$ ,  $\text{Mg}^{2+}$  and  $\text{SO}_4^{2-}$ . Zeta potential in a colloid system, measures the difference in the electrical charge between the dense layer of ions surrounding the particle and the charge of the bulk of the suspended fluid surrounding the particles (Strand et al., 2006). In SK chalk particles both  $\text{Ca}^{2+}$  and  $\text{SO}_4^{2-}$  are able to modify the surface charge when NaCl suspension is added (Pierre et al., 1990). The zeta potential measurements, done by Strand et al. (2006), were performed on a suspension with 4 wt% of milled chalk in NaCl brine containing different ratios of  $\text{Ca}^{2+}$  and  $\text{SO}_4^{2-}$ . The zeta potential is plotted in Figure 5.7 as a function of the concentration difference  $[\text{Ca}^{2+}] - [\text{SO}_4^{2-}]$ . Strand et al. (2006) concluded with that  $\text{Ca}^{2+}$  and  $\text{SO}_4^{2-}$  play an important role in the wettability alternating process, and adsorption of  $\text{SO}_4^{2-}$  onto chalk surface desorbs negatively charged carboxylic material by changing the surface charge of chalk. Adsorption of

$\text{Ca}^{2+}$  increases the concentration of  $\text{Ca}^{2+}$  close to chalk surface, and will contribute to release the carboxylic group. High concentration of  $\text{Ca}^{2+}$  has a positive surface charge, while high concentration of  $\text{SO}_4^{2-}$  has a negative surface charge.  $\text{Mg}^{2+}$  ions do not interact with surface at low temperatures.

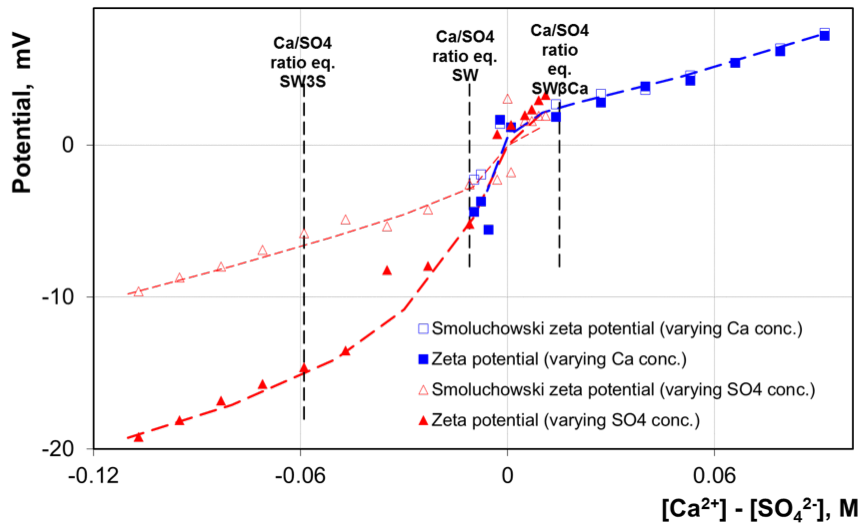


**Figure 5.7:** Zeta potential measurements on 4 wt% chalk suspension in NaCl-brine with  $[\text{Ca}^{2+}] = 0.013 \text{ mol/l}$  and varying sulfate concentration, or in NaCl-brine with  $[\text{SO}_4^{2-}] = 0.012 \text{ mol/l}$  and varying calcium concentration (Stand et al., 2006).

The effect on oil recovery for these ions are different and the effect of  $\text{SO}_4^{2-}$  in the seawater at 100 °C are that oil recovery increase with the concentration of sulfate (while keeping concentration of the other ones). The same effect is seen for  $\text{Ca}^{2+}$  when sulfate concentration is remained constant. As mentioned earlier,  $\text{Mg}^{2+}$  at low temperatures does not interact with the surface, but at higher temperature  $\text{Mg}^{2+}$  in seawater can displace  $\text{Ca}^{2+}$  from the rock, formatting  $\text{MgCO}_3$ .  $\text{Mg}^{2+}$  has a strong hydration energy, and this makes the ion less reactive at low temperature (Austad, 2013). The process is shown in the following equilibrium and Figure 5.8:



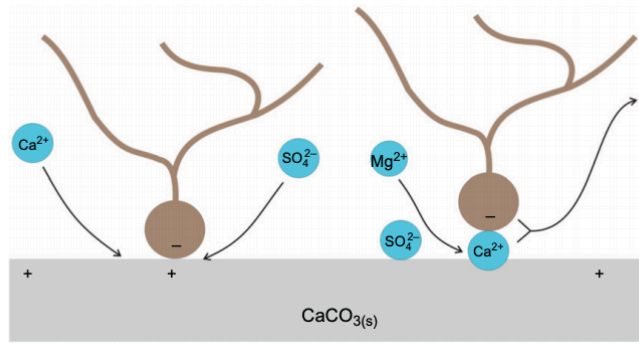


**Figure 5.8:** Illustration of the suggested chemical mechanism for wettability of carbonate by SW (Zhang et al., 2007)

$Mg^{2+}$  also bonds with the negatively charged acidic component, but this bonding is more weak than  $-COO^- - Ca^{2+}$  bond. The wettability of a rock is controlled by the polar organic components in the crude oil, and the negatively charged acidic components ( $-COO^-$ ) are strongly attached to the surface of the rock. To release the anchor component from the rock, chemicals like  $SO_4^{2-}$  and  $Ca^{2+}$  are need.  $SO_4^{2-}$  which will react with the double layer surface of  $Ca^{2+}$  and  $Ca^{2+}$  which will interact with the acidic component in the crude oil and release it from the surface, as demonstrated in Figure 5.9. It is also demonstrated in the figure that wettability alteration efficiency increases with reduced salinity.

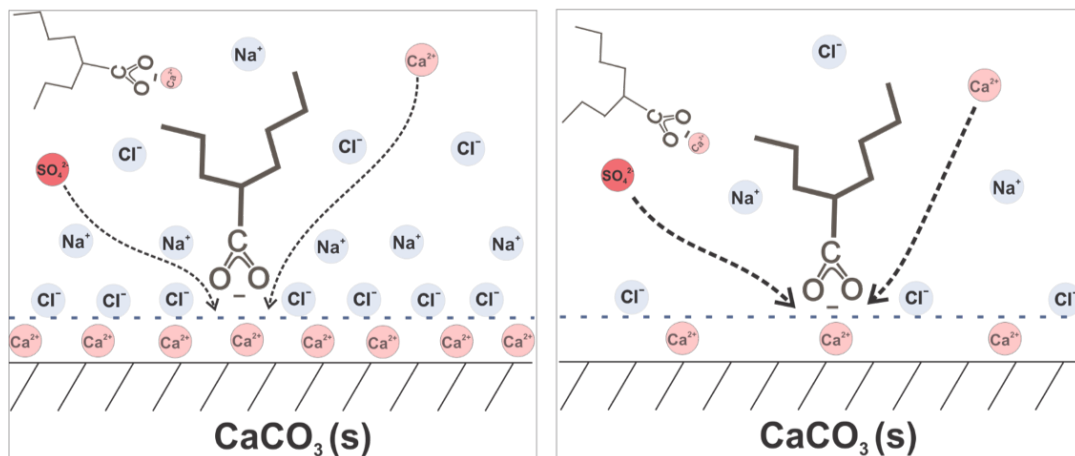


**Figure 5.9:** Chemical wettability alteration model for carbonates (Smart Water IOR group, 2019).

## 6 SENDRA Simulator

SENDRA is a coreflood simulator with a fully implicit two-phase core flow simulator designed to simulate and verify SCAL experiments. It can be used for both imbibition and drainage processes, for oil-water, gas-oil or gas-water experiments. It also covers experimental approaches like unsteady-state, steady-state and centrifuge experiments. SENDRA simulator history matches the recovery and pressure drop data, and creates relative permeability curves using Corey correlations and capillary pressure curves using Skjæveland correlations based on recovery and pressure drop input data (Lenormand et al., 2017). In this chapter the correlations are described in more detail.

During a smart water injection, the reservoir will merge a wettability alteration from oil-wet/mixed-wet/slightly water-wet conditions towards more strongly water-wet conditions. Reservoir simulations require relative permeability data to predict fluid flow in the reservoir. In SENDRA, two sets of relative permeability data is needed, one for the initial wettability and one for the final wetting established at the end of smart water injection.

### 6.1 Laboratory measurements of relative permeability and fluid saturations

Relative permeability is the permeability measured at a specific fluid saturation expressed as a fraction of the absolute permeability. There are many methods for measuring permeabilities at various saturations to obtain relative permeabilities. Two methods are unsteady-state and steady-state method and illustrated in Figure 6.1.

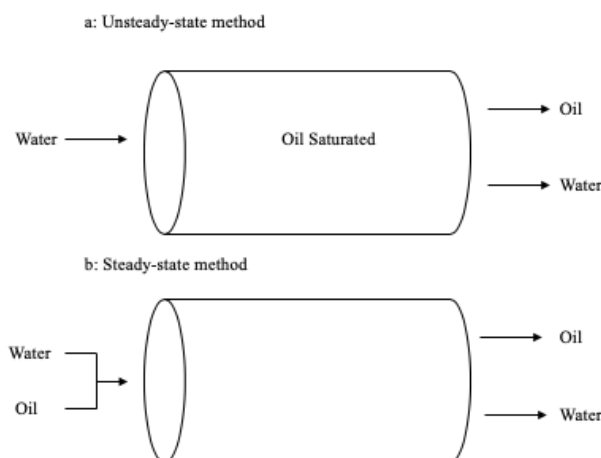


**Figure 6.1:** Illustration of unsteady-state and steady state methods of measuring two-phase oil and water relative permeability.



The most accurate method is the steady-state method, but this method is time consuming and expensive. Both oil and water are injected into the core simultaneously until output rates are equal to input rates, and Darcy's law is applicable to calculate the effective permeability for each phase. Unsteady-state method is less accurate, but is faster and cheaper. The core is already saturated with oil, and only water is injected to the core. These two methods gives different relationship between relative permeability and saturation. Another method are even faster and cheaper, involving measuring the effective permeabilities at  $S_{wi}$  and  $S_{or}$  (Lucia, 1999). It measured the end point relative permeabilities, and the relative permeability curves can be estimated using Corey correlations, which is described in the next section 6.2.

During an unsteady state flow, Darcy's law is not applicable, but the Johnson-Bossler-Naumann (JBN) method can be used. The JBN method is a function of saturation and fluid distribution, and requires pressure drop data, at initial conditions and during the injection, and volume of produced water and oil. These experimental data can calculate the value of  $S_w$ ,  $k_{ro}$  and  $k_{rw}$  and also the ratio between  $k_{ro}$  and  $k_{rw}$  (Johnson et al., 1959).

As mentioned, relative permeability measurements depends greatly on determination of fluid saturation and there are mainly two methods to determine fluid saturation in a core: external and internal techniques. External techniques are either material balance or gravimetric method. The material balance deduce saturation from fluid production (fluid in – fluid out = fluid retained in core), which is an average values for the core. The gravimetric method, is the difference between the weight of the saturated core compared with the weight of the dry core, and the saturation is estimated from the difference in weights. Internal techniques measures directly the quantity of fluids in the core. The best method is the internal method, which measure different saturation levels along the length of the core, rather than the average value of the core (Apostolos et al., 2016).

## 6.2 Relative permeability curves with Corey correlations

Corey correlations (Brooks & Corey, 1964) are used for relative permeability curves based on history matching, and Equations 6.1 and 6.2 shows correlations for calculate relative permeability to water and oil:

$$k_{rw} = k_{rw}^0 (S_w^*)^{N_w} \quad (6.1)$$

$$k_{ro} = k_{ro}^0 (1 - S_w^*)^{N_o} \quad (6.2)$$

Where:

- $k_{rw}^0$  Relative permeability of water at residual oil saturation ( $S_{or}$ )
- $k_{ro}^0$  Relative permeability of oil at initial water saturation ( $S_{wi}$ )
- $S_w^*$  Normalized water saturation
- $N_w$  Corey parameter for water
- $N_o$  Corey parameter for oil

The shape of water and oil relative permeability curves is attained by parameters  $N_w$  and  $N_o$ . SENDRA simulator constructs these relative permeability curves by changing  $N_w$  and  $N_o$ , keeping end point saturations,  $S_{wi}$  and  $S_{or}$ , constant. The normalized water saturation can be calculated as:

$$S_w^* = \frac{S_w - S_{wi}}{1 - S_w - S_{or}} \quad (6.3)$$

Where:

- $S_w^*$  Normalized water saturation
- $S_{wi}$  Irreducible water saturation
- $S_{or}$  Residual oil saturation

### 6.3 Two-phase capillary pressure curves with Skjæveland correlations

Skjæveland correlations (Skjæveland et al., 2000) are used for capillary pressure curves based on history matching. Four capillary pressure curves for a mixed-wet reservoir that comprises both drainage and imbibition as can be seen in Figure 6.2.

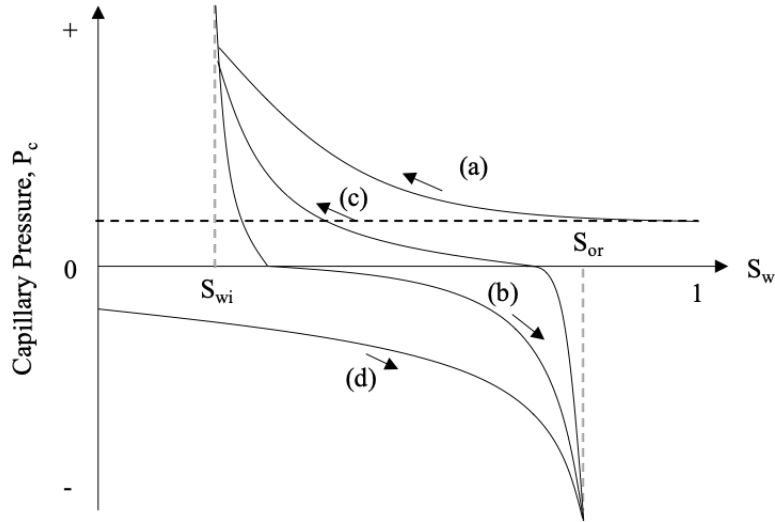


**Figure 6.2:** Schematic of bounding curves, capillary pressure,  $P_c$ , as a function of water saturation,  $S_w$ : (a) primary drainage to establish  $S_{wi}$ , (b) Spontaneous imbibition at positive  $P_c$  and forced imbibition at negative  $P_c$ , (c) secondary drainage and (d) primary imbibition. Redrawn from Skjæveland et. al (2000).

The general expression is:

$$P_c = \frac{c_w}{\left(\frac{S_w - S_{wi}}{1 - S_{wi}}\right)^{a_w}} + \frac{c_o}{\left(\frac{1 - S_w - S_{or}}{1 - S_{or}}\right)^{a_o}} \quad (6.4)$$

Where:

- $P_c$  Capillary pressure
- $S_w$  Water saturation
- $S_{wi}$  Initial water saturation
- $S_{or}$  Residual oil saturation

$a_w$ ,  $a_o$ ,  $c_w$ ,  $c_o$  are four Skjæveland constants.  $a_w$ ,  $a_o$  and  $c_w$  are positive numbers and  $c_o$  are negative number.

## 7 Experimental work

In this thesis work the effect of core wettability on relative permeability and waterflooding in chalk material is studied. In this chapter, the materials and the methodology used in the experiments investigating the influence of wettability in relative permeability, fluid distribution and mobilization will be described.

### 7.1 Materials

In following sections materials and fluids used in the experiments will be presented.

#### 7.1.1 Core materials

Outcrop chalk material from Stevns Klint (SK), Copenhagen, Denmark, was used as the porous media in this study. SK chalk is highly porous (45-50%) and low in permeability (2-5 mD) (Punternold et al., 2007). The material is similar to some North Sea chalk oil reservoirs (Frykman, 2001); homogeneous and composed mainly of fine-grained, coccolithic matrix, i.e. the skeleton from planktonic algae called coccolithophorids. A single chalk grain has a general size of 1  $\mu\text{m}$  and has a specific surface area of about 2  $\text{m}^2/\text{g}$ . The cores were drilled in the same direction and from the same block of outcrop chalk, by an oversized bit following the procedure set by Punternold et al. (2007). Before further using of the cores, they were dried, shaved and cut into properly dimensioned cores, with approximately a diameter of 3.8 cm and a length of 7 cm.

All tests in this experimental study were performed using two chalk cores with almost identical properties: core C2 and C5. Core C2 was tested first and core C5 was to validate and strengthen the results. Included, two reference cores (CR1 and CR2) were also prepared and tested for comparison of wettability. Cores CR1 and CR2 were strongly water-wet, while C2 and C5 had a fractionally wetted system. Properties of the cores are utilized in this experiment are presented in Table 3.

**Table 3:** Core properties

Core	CR1	CR2	C2	C5
<b>Dry weight [g]</b>	109.10	107.68	107.15	105.36
<b>Length [cm]</b>	7.06	7.07	7.12	7.03
<b>Diameter [cm]</b>	3.78	3.79	3.79	3.79
<b>Pore volume [ml]</b>	37.53	39.17	39.80	39.90
<b>Porosity [%]</b>	47	49	50	50
<b>S<sub>wi</sub> [%]</b>	20	20	20	20
<b>Permeability [mD]</b>	4.02	4.09	4.16	4.30

Determination of pore volume is based on the dry weight of the core, the fully saturated weight of the core and the density of DI-water. Equation 7.1 illustrates how to calculate pore volume:

$$PV = \frac{m_{dry} - m_{sat}}{\rho_w} \quad (7.1)$$

Where:

- $PV$  Pore volume [ml]
- $m_{dry}$  Saturated weight of core [g]
- $m_{sat}$  Dry weight of core [g]
- $\rho_w$  Density of water, 0.998 [g/cm<sup>3</sup>] or [g/ml]

Both pore volume and bulk volume are needed to measure core porosity. Bulk volume of the core can be determined by measuring the dimensions (length and diameter), and PV is measured by using Equation 7.1. Finally the porosity of different cores were determined by Equation 7.2:

$$\phi = \frac{PV}{L \cdot \pi \cdot \frac{d^2}{4}} = \frac{PV}{V_b} \quad (7.2)$$

Where:

- $\phi$  Porosity
- $L$  Length of the core [cm]
- $d$  Diameter of the core [cm]
- $V_b$  Bulk volume [cm<sup>3</sup>] or [ml]

Absolute permeability is determined in section 7.3.1.1 and Equation 7.4.

### **7.1.2 Oils**

The model oils were centrifuged for an hour at high rotation speed, and then filtrated with a 5  $\mu\text{m}$  Millipore filter, to separate particles from the oil. Oil properties are given in Table 4. The mineral oil were prepared with Marcol 85 which was diluted with heptane in the ratio of 42/58 heptane/marcol by volume. Oil A, B and C was prepared to have three different acid numbers, and oil B is the model oil used in this experiment with an AN = 0.34. AN affects the wettability of the rock, and higher AN makes the core surface more oil-wet (Fan & Buckley, 2007).

#### **Heidrun**

Heidrun crude oil with AN=2.80 and BN=0.74 mgKOH/g was used as a reference crude oil. This oil was sampled from a real well during a well test.

#### **RES40**

The RES40 was prepared by diluting Heidrun oil with n-heptane with a ratio of 60/40 by weight%. After stirring the mixture with a magnetic stirrer for one week, the mixture was centrifuged and filtrated. The AN and BN was measured to be AN=2.40 and BN=0.84 mgKOH/g. Dilution with heptane was preformed to reduce oil viscosity and required pressure to displace the oil.

#### **RES40-0**

This oil was prepared by adding 20 vol% of silica gel to the RES40 oil in two steps, and left for stirring for a week each time. In total 40 vol% of silica gel was added. The silica gel was added to remove surface-active components in the oil, mostly the carboxylic acid groups but also the basic material. After adding all of the silica gel, and the mixture was stirred for a week, the mixture was centrifuged to separate oil from the silica gel. Silica gel was settled at the bottom of the centrifuge bottle, and the oil on the top was filtrated. The acid and base number were measured to be AN=0.06 and BN=0.1 mgKOH/g.

#### **Oil B**

Oil B was prepared by mixing 100 ml of RES40 and 900 ml of RES40-0, to get an oil with an acid number of 0.35 mgKOH/g. The right amount of RES40-oils were calculated by 100ml of

RES40\*AN of RES40 + 900 ml of RES40-0\*0.06. The acid and base number for oil B was measured to be AN=0.34 and BN=0.26 mgKOH/g.

### Mineral oil (M-OIL)

The mineral oil does not contain any polar components that could influence the core wettability during flooding. It is made of 58vol% of Marcol 85 and 42vol% of n-heptane and is based on the viscosity of the other oils. The goal was to find the best ratio of Marcol and n-heptane that matched the viscosity of the model oils. The final result was when 58vol% of Marcol and 42vol% of n-heptane to get viscosity of 2.7 mPas.

**Table 4:** Oil properties

Oil types	Heidrun	RES 40	RES 40-0	OIL B	Marcol 85	n-heptane	M-OIL
Viscosity [mPas]	-	2.7	2.4	3.5	28.3	0.4*	2.7
Density [g/cm <sup>3</sup> ]	-	0.820	0.809	0.814	0.847	0.684	0.783
IFT [mN/m]	-	14	27	23	45	34	41
AN [mgKOH/g]	1.93	2.40	0.06	0.34	-	-	-
BN [mgKOH/g]	0.18	0.84	0.01	0.26	-	-	-

\* Theoretical value

### 7.1.3 Brines

Brines used in this study were synthetically prepared in the laboratory by dissolving the correct needed amount of salts in deionized (DI) water. All chemicals used to prepare brines were delivered by Merck laboratories. Brines containing chloride, sulfate and carbonate were first dissolved separately in DI water to avoid precipitation during the mixing process. Then, all solutions were mixed to one solution and diluted to 1 liter in a volumetric flask. The solution was left for stirring on a magnetic stirrer for approximately 4 hours, to ensure full dissolution. All brines were filtrated through a 0.22 µm Millipore filter, using VWR vacuum gas pump to remove particles and dissolved gas. Table 5 shows the composition of the various brines. A brief explanation of the different brines used in this experiment is shown below:

**SW:** Synthetic seawater. The brine was used as a reference for the chromatographic wettability test and contain  $SO_4^{2-}$ , but not  $SCN^-$ .

**SW0T:** Synthetic seawater for first part of the chromatographic wettability test. The brine does not contain  $SO_4^{2-}$  and  $SCN^-$ .

**SW1/2T:** Synthetic seawater for chromatographic wettability test. The brine has equal amounts of  $\text{SO}_4^{2-}$  and  $\text{SCN}^-$ , and is used in the secondary seawater flooding after reaching  $S_{\text{or}}$  with SW0T.

**Table 5:** Composition and properties of brines

<b>Brine</b>	<b>SW</b>	<b>SW0T</b>	<b>SW1/2T</b>
Ions	[mmol/l]	[mmol/l]	[mmol/l]
$\text{HCO}_3^-$	2	2	2
$\text{Cl}^-$	525	583	538
$\text{SO}_4^{2-}$	24	0	12
$\text{SCN}^-$	0	0	12
$\text{Mg}^{2+}$	45	45	45
$\text{Ca}^{2+}$	13	13	13
$\text{Na}^+$	450	46	427
$\text{Li}^+$	0	0	12
$\text{K}^+$	10	10	22
$\text{Ba}^{2+}$	0	0	0
$\text{Sr}^{2+}$	0	0	0
<b>Density 20°C [g/cm<sup>3</sup>]</b>	1.024	1.024	1.024
<b>TDS [g/l]</b>	33.39	33.39	33.39

#### 7.1.4 Chemicals

DI water was used as formation water, as the displacing fluid and to clean the core, and the lines in the flooding set ups. The n-heptane was used for dilution of Marcol 85 to obtain the right viscosity of the mineral oil, and also for cleaning the lines in the flooding set-ups and cleaning the cores after flooding.  $\text{N}_2$  was also used to clean the flooding set ups before using vacuum. The chemicals used for AN and BN measurements are presented later in Appendix.

## 7.2 Analyses

A brief description of the analysis performed as part of experiments is presented in the following section.

### 7.2.1 pH measurements

pH measurements were done using the pH meter seven compact™ from Mettler Toledo. The electrode used was semi micro-pH and repeatability of the measurement was  $\pm 0.01$  pH units at room temperature.



### 7.2.2 Density measurements

Densities of brines and oils were measured using DMA-4500 Density Meter from Anton Paar at ambient temperature. First the apparatus was cleaned with white spirit, acetone and DI water. Then, small amount of the sample was injected into the density meter and the density was measured. The measurements were repeated 3 or 4 times to ensure accuracy, and the repeatability was  $\pm 0.001 \text{ g/cm}^3$ .

### 7.2.3 Viscosity measurements

The viscosity of brines and oils were determined using the rotational rheometer Physica MCR 302 from Anton Paar at ambient temperature. Approximately  $800 \mu\text{l}$  of an oil sample was placed on a metal plate, and then the apparatus was set to measure position with the plates close to each other. The viscosity of oils were determined through shear stress and shear rate relation. When determined the viscosities of different RES40 oils, the viscosity of the mineral oil should be the same and it could be determined to get the right ratio of n-heptane/marcol. The shear rates ranged from  $50$  to  $500 \text{ s}^{-1}$  and the repeatability was  $0.01 \text{ mPa}\cdot\text{s}$ .

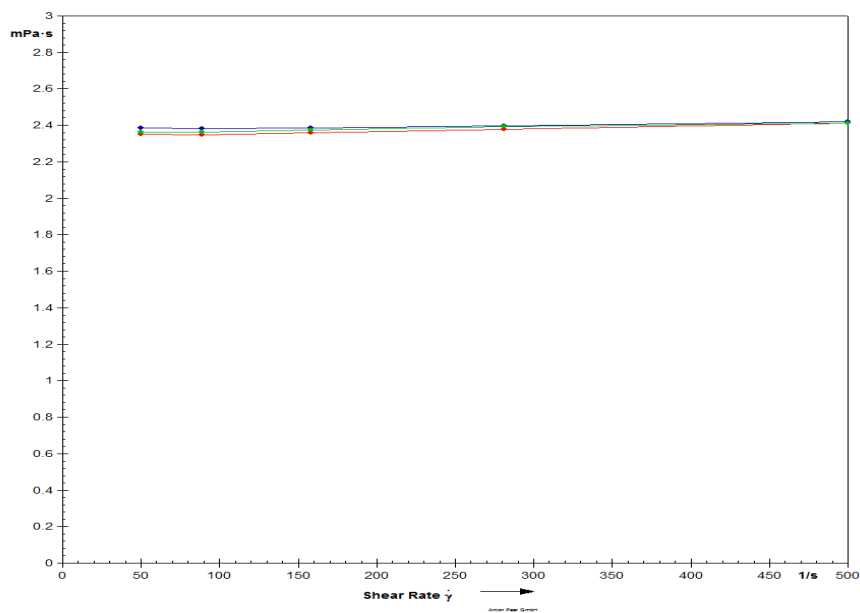


*Figure 7.1:* Illustration of viscosity measurements

### 7.2.4 Interfacial tension measurements

Interfacial tension was measured using Krüss K6 with the DU Noüy ring method. 1.5 cm of DI water was placed in a cup. A ring was lowered into the water to be fully contacted with the water. Then 1 cm of oil were placed on top of the water using a pipette. IFT was measured when the ring went from water to oil, and IFT is the force required to pull the wire ring off the

interface. A lamella was made when ring went from water to oil (Adamson & Gast, 1997). Interfacial tension measures the force of attraction at the interface of two fluids. Fluids with high interfacial tension will not mix and in case of an oil recovery process higher capillary forces are needed. In the case where interfacial tension is lowered, oil recovery increases and less force is needed to extract the oil.

### 7.2.5 Determination of AN and BN

Acid number (AN) and Base number (BN) measurements of oil samples were done with Mettler Toledo T55 auto-titrator by potentiometric titrations, and the methods used were developed by Fan and Buckley (2007). The standards are modified versions of ASTM 2896 and ASTM 664

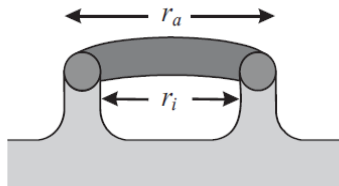


**Figure 7.2:** Du Noüy ring method for IFT measurement (Moradi et al., 2015).

for BN (mg KOH/g) and AN (mg KOH/g). The instrument uses a blank test as a reference during potentiometric titration of oil samples, where measurement of electronic potential is converted to equivalent acid and base number. Each measurement requires titration solvent and spiking solution, the composition of these can be found in Appendix A.1 and A.2. To secure the test repeatability, a Mettler Toledo weight instruments with accuracy down to the fourth decimal was used and the test was repeated to three equal numbers. Reproducibility of the analyses was better than  $\pm 0.02$  mg KOH/g oil added.

### 7.2.6 Ion chromatography

Effluent brine samples were collected during the chromatographic wettability test using a Gilson GX-271 auto-sampler. The effluent brine were diluted 1000 times with DI water using the trilution™ LH system from a Gilson GX-271 liquid handler. The diluted sampler were further filtrated through a  $0.22 \mu\text{m}$  filter and put into small glasses for analysis. Then, DIONEX IC-5000<sup>+</sup> ion chromatograph was used for chemical analysis of anions and cations. The software controlling the chromatograph uses retention time, which is travel time through the columns. When the analysis is finished, it plots a graph of conductivity versus the retention time where the area under each peak the represents an ion corresponds to their relative

concentrations. The ion concentrations of the effluent were calculated based on external standard method.

### **7.2.7 Scanning electron microscopy (SEM), EDAX**

Scanning Electron Microscope (SEM), *Zeiss Gemini Supra 35VP*, was used to collect images of rock surface and analyze the core structure and size distribution. SEM is a very important electron beam technology invention, which creates an image by scanning the surface of the sample. Prior to the scanning, the sample was prepared with *Emitech K550*. This device was used to prevent erosion prior to scanning. The mineral was vacuumed and coated with palladium in argon gas environment. An EDAX detector was used for elementary analyses of the same rock sample.

### **7.2.8 Data analysis with Sendra**

In this project, SENDRA was used to estimate proper relative permeability curves for the water-wet reference cores and fractionally wetted core. Input parameters are listed in Appendix C. History matching was simulated using unsteady-state flow, imbibition for water-oil.

## **7.3 Methods**

In this section different methods utilized in the experiment are explained.

### **7.3.1 Initial core preparation**

All cores were prepared and restored before oil recovery test. Below, core cleaning, restoration and oil flooding is described.

#### **7.3.1.1 Core cleaning**

Cores were initially placed in a Hassler cell (illustrated in Figure 7.3) for cleaning. The cleaning process is done to easily remove soluble salts, like  $\text{SO}_4^{2-}$ , which can affect initially wettability of the core (Punternold et al., 2007). Cores were flooded with 250 ml of DI water at a rate 0.1 ml/min at ambient temperature. The applying confining pressure were 20 bars and during the flooding, effluent from the core was tested for sulfate by a batch test using  $\text{Ba}^{2+}$ . If there was any soluble sulfate in the effluent, it would visually produce precipitation of  $\text{BaSO}_4$ . After cleaning, cores were placed in an oven with temperature 90 °C and dried overnight to a constant weight. The chemical reaction for a batch test is represented in Equation 7.3.

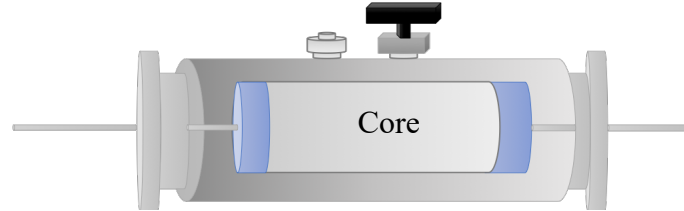


**Figure 7.3:** Hassler cell used in experiments.

Absolute permeability of different cores was also calculated during core cleaning by using Darcy's law, presented in Equation 7.4:

$$k = \frac{q\mu L}{A\Delta P} \quad (7.4)$$

Where

k permeability [ $\text{m}^2$ ]

q flow rate [ $\text{m}^3/\text{s}$ ]

$\mu$  viscosity [Pas]

L length of the core [m]

A cross sectional area [ $\text{m}^2$ ]

$\Delta P$  pressure drop [Pa]

### 7.3.1.2 Core restoration

The initial water saturation was established using the desiccator technique described by Springers et al. (Springer et al., 2003). After the core was dried in the heating chamber, it was placed in a desiccator, illustrated in Figure 7.4. The core was saturated under vacuum with the formation water (DI water). After fully saturating the core, it was placed into a desiccator containing silica gel, which is used as an adsorbent, to vaporize water molecules. Once the desired weight of the core was reached ( $S_{wi} = 20\%$  of DI-water), the core was stored in a sealed container and equilibrated for 72 hours to reach an even ion distribution.

Calculation of desired weight with 20 % initial water saturation was done by using Equation 7.5:

$$m_{S_{wi}=20\%} = m_{dry} + PV * S_{wi} * \rho_w \quad (7.5)$$

Where:

$m_{S_{wi}=20\%}$	Desired weight [g]
$m_{dry}$	Dry weight [g]
$PV$	Pore volume [ml]
$S_{wi}$	Initial water saturation, 20 [%]
$\rho_w$	Density of DI-water, 0.998 [g/cm <sup>3</sup> ]

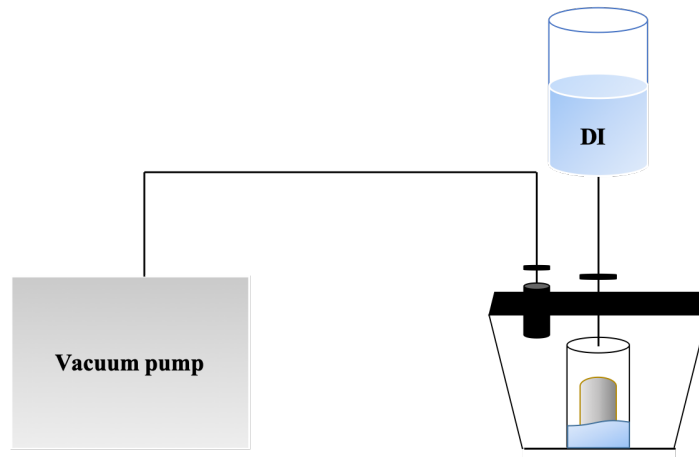


**Figure 7.4:** Illustration of vacuum pump set-up for water saturation of core

### 7.3.1.3 Crude oil saturation

The cores were first saturated with crude oil in a set-up illustrated in Figure 7.5, then chalk cores were placed in a protective rubber sleeve and mounted into a Hassler core holder inside a chamber, illustrated in Figure 7.3. Before oil flooding, the system was vacuumed to remove air from the system. During oil flooding confining pressure was set to 20 bars, while backpressure was set to 10 bars. The cores were flooded 2 PV of crude oil, at a constant rate 2PV/day, in each direction, in total 5 PV of crude oil was flooded, including the 1 PV oil saturation in the vacuum pump set-up. Following the crude oil flooding, the cores were aged for 72 hours before flooding the mineral oil. According to Hopkins (2017), aging is not necessary because the acidic crude oil components adsorb onto the chalk core surface

immediately upon contact (Hopkins, 2016). The water-wet reference cores were only saturated with M-OIL (described in next section), which does not contain any polar element that could affect the core wettability.

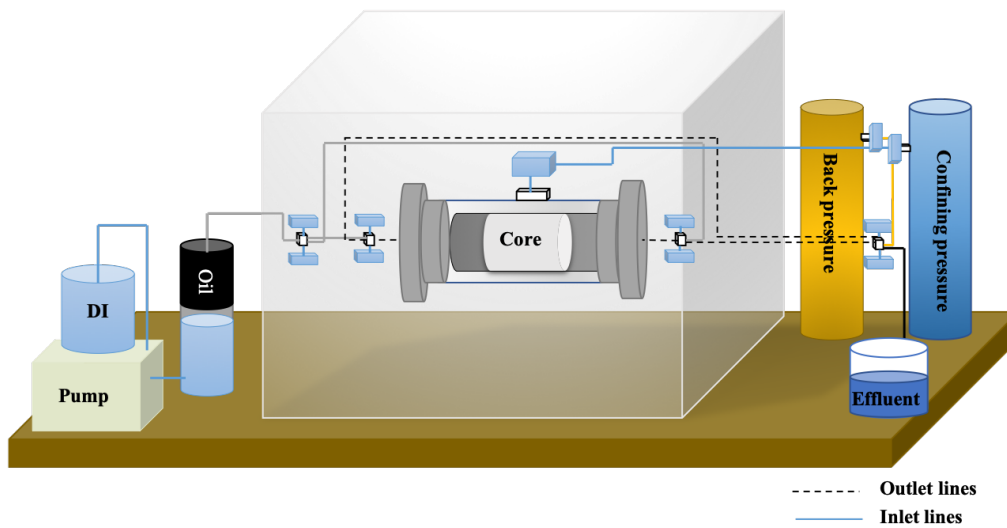


**Figure 7.5:** Illustration of oil flooding set-up

#### 7.3.1.4 Mineral oil flooding

After aging, the mineral oil with n-heptane/marcol for 5 PV, four with 2 PV/day and one with 1 PV/day to get the appropriate pressure drop for oil flooding. Pressure drop was recorded and effective permeability of oil was calculated using Darcy's equation, Equation 7.4. The mineral oil is introduced because all cores at different wetting should have the same oil present. This will reduce the effect of crude oil on wettability, since all crude oils have different wetting properties.

Effluent samples of produced oil were collected, to see the color difference (Figure 7.6). The effluent after 5 PV should almost not be polluted with crude oil minerals. But not all of the crude oil should be displaced, since the polar components in the crude oil dictates which wetting state the core has.

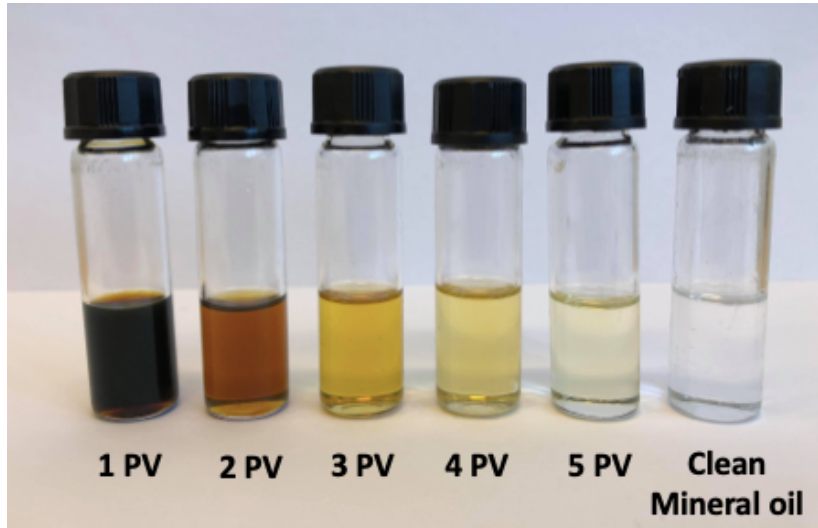


**Figure 7.6:** Effluent samples of produced oil during mineral oil flooding

### 7.3.2 Oil recovery

After oil flooding process, cores were ready for oil recovery. In this experiment both spontaneous imbibition and forced imbibition was used. It is important to notice that core C2 had forced imbibition first, and was restored again before spontaneous imbibition process. Core C5 was only restored in the beginning and followed by spontaneous imbibition and forced imbibition. In the following subsections, oil recovery by spontaneous and forced imbibition are described.

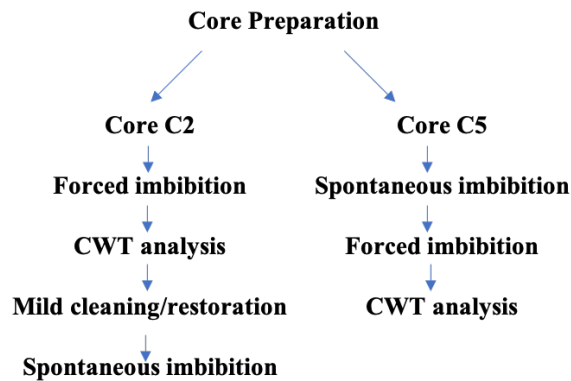


**Figure 7.7:** Schematic of experimental stages for cores C2 and C5

#### 7.3.2.1 Spontaneous imbibition

Cores were immersed in formation water (DI-water) inside an Amott imbibition glass cell at ambient temperature. A schematic of spontaneous imbibition procedure can be seen in Figure 7.8 below. During the imbibition of DI-water, oil was produced. The produced oil in ml was

collected at the top of the imbibition cell. The cumulative oil recovery was recorded as percentage of OOIP (original oil in place) versus time, until a plateau was reached. The %OOIP was calculated by the Equation 7.6:

$$\%OOIP = \frac{\text{Produced oil}}{\text{Original Oil in Place}} * 100 = \frac{\text{Produced oil}}{S_{oi} * V_p} \quad (7.6)$$

Where:

%OOIP Oil recovery percentage of OOIP

$S_{oi}$  Initial oil saturation

$V_p$  Pore volume in the core

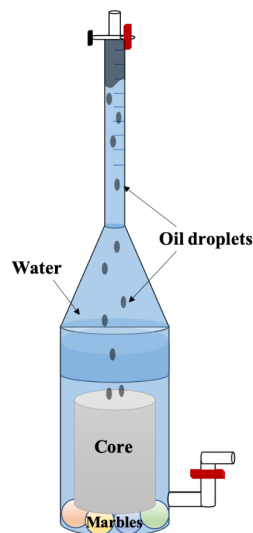


**Figure 7.8:** Schematic of spontaneous imbibition procedure

### 7.3.2.2 Forced imbibition

Cores were placed into a rubber sleeve and mounted into a Hassler core holder. The overburden pressure were set to 20 bars and the back pressure to 10 bars. The formation brine (DI water) was flooded through cores at the rate 1 PV/day at ambient temperature. Viscous flooding are a similar experiment as spontaneous imbibition. The difference is that the water is now pushed through cores by a piston cell, forcing displacement of oil. Produced oil was collected in a burette and oil recovery (% of OOIP) was reported versus pore volume. When the production and pressure drop had reached a plateau, the flow rate was increased to 4 PV/day to force out any oil left. The injection rates for each core are presented in Table 6.



**Table 6:** Pore volumes of cores and injection rates during forced imbibition

Core	CR1	CR2	C2	C5
PV [ml]	37.53	39.17	39.80	39.90
1 PV/day [ml/min]	0.026	0.027	0.028	0.028
4 PV/day [ml/min]	0.104	0.108	0.112	0.112

### 7.3.3 Mild core cleaning

Cores were restored during a mild cleaning, and then cores were for imbibition processes again. Mild cleaning procedure involves flooding the cores with DI-water, followed by heptane. The mild cleaning aims to preserves the surface-active material on the core surface rather to remove it (Hopkins, 2016). Heptane has low or reduced solubility of large oil component, and the aim is to displace residual oil without removal of polar organic components (POC) adsorbed to the rock surface dictating rock wettability. Cores were cleaned with 200 ml of DI water and 250 ml of n-heptane at a rate of 0.1 ml/min. The water and heptane were removed by evaporation in a standard heating chamber at 90 °C until constant weight. After drying the core, new core restauration with  $S_{wi}$  and saturated with mineral oil.

### 7.3.4 Chromatographic wettability test

Chromatographic wettability test was performed after the forced imbibition (Figure 7.9), and this test determines the water-wet area inside the carbonate core. This is based on the measured separation of a non-adsorbing tracer and sulfate, as described in section 4.5.5. Cores were first flooded with SW0T, with neither tracer nor sulfate at 0.2 ml/min for 1 day to get any oil left in the core out of the system. Finally, cores were flooded with SW1/2T, a seawater containing equal amount of both tracer and sulfate a seawater containing the equal amount of tracer and sulfate. The effluent was collected by an auto-sampler from Gilson, and concentration of cations and anions were determined by ion chromatography analysis. The results were compared to strongly water-wet cores as an indication of core wetting state. Separation area between the thiocyanate and sulfate curves were calculated for all the cores by using trapezoidal method. The WI was also calculated using Equation 5.1 in section 4.3.5.

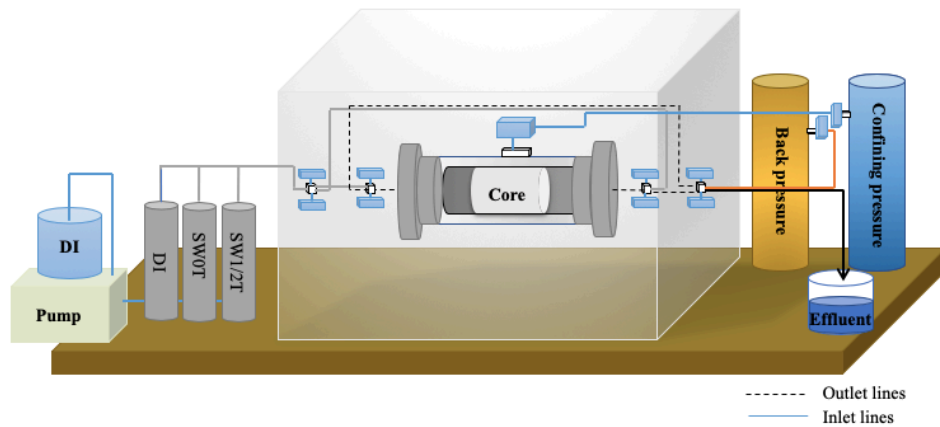


**Figure 7.9:** Illustration of the flooding set-up for chromatographic wettability test

### 7.3.5 Determining relative permeability

Pressure drop data were collected when the pressure drop over the core was stable. This stable pressure drop can calculate the absolute permeability of the core and effective permeability during oil and waterflooding. The absolute permeability was calculated during core cleaning, where only DI-water flow through the core. Pressure drop was collected at different rates, and absolute permeability were calculated using equation 7.4. During M-OIL flooding pressure drop data were collected at 1 PV/day. When the pressure drop was stable, the effective permeability of oil at  $S_{wi}$  could be calculated using equation 7.4. The stable pressure drop during water flooding, assuming no more production of oil, can calculate the effective permeability of water at  $S_{or}$ . The rate was 1 PV/day, and effective permeability of water can be calculated using equation 7.4.

The end point relative permeability were calculated by effective permeability as a fraction of absolute permeability (see Equation 4.9). End point relative permeabilities were calculated for using in SENDRA simulator. It was only calculated for CR1, CR2, C1, C2 and C3, since other cores were not history matched. In Table 7 the constant pressure drop data ( $\Delta P$ ), residual oil saturation ( $S_{or}$ ) absolute permeability ( $k$ ), effective permeability ( $k_e$ ) and relative permeability ( $k_r$ ) of each core is listed. Rate of each core is listed in Table 6.  $S_{wi}$  for all cores, as mentioned before, were 0.2.  $S_{or}$  after rate 1 PV/day are calculated by using Equation 7.7.

$$S_{or} = \frac{(1-S_{wi})PV-PO}{PV} \quad (7.7)$$

Where:

$S_{wi}$  Irreducible water saturation

$PV$  Pore volume [ml]

$PO$  Produced oil [ml]

**Table 7:** End point relative permeabilities with important factors to calculate them.

<b>Core</b>	<b>CR1</b>	<b>CR2</b>	<b>C1</b>
$\Delta P_{oil}$ [mbar]	231	228	293
$\Delta P_{water}$ [mbar]	659	828	679
$k$ [mD]	4.02	4.09	4.12
$k_{eo}$ [mD]	3.22	3.37	2.58
$k_{ew}$ [mD]	0.36	0.29	0.35
$k_{ro}$	0.80	0.82	0.62
$k_{rw}$	0.09	0.07	0.09
$S_{or}$	0.25	0.23	0.22

## 8 Results and discussion

Experimental and simulator results are described and discussed in this chapter.

### 8.1 Chalk core characterization

SEM images of small rock samples from the uncleaned SK chalk cores were collected to get a closer look at the pore size distribution. An unflooded core is presented in Figure 8.1, and the picture is magnified 5000 times. One can clearly see some ring structures from the intact coccolithic rings with average particle size of approximately 2-4  $\mu\text{m}$ . Mostly there are fragmented grains with an average particle size of 1  $\mu\text{m}$ . The darker areas between the grains represent the pore system in the core. The structure is commonly main heterogeneous.

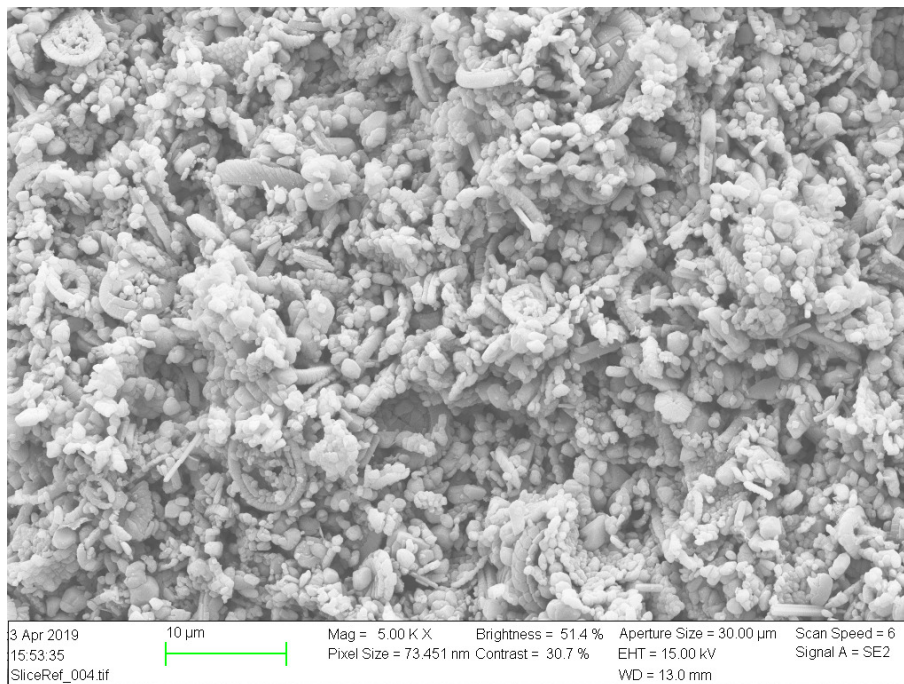


**Figure 8.1:** Scanning electron microscopy (SEM) picture of the outcrop SK chalk core, magnified 5000x.

#### 8.1.1 Energy dispersive x-ray spectroscopy (EDS)

Energy dispersive x-ray spectroscopy (EDS) analyzed the composition of the core. In Table 8, an values of atomic weight (At%) is presented. Calcium, Ca, shows a high value of 98.3%, which indicates very pure  $\text{CaCO}_3$ . A small value, like magnesium have, could be linked to dolomite or  $\text{MgCO}_3$ . Sulphur, S, can be linked to anhydrite or gypsum ( $\text{CaSO}_4$  components), but the value is very low and content is minor. Silicon (Si) and Aluminum (Al) can indicate silica ( $\text{SiO}_2$ ) and clays but as for Mg and S the values are very low and is almost negligible.

**Table 8:** Composition analysis by energy dispersive x-ray spectroscopy of SK chalk.

Element	Atomic weight, At [%]
Mg	0.18
Al	0.15
Si	1.01
S	0.36
Ca	98.3

### 8.1.2 Effluent pH analysis

pH of the effluent from the produced water at the oil recovery test was performed regularly to link the charge of the organic materials. pH of the formation water (DI-water) before entering the core, was measured to be 6.16. The pH of formation water effluent was measured to be above 7, and the average was approximately 7.5 as seen in Figure 8.2 below. The pH confirms that the environment is slightly alkaline, hence we have dissociated acids and neutral base components as shown by the charge of the organic material at various pH:



At alkaline conditions, the basic components are neutrally charged and it is the negatively charged acidic components that should be active towards the chalk surface. Adsorption of acid components has been studied before and the results are corresponding with what Hopkins (2017) did. pH of effluent from all cores are listed in Appendix B.3.

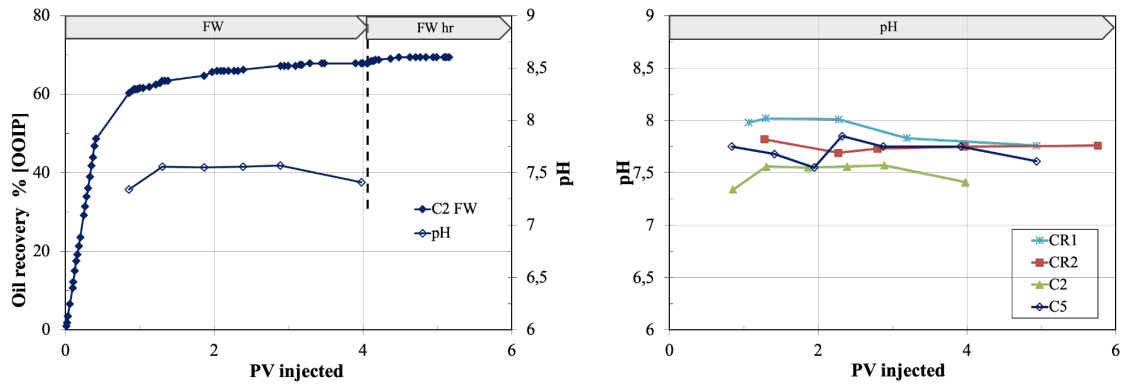


**Figure 8.2:** Example of pH at different PV injected of the water effluent during an viscous force oil recovery test.

## 8.2 Oil characteristics

Oil used in this experiment are crude oils and the mineral oil. Below, descriptions of preparations and characteristics are explained

### 8.2.1 Preparation of mineral oil (M-OIL)

To prepare the right solution of the mineral oil, the viscosity of model crude oils needed to be known. The mean viscosity of crude oils were 2.6 mPas, and the goal was to obtain the same viscosity for the M-OIL. The results from the viscosity experiments are presented in figure. The viscosity of the mixture increases with increasing amount of Marcol and decreasing amount of n-heptane in weight percent. Finally, after adjusting the mixing ratio, the best match was measured to be when the mixture had a 58 wt% of Marcol and 42 wt% of n-heptane. In Figure 8.3 Marcol in n-heptane and mean oil viscosity are illustrated, and the best match was at 58 wt% of Marcol.

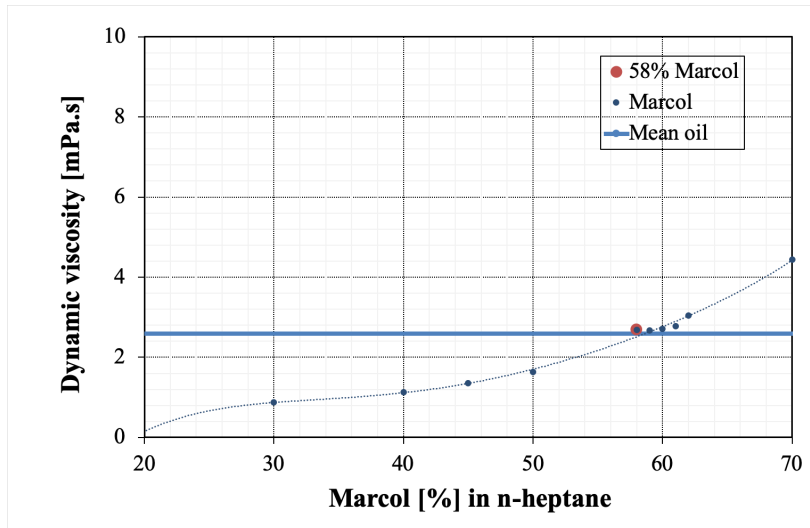


**Figure 8.3:** Viscosity vs percent of Marcol in n-heptane

### 8.2.2 The effect of AN on IFT

Interfacial tension and acid number was measured for all oils, and are listed in Table 4 section 7.1.2. As seen in Figure 8.4, increasing AN contributes to a decrease in IFT. According to Buckley and Fan (2007), acid number is an important crude oil property with respect to IFT, which also confirmed that IFT decreases with higher AN (Buckley & Fan, 2007).

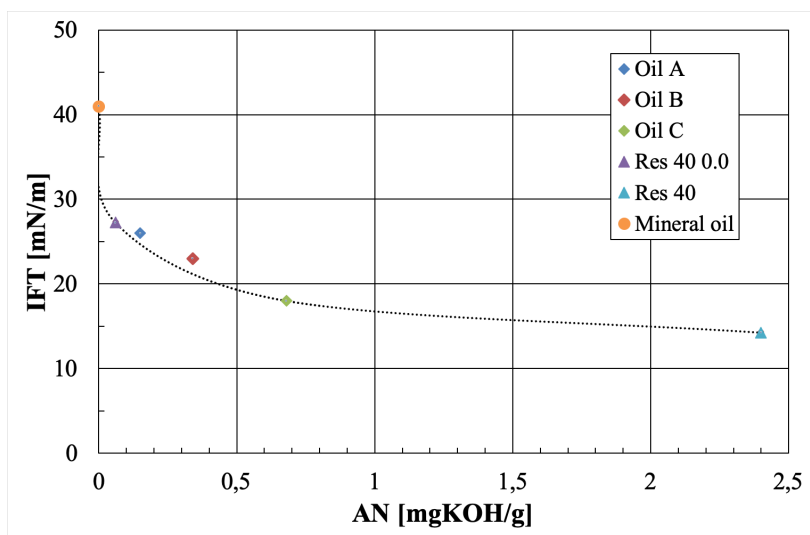


**Figure 8.4:** Acid number dependence of interfacial tension

Higher AN lowers the IFT, and when IFT decreases capillary pressure also decreases (see Equation 2.7). A decrease in capillary pressure will give a better flow of water which result in earlier water breakthrough, and lower recovery. To recover all moveable oil, more pore

volumes of water needs to be injected and other recovery methods needs to be considered (Kootiani & Samsuri, 2012).

### **8.3 Oil recovery from water-wet reference cores**

Two reference cores with a wettability of strongly water-wet were used to compare the results with the other cores. Stevns klint (SK) chalk cores behaves very water-wet, which is confirmed with the spontaneous imbibition (SI) test and chromatographic wettability test (CWT). The reference cores were flooded only with the M-OIL with no polar components that could interact with the core surface.

#### **8.3.1 Forced imbibition**

Forced imbibition experiments were performed on two parallel cores, CR1 and CR2 at an injection rate of 1 PV/day and ambient temperature. At the end of production, the injection rate was increased to 4 PV/day (rates can be found in Table 6). Both oil production and pressure drop, to avoid unrealistic high pressure drop during water injection, was measured. The oil recovery (%OOIP) was relatively high, close to 70 %OOIP for both cores during forced imbibition, as seen in Figure 8.5. Pressure drop data was collected and water injection continued until stabilized pressure drop. The reason is because stable pressure data is needed as input data for simulator SENDRA and for calculating effective and relative permeabilities.

In the beginning, the pressure drop increases gradually for approximately 0.4 PV as oil recovery increases. This could be explained by strong capillary forces promoting water imbibing and forcing oil out of the smaller pores (Equation 2.7). When capillary forces inside gradually decreases, oil recovery starts to stabilized and pressure drop decreases. After the recovery plateau is reached, one can still observe a decline in the pressure drop for about 2 PV. When the pressure drop were stabilized, the injection rate was increased from 1 to 4 PV. A new rapid increase in pressure drop was observed, and gradually decreasing. This could be explained by lack of capillary forces disturbing the pressure drop profile. About 1 %OOIP extra oil was produced in both parallel experiments. The uncertainty of the two reference cores are 70 +/- 2%OOIP.



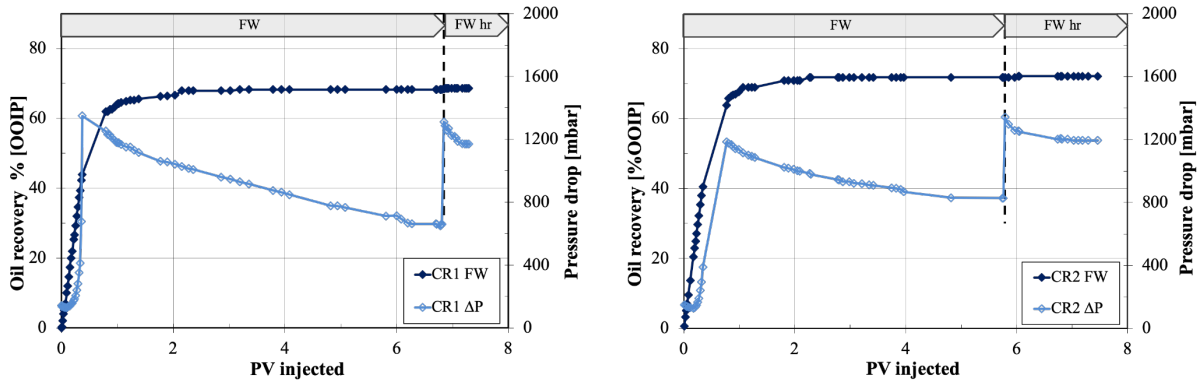


**Figure 8.5:** Oil recovery and pressure drop data vs pore volumes injected during forced imbibition at ambient temperature for left: CR1 (69%OOIP) and right: CR2 (72%OOIP) with two different rates, 1 PV/day and 4 PV/day. DI-water was used as the displacing fluid, and M-OIL was used as the displaced fluid.

The uncertainty of the two reference cores are  $70 \pm 2\%$ OOIP. So the reproducibility of the oil recovery for strongly water-wet cores are good. In Figure 8.6, both very water-wet cores at rate 1 PV/day are illustrated. Production curve has equal shape, but there is a minor difference in pressure drop development. Both cores have high capillary forces in the beginning imbibing water into the core and producing oil in a piston-like shape. Core CR1 were flooded 1 PV longer than core CR2 to reach a stabilized pressure drop.

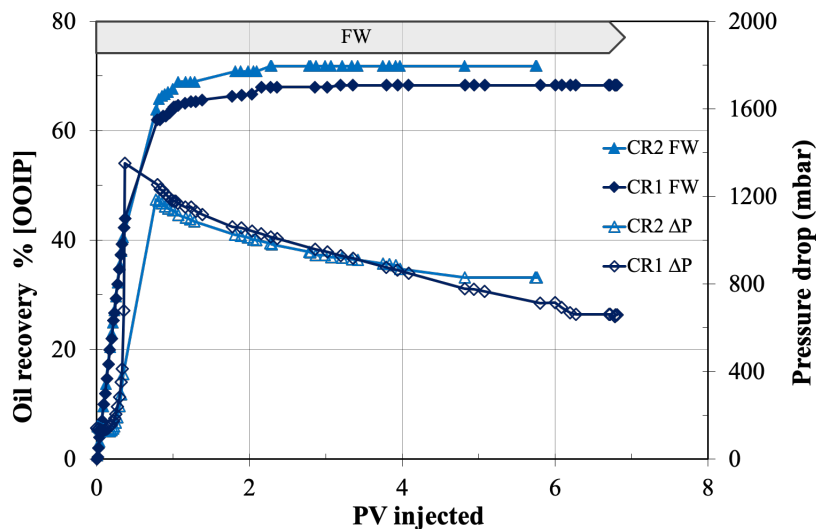


**Figure 8.6:** Oil recovery and pressure drop data vs pore volume injected during forced imbibition at ambient temperature for cores CR1 and CR2 at rate 1PV/day.

### 8.3.2 Spontaneous imbibition

Both water-wet cores were restored with  $S_{wi}=20\%$  of DI-water and M-OIL. Then, cores were exposed to SI at ambient temperature. The spontaneous imbibition test confirms strong capillary forces and a rapid production of oil. DI-water was used as imbibing brine. The oil production (M-OIL) from the two reference cores, CR1 and CR2, were respectively 67 % and 75 % OOIP. Due to strong capillary forces, oil was produced quickly (Figure 8.7, left) and nearly all oil was produced within 2 hours. Since almost all oil are produced within 2 hours, it is better to plot a log-plot (Figure 8.7, right). In the log-plot, one can see what happens at low time data. In Figure 8.7, left, it seems like production before water breakthrough is equal for cores CR1 and CR2, but in the right figure, the production is not equal. Even though a difference can be seen, the difference is very small and the reproducibility of the very water-wet cores are quite good.

The uncertainty for the reference cores are  $71 \pm 4\%$  OOIP. High capillary forces also confirms very water-wet cores. In spontaneous imbibition, water imbibe into all open pores, and not only from one side of the core like for forced imbibition. Even though it is not correct to compare production from two different processes, it is interesting to note that the ultimate recovery is almost the same for FI and SI (70-71 %OOIP). This indicates that capillary forces are important in oil recovery from low permeable water-wet cores.

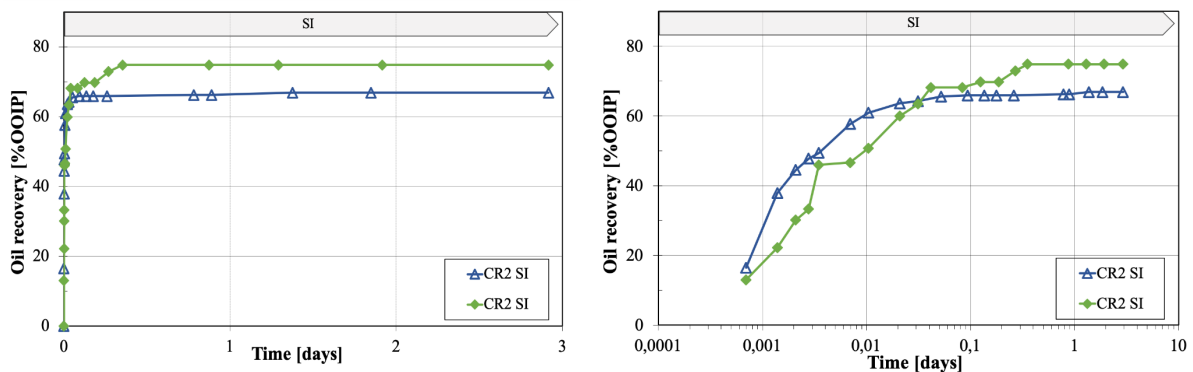


**Figure 8.7:** Oil recovery vs time by spontaneous imbibition of DI-water displacing M-OIL on two water-wet reference restored cores, CR1 and CR2, at ambient temperature. Left: Oil recovery vs time. Right: Oil recovery in a semilog-plot.

The oil recovery (%OOIP) by spontaneous imbibition from the reference (very water-wet) core,  $SI_{WWC}$ , is then the average of these two cores, CR1 and CR2, 71 %OOIP. The  $SI_{WWC}$  is used as a reference for calculating the modified Amott wettability index,  $I_{W-SI}^*$ , for the fractionally wet cores during spontaneous imbibition (see Equation 4.7).

### 8.3.3 Spontaneous and forced imbibition for reference core CR2

After spontaneous imbibition, one of the reference core (CR2) went through forced imbibition again. As seen in Figure 8.8 all recoverable oil was produced during the spontaneous imbibition process. This result confirm a very water-wet condition.

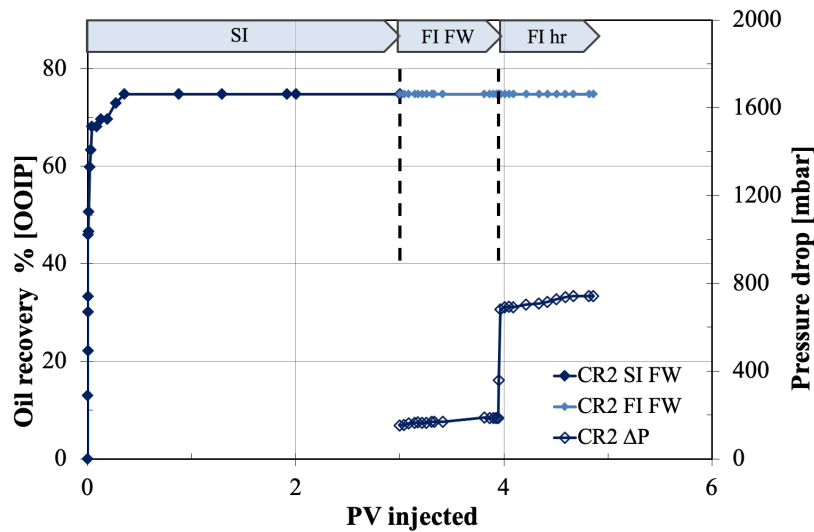


**Figure 8.8:** Oil recovery by spontaneous imbibition and forced imbibition on water-wet reference core, CR2 after second restoration at ambient temperature.

The pressure drop for forced imbibition process in this case do not increase rapidly, like it did for the FI in section 8.3.1, and the reason is because there is no more capillary forces left, and the viscous forces kicks in giving no more oil was produced. At high rate the pressure drop increase as a function of rate, but the pressure drop stabilize really quick with no extra oil produced.

Using Equation 4.4 from section 4.3.3, one can determine the “displacement-by-water-ratio”,  $I_w$  for core CR2. The value is 1 and clearly indicate a 100 % water-wet system.

$$I_{w,CR2} = \frac{0.75}{0.75 + 0.00} = 1 \quad (8.1)$$

### 8.3.4 Chromatographic wettability test of reference cores

Chromatographic wettability tests was also performed in order to define a measurement of a completely water-wet surface area for SK chalk (Figure 8.9). The test was performed at ambient temperature by flooding first with SW0T, then by SW1/2T brines. As seen in Figure 8.9, 100% water-wet cores had a water-wet surface area of  $A_{\text{water}} = 0.301$  and  $A_{\text{water}} = 0.263$ , and by taking the average of these two surface areas,  $A_{\text{water}} = 0.282$ , and this is the wettability index (WI) equal to 1. The values are in line with previously published data for SK cores (Fathi, 2012; Hopkins, 2016).

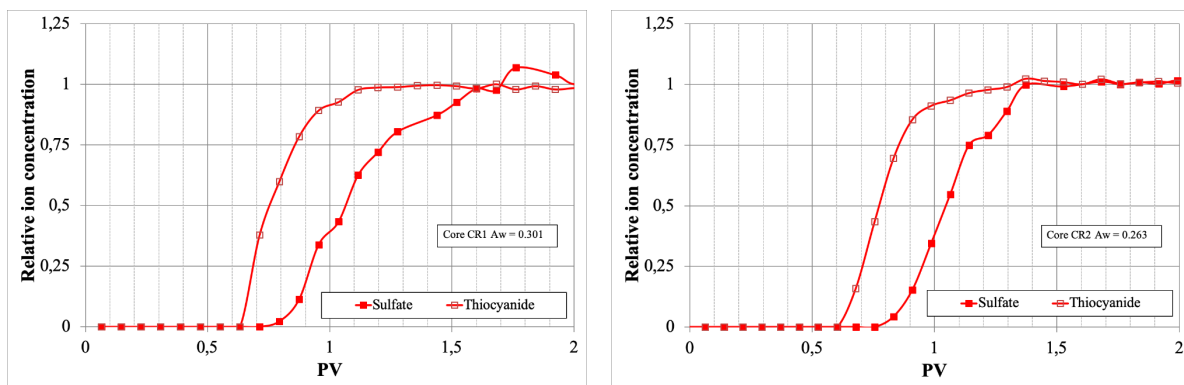


**Figure 8.9:** Chromatographic wettability test (CWT) results performed on reference cores at 23 °C. Left: CR1 with a surface area of  $A_{\text{water}} = 0.301$ . Right: CR2 with a surface area of  $A_{\text{water}} = 0.263$ .

## 8.4 Oil recovery and wettability for fractional-wet cores

Two cores were exposed to crude oil with  $AN=0.34$  mg KOH/g (Oil B) to reduce the water wetness of the very water-wet SK cores. After the crude oil flooding, cores were aged for 3 days, then the mineral oil with no polar components was flooded into the core. The first core, C2, went through forced imbibition first, then it was saturated with water again, establishing  $S_{\text{wi}}$  and saturated with mineral oil before spontaneously imbibition. The second core, C5, was spontaneously imbibed first, then forced imbibed.

### 8.4.1 Forced imbibition for fractional wet core C2

Core C2 with  $S_{\text{wi}}=20\%$  was exposed to 5 PV of oil B ( $AN=0.34$ ), to reduce the water wetness, before the oil phase was displaced with M-OIL. The oil recovery for core C2 was also high at low injection rate and close to the very water wet cores. The total recovery was close to 70 %OOIP, and results are presented in Figure 8.10. The high recovery and piston-like shaped curve indicates high enough capillary forces, even though the wettability should be reduced

compared to the reference cores. The same gradually increase in pressure drop is observed during water injection for rate 1 PV/day, as observed for the very water wet cores. Both the recovery and pressure drop stabilize at the same time, at less than 4 PV injected. At the end, the injection rate was increased to 4 PV/day. Rapid increase in pressure drop was observed without given extra oil ( $\sim 1$  %OOIP).

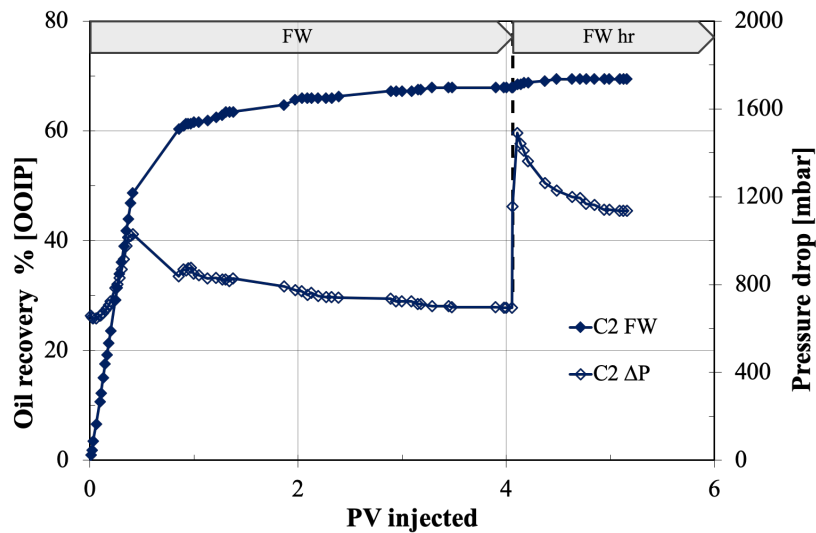


**Figure 8.10:** Oil recovery and pressure vs pore volume injected during forced imbibition for fractionally-wet core C2 at ambient temperature and two different rates, 1 PV/day and 4 PV/day. DI-water was used as the displacing fluid, and M-OIL was used as the displaced fluid. The total oil recovery after changing the rate was 71 %OOP.

IFT from the produced (M-OIL) oil were measured, and it was lowered from 41 to 28 mN/m. This IFT is still very high, compared to typical crude oils. This reduction is from the polar organic components from oil B at the core surface. By decreasing the IFT, the capillary forces inside the core will reduce (see Equation 7.6). That is an effect one will see in the spontaneous process, C5 in 8.4.3.

In Figure 8.11, one can see a comparing of the very water-wet references and fractional wet core C2 at low rate. Oil production curve follows the same trend as production curves for the water-wet reference cores. The oil recovery differs from 68 % and 72 %OOIP which is a very small difference in oil recovery. On the other hand, pressure drop is different, which could be explained by capillary forces imbibing water and forcing oil out from the smaller pores. The pressure drop is lower for the fractionally wet core, than for the reference core. But, the capillary forces, due to high IFT, for core C2 were high enough since the recovery was almost the same

as for the very water-wet reference cores. Pressure drop gradually increases until 0.4 PV and then decreases until pressure drop stabilizes when recovery plateau is reached approximately at 3 PV.

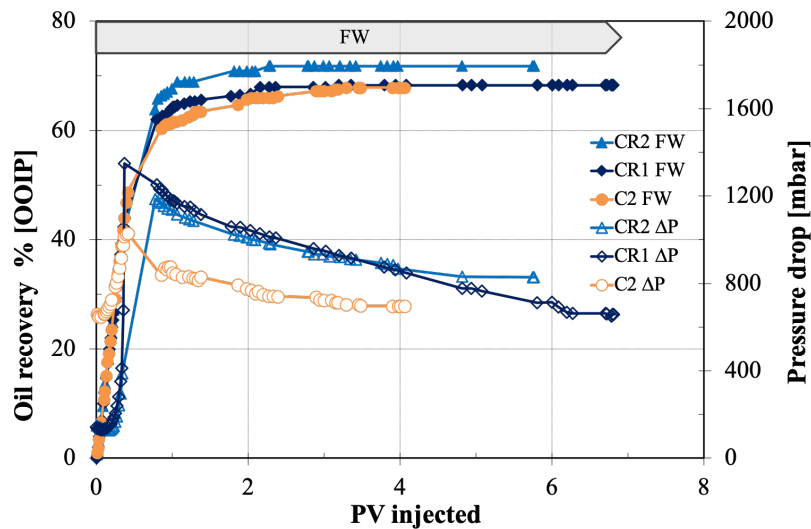


**Figure 8.11:** Forced imbibition process for reference cores (CR1 and CR2) and core C2 at ambient temperature. Oil production is almost the same, but the pressure drop for C2 is lower than for reference cores.

#### 8.4.2 Spontaneous imbibition of restored core C2

After forced imbibition, core C2 were restored with  $S_{wi} = 20\%$  of DI-water and M-OIL. The oil recovery by spontaneous imbibition of the core were relatively high of what was expected (Figure 8.12). The recovery was 58 %OOIP within less than a day. The high recovery can also be explained by the capillary forces. After restoration, mild cleaning, the IFT between M-OIL and DI-water could be higher and therefore increasing the capillary forces (see Equation 7.6). Mild cleaning is a process that reduces the effect of POC from pore surface (Hopkins, 2016), but this is minor, so the wetting of the core should not change that much. Increase in capillary forces can be affected of the system has become somewhat more water-water (lower contact angle) after the mild cleaning, but the IFT could also have increased compared to the IFT of effluent M-OIL measured after FI.

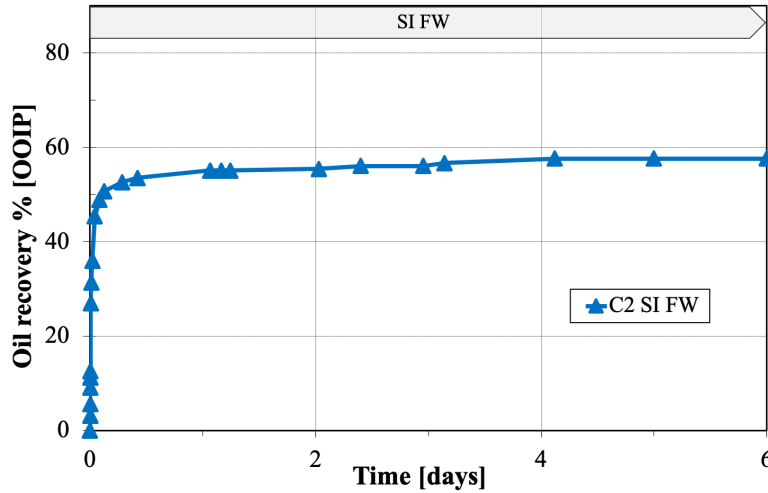


**Figure 8.12:** Oil recovery vs time during spontaneous imbibition of core C2 at ambient temperature. DI-water as displacing fluid and M-OIL as the displaced fluid. Total recovery after 6 day was 58 %OOIP.

The modified Amott wettability index for water,  $I_{W-SI}^*$ , can be used to indicate the water wetness of C2. The equation can be found in section 4.3.2, Equation 4.4. The water wettability index for core C2 is 0.82, which indicates a water-wet system:

$$I_{W-SI}^* = \frac{58}{71} = 0.82 \quad (8.2)$$

### 8.4.3 Spontaneous imbibition of core C5

Core C5 were flooded with oil B and M-OIL, and were immersed into a spontaneous imbibition cell. The oil recovery was 37 %OOIP, and this is lower than for core C2. The IFT in core C5 was probable lower than for core C2, which gives lower capillary forces imbibing water and forcing oil though the core and lower oil recovery. Figure 8.13 shows the oil recovery (%OOIP) versus time.

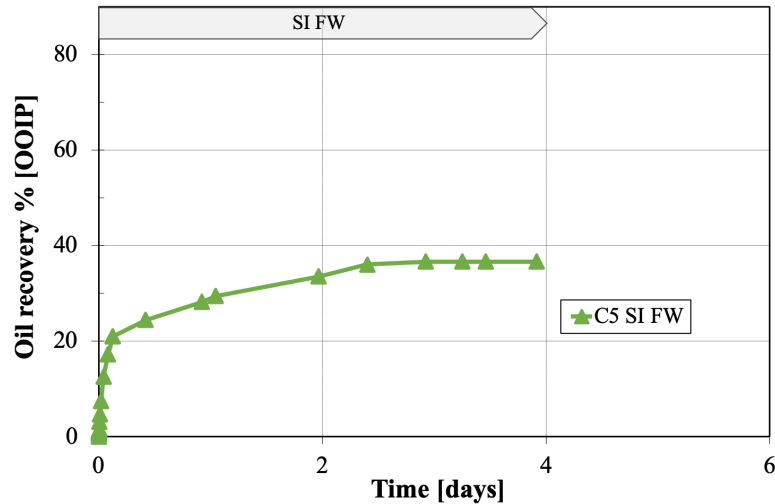


**Figure 8.13:** Oil recovery vs time during spontaneous imbibition of core C5 at ambient temperature. DI-water as displacing fluid and M-OIL as the displaced fluid. Total recovery after 4 day was 37 %OOIP.

As for core C2, the modified Amott water wettability index can also be used for core C5. The equation can be found in section 4.3.2, Equation 4.4. The water wettability index for core C5 is 0.52, which indicates a less water wet system then for core C5:

$$I_{W-SI}^* = \frac{37}{71} = 0.52 \quad (8.3)$$

This wettability is more representative to the wettability during forced imbibition on core C2.

In Figure 8.14, a comparison of the oil recovery of each core during spontaneous imbibition is illustrated. The semi-log plot (right figure) shows a significant changes in speed of imbibition. Even though cores CR1, CR2 and C2 were restored, a clear difference in the very water-wet cores and fractionally-wet cores are observed. For the case of the water-wet reference core, the IFT will not be different since the core surface are not affected by any surface active agents, and therefore will the capillary forces be the same before and after mild cleaning. For parallel cores C2 and C5, there are a recovery difference in 20 %OOIP, which is a big difference and indicates the difference in capillary forces due to the different processes the cores have been exposed to.



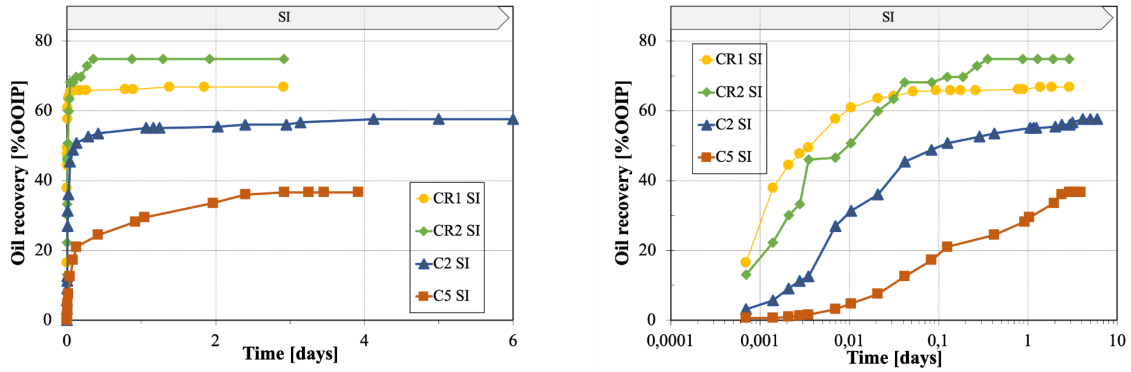


**Figure 8.14:** Comparing oil recovery vs time during spontaneous imbibition of all cores at ambient temperature.

### 8.4.4 Spontaneous and forced imbibition of core C5

As described in section 8.4.3, the recovery for C5 after spontaneous imbibition is 37% of OOIP, and the rapid production in the beginning indicates strong capillary forces imbibing water. The forced imbibition at low rate followed, further increases the production to 54% after 9 day. Increasing the injection rate from 1 PV/day to 4 PV/day increased the production to 65%.

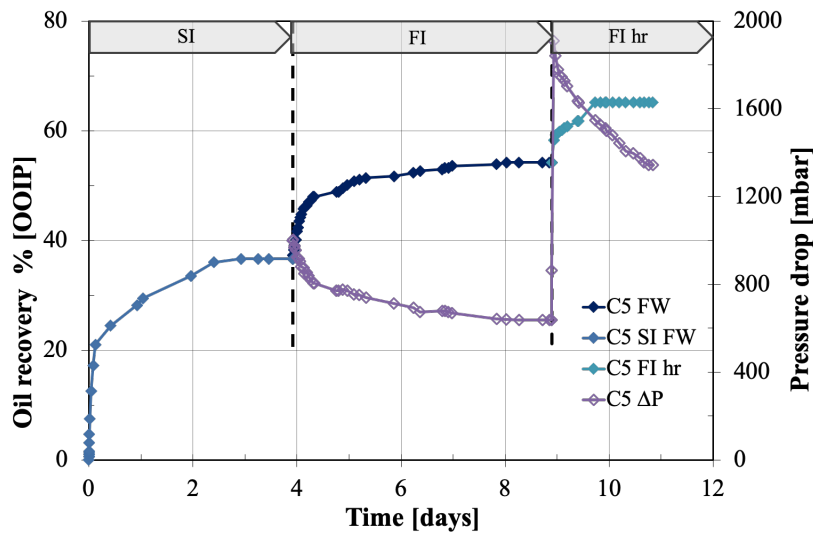


**Figure 8.15:** Oil recovery vs times during SI and FI (at two different rates) with DI-water as displacing fluid and M-OIL as displaced fluid at ambient temperature for core C5. The total recovery after high rate was 65%.

The pressure drop profile is different from the other cases seen in section 8.4.1 and 8.3.1. After a spontaneous imbibition process where the oil is produced by capillary forces, the forces decreases. When FI starts, a rapid pressure build up can be seen, then the pressure drop gradually decreases, which indicates lack of capillary forces which disturbs the pressure drop

profile. The pressure drop stabilizing after approximately 3 PV. When the pressure drop stabilizes, the injection rates was increases, and a new rapid increase in pressure drop was observed, gradually decreasing.

Using Equation 4.4 from section 4.3.3, one can determined the “displacement-by-water-ratio”,  $I_w$ , as calculated below for core C5.

$$I_{w,C5} = \frac{0.37}{0.37 + 0.28} = 0.57 \quad (8.4)$$

Figure 8.16 illustrates the recovery difference in CR2 and C5. Spontaneous imbibition is a strong indicator of the wettability of the core. Due to lack of capillary forces in the FI process, the total production of core C5 is lower. The higher recovery from core CR2 indicates that this core is more water-wet than core C5. As mentioned before core CR2 did not produce any oil during FI after SI and all mobile oil has been displaced during SI. During FI core C5 produces more oil, and since the capillary forces are low, the viscous forces, forcing water to displace more oil and recovery of oil increases.

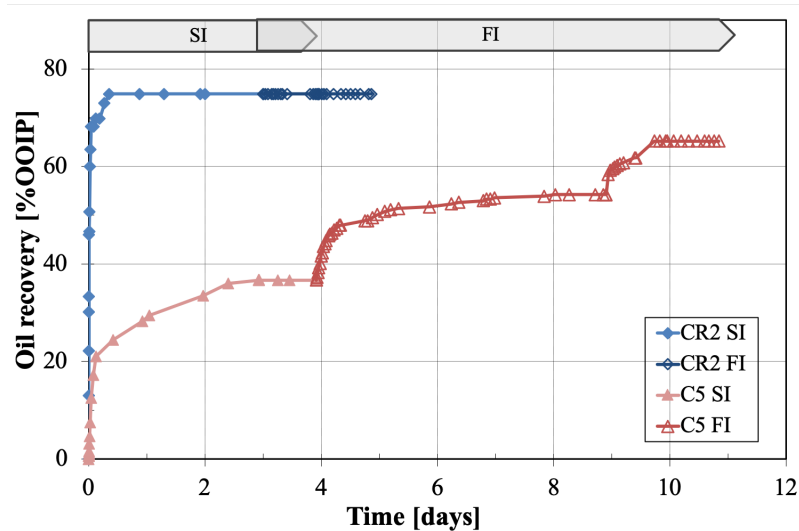


**Figure 8.16:** Spontaneous and forced imbibition comparison for core CR2 and C5 at ambient temperature.

#### 8.4.5 Chromatographic wettability test

Following the forced imbibition, the cores were flooded until  $S_{or}$ , and then a chromatographic wettability test was performed. Results are presented in Figure 8.17. Area between  $SCN^-$  and

$\text{SO}_4^{2-}$  was calculated to be 0.207 for core C2 and 0.248 for C5, which indicates water-wet cores compared with very water wet cores with a wettability index of 0.282.

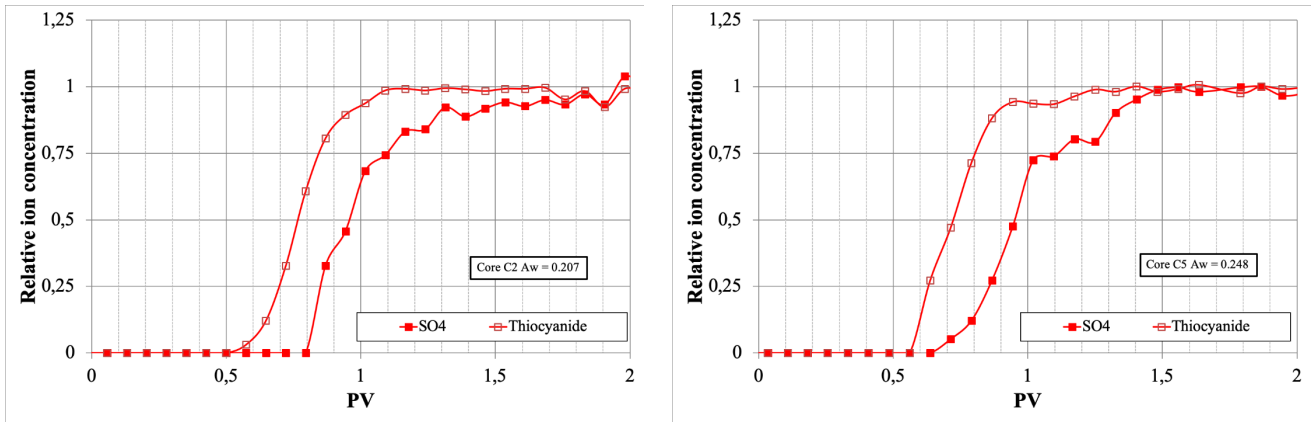


**Figure 8.17:** Chromatographic wettability test (CWT) results performed on fractionally-wet cores at 23 °C. Left: C2 with a surface area of  $A_{\text{water}} = 0.207$ . Right: C5 with a surface area of  $A_{\text{water}} = 0.248$ .

The wettability index (WI) is defined in section 4.3.5, Equation 4.8 and can calculate the wettability index for both core C2 and C5:

$$WI = \frac{0.207}{0.282} = 0.73 \quad (8.5)$$

$$WI = \frac{0.248}{0.282} = 0.88 \quad (8.6)$$

The wettability index confirms reduced water wet surface area after crude oil exposure. The explanation between the difference in wettability index, could be that core C5 have gone through more processes before chromatographic wettability test, and through these processes the core has become more water-wet. Both cores confirms that the core is quite water-wet.

### 8.5 Comparing oil recoveries with cores with different initial wettability

During the experiment, a crude oil with AN = 0.34 mgKOH/g where used. The fellow students were conducting the same experiments with a different AN in model crude oils. The lowest AN (0.15 mgKOH/g) was expected to have the most water-wet system, while the crude oil with the highest AN (0.68 mgKOH/g) was expected to give the least water-wet core. The average recovery values for strongly water-wet reference cores, CR1 and CR2, were used as reference values. And these are listed in Table 9:

**Table 9:** Reference vaules from reference cores, CR1 and CR2.

Core	CR1	CR2	Average
<b>SI<sub>WWC</sub> (SI recovery in %OOIP)</b>	67	75	71
<b>CWT A<sub>water</sub> (separation area)</b>	0.301	0.263	0.282

Some of the cores (CR1, CR2, C1, C2 and C3) were restored 2 times during experiments and others were only restored 1 time (cores CR2\*, C4, C5 and C6). CR2\* is the same core as CR2, but this core was first during forced imbibition, then the core was restored with a  $S_{wi} = 20\%$  and saturated with M-OIL. After core restoration, the core went through spontaneous imbibition followed by forced imbibition again. In Tables 10 and 11 comparison of result from all cores are listed.

**Table 10:** Comparison of results from cores ( 2 restoration) with varying wettabilities, Case 1

Cores					
	CR1	CR2	C1	C2	C3
<b>Oil AN</b>	-	-	0.68	0.34	0.15
<b>SI Recovery (in %OOIP)</b>	67	75	51	58	63
<b>FI Recovery (in %OOIP) at 1PV/day</b>	68	72	73	68	67
<b>FI Recovery (in %OOIP) at 4PV/day</b>	1	-	1	1	8
<b>Total FI (in %OOIP)</b>	69	72	74	69	70
<b>Separation area</b>	0.301	0.263	0.205	0.207	0.281
<b>WI</b>	1	1	0.73	0.73	0.99
<b>I*<sub>w-SI</sub></b>	1	1	0.72	0.82	0.89

**Table 11:** Comparison of result from cores (1 restoration) with varying wettabilities, Case 2

Cores				
	R2*	C4	C5	C6
<b>Oil AN</b>	-	0.68	0.34	0.15
<b>SI Recovery (in %OOIP)</b>	75	6	37	58
<b>FI Recovery (in %OOIP) at 1PV/day</b>	-	61	17	2
<b>FI Recovery (in %OOIP) at 4PV/day</b>	-	2	11	2
<b>SI+FI (in%OOIP)</b>	75	69	65	62
<b>Separation area</b>	0.263	0.174	0.248	0.306
<b>WI</b>	1	0.62	0.88	1.09
<b>I<sub>w</sub></b>	1	0.09	0.57	0.94
<b>I*<sub>w-SI</sub></b>	1	0.08	0.52	0.82

As seen in these two tables (10, 11), recovery by spontaneous imbibition increases with decreasing acid number. For forced imbibition, there are no clear differences. All cores produce around 70 +/- 5 % OOIP. The only big difference is that all cores except core C3 and C5, produces 1-2%OOIP after increasing the rate. Core C3 produces 8%OOIP and core C5 produces 11%OOIP after increasing the rate. The reason for more production from core C3, can be due to more moveable oil left ( $S_{or}$  not reached) in the core and the increasing viscous forces (at increasing rate) forcing the remaining oil out of the core. During FI in core C5, there was no strong capillary forces observed. The pressure drop decreased immediately after starting the FI recovery process. During the low and high rate viscous forces are the forces acting on the rock, and after stabilizing production and pressure drop, the rate was changed and even more oil was produced. There is more moveable oil left in the core after SI and low rate FI, and by increasing the rate it seems that the increasing viscous forces force the remaining oil out of the system.

In the case (2) where spontaneous imbibition was conducted first, followed by forced imbibition, the recovery was much lower for SI. Cores C4, C5, C6 has the same AN as C1, C2, C3. The same recovery trend can be seen in Figure 8.18 compared to Figure 8.19, where the core with highest AN (C4) has the lowest oil recovery and the core with lowest AN (C6) has highest recovery. The only difference is that the recovery in this case is lower for the fractionally-wet cores (Figure 8.18). The lower recovery has been discussed before, and it is due to lower capillary forces. IFT between water and M-OIL has been lowered due to POC at pore surface. This SI test describes the initial core wettability for all cores.

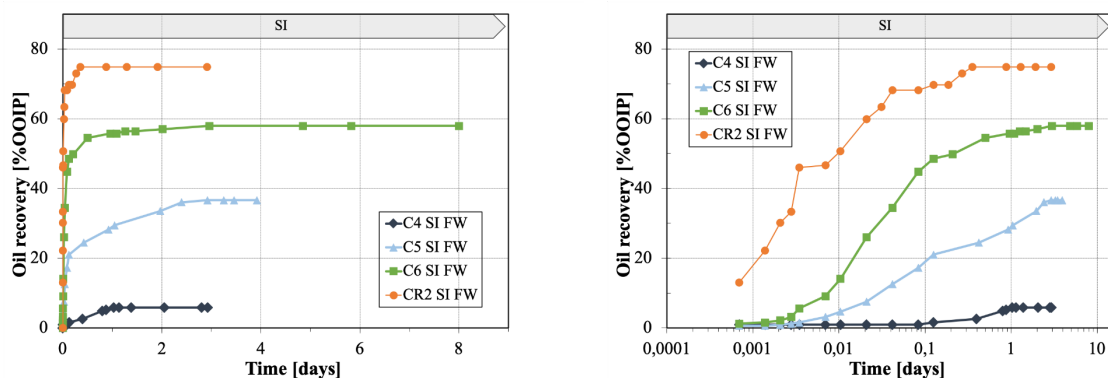


**Figure 8.18:** Comparing oil recovery by SI from core CR2, C4, C5, C6 at ambient temperature. Left: Oil recovery vs time. Right: Oil recovery in a log-plot.

In the case where spontaneous imbibition was conducted after restore no. 2, one can see in Figure 8.19 that oil recovery for all cores (CR1, CR2, C1, C2 and C3) was rapid, and quite high. In this case the IFT was higher, due to the high IFT between water and M-OIL. The polar organic components (POC) are still adsorbed onto chalk surface, but after the mild cleaning POC does not seem to lower the IFT. Higher capillary forces acts in the core, and water is immediately imbibed into the core forcing M-OIL out of the core. Even though the recovery from these cores were rapid and high, a difference can be seen. The fractionally-wet core with highest AN (C1), the less water-wet core, produces less oil than the other cores. The fractionally-wet core with lowest AN (C3), the quite water-wet core, produces almost the same amount as the reference strongly water-wet cores.

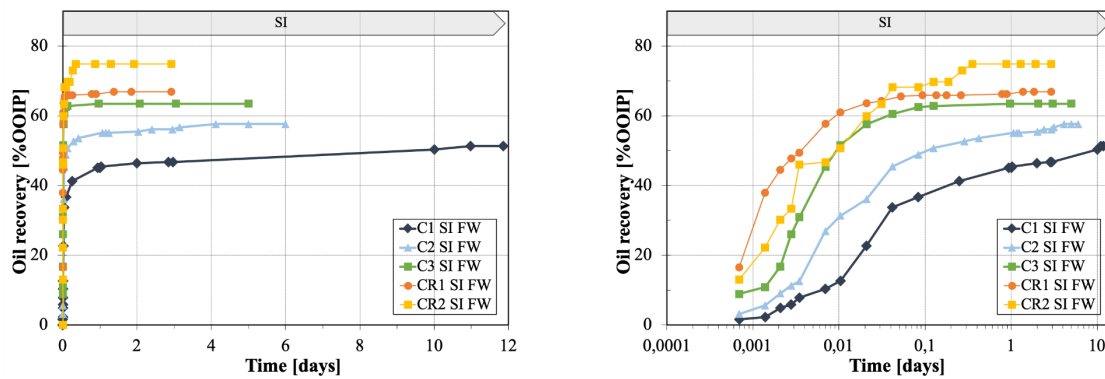


**Figure 8.19:** Comparing oil recovery by SI from core CR1, CR2, C1, C2, C3 at ambient temperature. Left: Oil recovery vs time. Right: Oil recovery in a log-plot.

Oil production during forced imbibition (Case 1) is almost the same for all cores. As mentioned before all cores produced 70+-5%OOIP. The pressure drop data for each core is different, but follows the same trend. In the beginning the pressure drop increases as capillary forces imbibe water and displaces oil. The pressure drop increases much higher for the strongly water-wet cores, than for the fractionally-wet cores. The high recovery corresponds to both high capillary forces in the beginning and viscous forces acting on the cores.

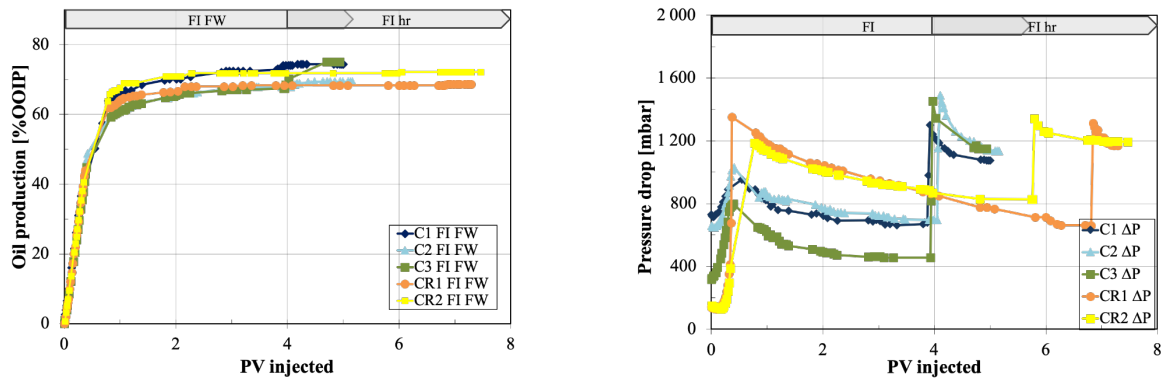


**Figure 8.20:** Comparing oil recovery (left) and pressure drop (right) vs PV injected for cores CR1, CR2, C1, C2, C3 at ambient temperature.

## 8.6 Numerical core analysis

In this analysis the effect of wettability on waterflooding and relative permeability curves on displacement of oil and water was used to history match the flooding experiments on measured two-phase properties. Simulator Sendra history matched experimental production and pressure drop data. Often in a simulator analysis, the  $P_c$  is considered negligible, but in this case  $P_c$  gave a better history match and is therefore considered. The history matching is based on recovery at low rate 1 PV/day, since the recovery after increasing the rate was minimized.

### 8.6.1 Methodology

Rock and fluid properties, listed in Appendix C1 and C2, for water-wet cores and fractionally-wet cores were used as input parameters in SENDRA simulation. Experimental data for forced imbibition were used for history matching, and these data are listed in Appendix B2.

The determined values to create relative permeability and capillary pressure curves are listed in table 12 and 13.

Before simulation, endpoint relative permeabilities for water and oil and  $S_{or}$  were calculated.  $S_{or}$  was calculated by using Equation 7.7, and,  $k_{rw}(S_{or})$  and  $k_{ro}(S_{wi})$  were calculated based on the effectives and absolute permeabilities using Darcy's law (equation 7.4) at stabilized pressure drop. When pressure drop was stabilized, it was checked for approximately 1 day. Assumptions were made that the pressure drop were stable afterwards as well and that  $S_{or}$  was reached, and that the pump rate was constant at all times. The calculated endpoint relative permeability and  $S_{or}$  are listed in table 7. Simulations were first based on the calculated endpoint relative permeabilities and  $S_{or}$ . This gave really poor results with no match at all.

For strongly water-wet cores, the automatic history match was poor, which is described and shown in next section. Table 12 shows the automatic history matching parameters. Automatic history matching is first done keeping always  $S_{wi}$  as a fixed value, while all other parameters were variable values during estimation. The automatic history match gave unrealistic Corey parameters. For relatively identical cores, as the water-wet reference cores are, the Corey parameter for water was quite different (see table 12).

**Table 12:** Corey and Skjæveland parameters for automatic history matching for cores CR1, CR2 and C2

<b>Automatic history matching</b>			
	<b>CR1</b>	<b>CR2</b>	<b>C2</b>
<b>Corey Parameters</b>			
$N_w$	2.72	1.00	3.15
$N_o$	2.24	2.69	3.83
$k_{rw}(S_{or})$	0.07	0.07	0.34
$k_{ro}(S_{wi})$	1.00	1.00	0.38
<b>Skjæveland Parameters</b>			
$C_w$	14917	14736	0
$A_w$	0.251	0.251	0.251
$C_o$	0	0	27843
$A_o$	0	0	0.251
<b>Saturation values</b>			
$S_{wi}$	0.20	0.20	0.20
$S_{or}$	0.24	0.13	0.12

By manually change the parameters, the history match for the strongly water-wet cores were improved. The methodology for changing the parameters starts with increasing the Corey parameters, but still favorable with a bit higher  $C_w$  than  $C_o$ . Lower Corey parameters seem to produce a piston-like displacement where both oil recovery and pressure drop curve increases until the curves stabilizes (see Figure 22). Capillary pressure are kept equal to zero. When the correct Corey parameters reflected the pressure drop curve,  $S_{or}$  was changed manually until the history matched production curve matched the experimental production curve. At last, the relative permeabilities were changed to get the best match of the first and last point of the pressure drop curve, and the shape of the production curve. By adding capillary pressure, the curves were even more modified. This will be shown in the next section. Table 13 shows the manually history matching parameters.



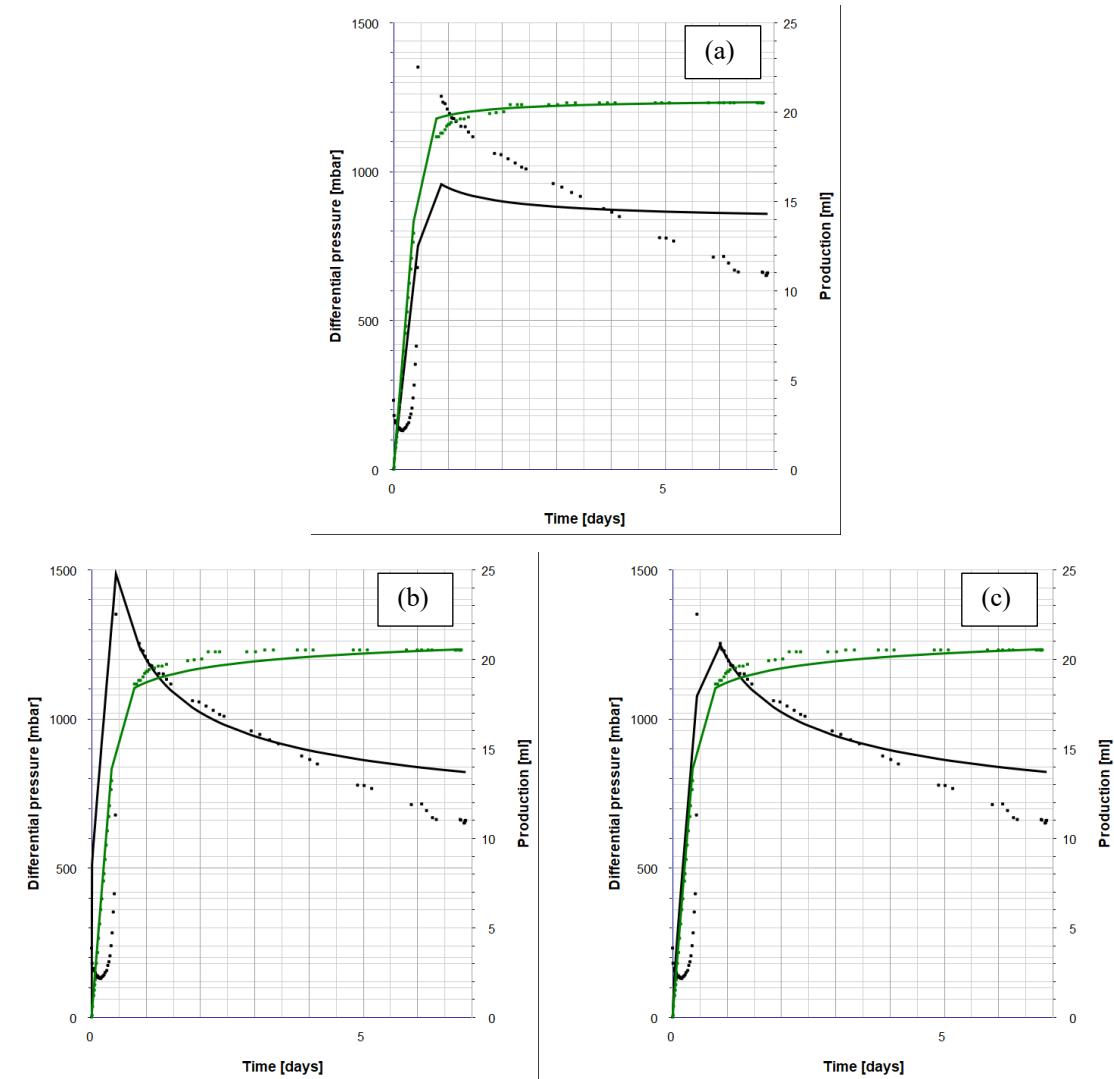
**Table 13:** Corey and Skjæveland parameters for manually history matching for core CR1 and CR2.

<b>Manually history matching</b>		
	<b>CR1</b>	<b>CR2</b>
<b>Corey Parameters</b>		
$N_w$	4.00	3.50
$N_o$	3.00	2.80
$k_{rw}(S_{or})$	0.10	0.12
$k_{ro}(S_{wi})$	0.40	0.20
<b>Skjæveland Parameters</b>		
$C_w$	37938	49659
$A_w$	0.251	0.251
$C_o$	0	0
$A_o$	0	0
<b>Saturation values</b>		
$S_{wi}$	0.20	0.20
$S_{or}$	0.20	0.13

As a summary:  $S_{wi}$  during the analysis was always used as a fixed value. At first, during the history matching, endpoint relative permeabilities and  $S_{or}$  were also used as fixed values. This gave poor matches both for production and pressure drop curves. When  $S_{or}$ ,  $k_{ro}(S_{wi})$  and  $k_{rw}(S_{or})$  were varying, the production profile was better. Even better matching for production and pressure drop curve was when manually changing the parameters.

### 8.6.2 History match for water-wet cores

Figure 8.22 illustrates the history matching for core CR1 based on automatic and manually parameters. The automatic matching (Figure 8.22 (a)) gave an acceptable production profile, but a poor pressure drop curve. The reason could be that the displacement of oil are almost piston-like, and the SENDRA simulates at piston-like pressure drop curve. It seems that the data requires not a piston-like displacement, but still a favorable displacement. Pressure drop curve in Figure 8.22 (a) is almost stable after production curve is stabilized. The endpoint relative permeabilities from automatic history matching are more similar to the calculated values (Table 7) than the endpoint relative permeabilities from manually history matching.



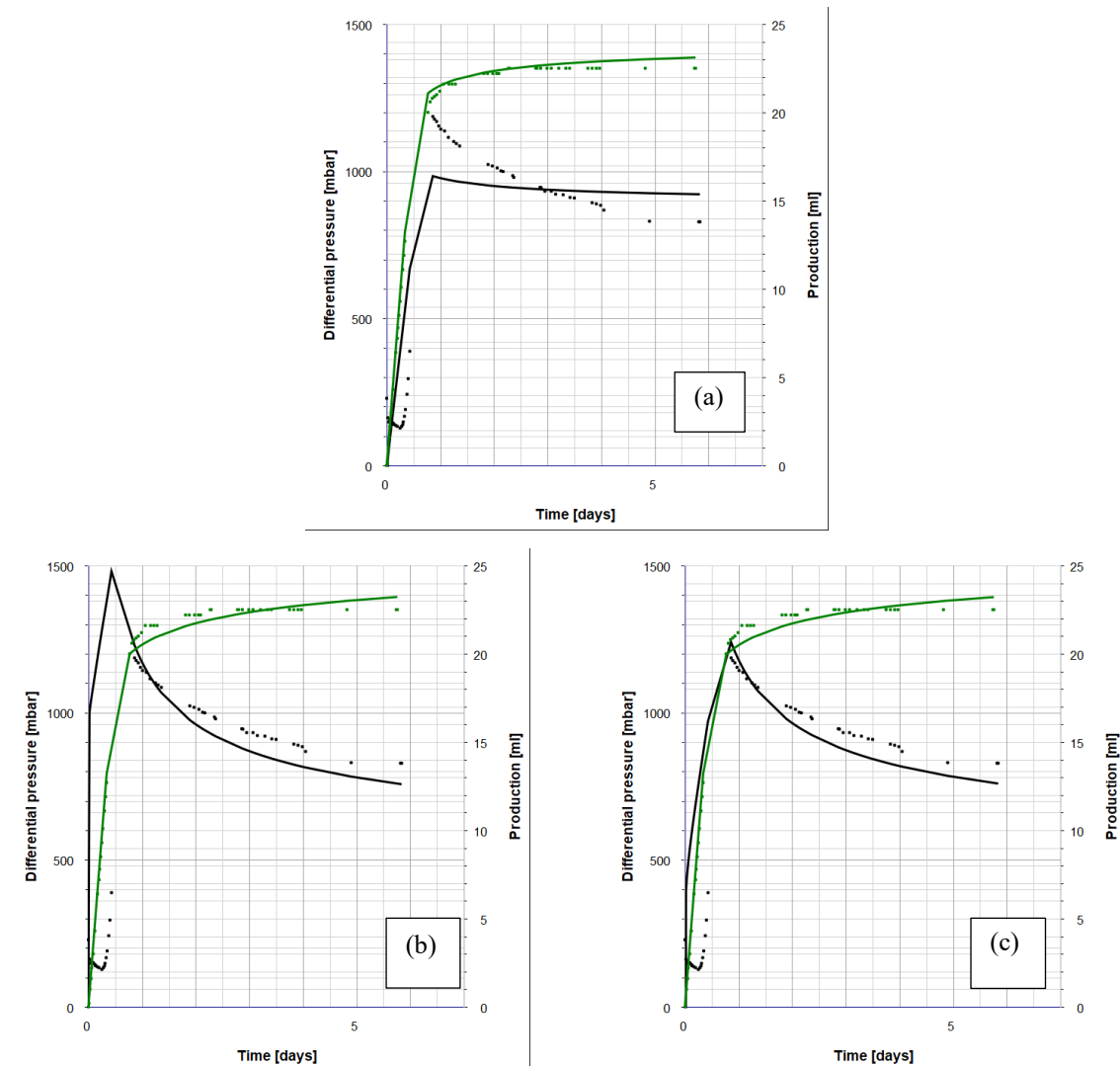
**Figure 8.21:** History matching of experimental production and pressure drop data of CR1. (a) Automatic history matching with  $P_c$ , (b) Manually history matching without  $P_c$  and (c) Manually history matching with  $P_c$ . Dots plots are the experimental data, and continuous lines are the history matched data.

Figure 8.22 (b) show the manually history matching without capillary pressure, which gave better matching than the automatic match. The manually history matching with capillary pressure (Figure 8.22 (c)) gave an even more improved match. It was more desirable to match the peak seen in the experimental pressure drop. By increasing the Corey parameters manually this the peak will be seen.

The endpoint relative permeabilities were not equal to the calculated values, from Table 7. The pressure drop data does not match at the end of production. The history matched values are higher than for the experimental data. The matched pressure drop data seem to decrease after end of production, even though the experimental pressure drop are virtually stable. The

matching could have been better if experimental pressure drop had been stable for a longer period. The endpoint relative permeability for water from SENDRA could also better if the matched pressure drop curve had been more stable at the end of the production. The matched production curve is relatively stable at the end, giving a  $S_{or} = 0.2$ . This value is not far from the calculated value (Table 7).

The same trend is seen for core CR2 (Figure 8.23) as for core CR1. Poor match for the pressure drop curve with automatic history matching, while an acceptable curve for production. Also in this case the endpoint relative permeabilities from automatic history matching are more similar to the calculated values (Table 7) than the endpoint relative permeabilities from manually history matching.



**Figure 8.22:** History matching of experimental production and pressure drop data of CR1. (a) Automatic history matching with  $P_c$ , (b) Manually history matching without  $P_c$  and (c)

Manually history matching with  $P_c$ . Dots plots are the experimental data, and continuous lines are the history matched data.

Manually history matching gave in this case also a better match, where it matches the pressure drop peak. The parameters are listed in table 13. The history matched pressure drop curve does not match the experimental curve in the end. Also in this case it seems to decline and will not stabilize at first. SENDRA interpolate the pressure drop, and therefore stabilized pressure drop data in SENDRA seem to be lower for CR2, than for the experimental values. Due to lower pressure drop, the  $k_{rw}(S_{or})$  will be higher than calculated, by small factors. The calculated  $k_{ro}(S_{wi})$  is quite high, but is lowered using matching. In this case, the matched pressure drop starts higher than the pressure drop measured in the laboratory. The end of production is assumed stabilized and at  $S_{or}$  in the experiment, while the matched production curve is still increasing, giving a lower  $S_{or}$  than calculated.

These two strongly water-wet cores, CR1 and CR2, should be relatively equal in the theory and the reproducible in laboratory experiments are good. Core CR2 produces 4 % more OOIP than core CR1. It interesting to notice that  $S_{or}$  and  $k_{ro}(S_{wi})$  are quite difference based on the manually history match. The reason for  $S_{or}$  being that low for core CR2, is because the manually history matched curve for oil production increases when the experimental curve seem to be stable. For core CR1, the match at the end of oil production seem to stabilize, and gives higher  $S_{or}$ . The main reason for the difference in  $k_{ro}(S_{wi})$  is because the simulator takes the first pressure drop point in manually matched curves to calculate the endpoint relative permeability for oil. The pressure drop in CR2 is higher than for CR1, which gives lower  $k_{ro}(S_{wi})$ . The Corey parameters and  $k_{rw}$  are quite equal for both cores.

The calculated values for endpoint relative permeabilities and  $S_{or}$  are based on stabilized pressure drop data during oil flooding ( $k_{ro}(S_{wi})$ ) and water flooding ( $k_{rw}(S_{or})$ ). Calculated  $k_{ro}(S_{wi})$  differs from manually history matched  $k_{ro}(S_{wi})$ . The manually matched values are lower, 0.4 and 0.2, while the calculated values are approximately 0.8 (see Table 7). If the goal was to match the calculated relative permeabilities and  $S_{or}$ , it would be better to use the automatic history match, shown in Table 12 and Figures 8.21a and 8.22a. The automatic history matching gave poor history matching and unrealistic Corey parameters, that were not equal for the two strongly water-wet cores.

### 8.6.3 History match for fractionally-wet core

The automatically history match for core C2 was significantly better than for the reference cores. It matches both production and pressure drop data. Figure 8.24 shows the history matching for core C2. Even though the match is good, the calculated endpoint relative permeabilities and  $S_{or}$  are not equal to what SENDRA matched automatically. One reason could be that absolute permeability in the core changes during the flooding, and is not consistent through the core. Another reason is that SENDRA extrapolate the production and the pressure drop curve. In this case the production seem to increase, giving a lower  $S_{or}$  than calculated. And matched pressure drop starts at a higher value and ends at a lower value than t measured stabilized pressure drops at oil flooding and water flooding, giving lower  $k_{ro}(S_{wi})$  and higher  $k_{rw}(S_{or})$ .

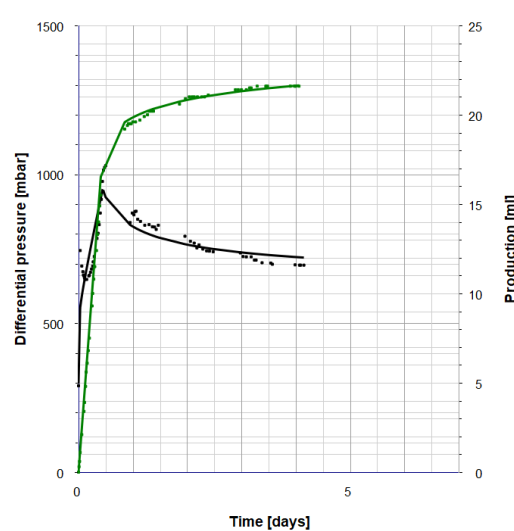


**Figure 8.23:** History matching of experimental production and pressure drop data of C2. Capillary pressure is negative. Dots plots are the experimental data, and continuous lines are the history matched data.

### 8.6.4 Relative permeability and capillary pressure curves.

Relative permeability curves and capillary pressure curves are based on Corey and Skjæveland parameters. The curves are made in ExCel using Equations 6.1 and 6.2 for relative permeabilities and Equation 6.4 for capillary pressures. In Figure 8.24, relative permeability curve and the corresponding capillary pressure curve for strongly water-wet conditions for cores CR1 and CR2. The relative permeability curves (Figure 8.24 a and b) indicates a crossover saturation (COS), where  $k_{ro} = k_{rw}$ , are close to 0.6. COS dictate the core wettability, and values larger than 0.5 can be characterized as a water-wet system (Craig, 1971).

The endpoint relative permeabilities can also be an indicator of the wettability. When endpoint relative permeability for a fluid is low, the tendency of that fluid to flow is low, and vice versa when endpoint relative permeability is high. In the case for the strongly water-wet cores, it was expected to have a high values for  $k_{ro}(S_{wi})$  and low for  $k_{rw}(S_{wi})$ . The reason for this expectation is because water breakthrough happens when almost all oil are produced during forced imbibition. From the figures, based on history matching, it seems that oil flows more poorly compared to the calculated value (Table 7). Water flow is low, and this was expected and calculated.

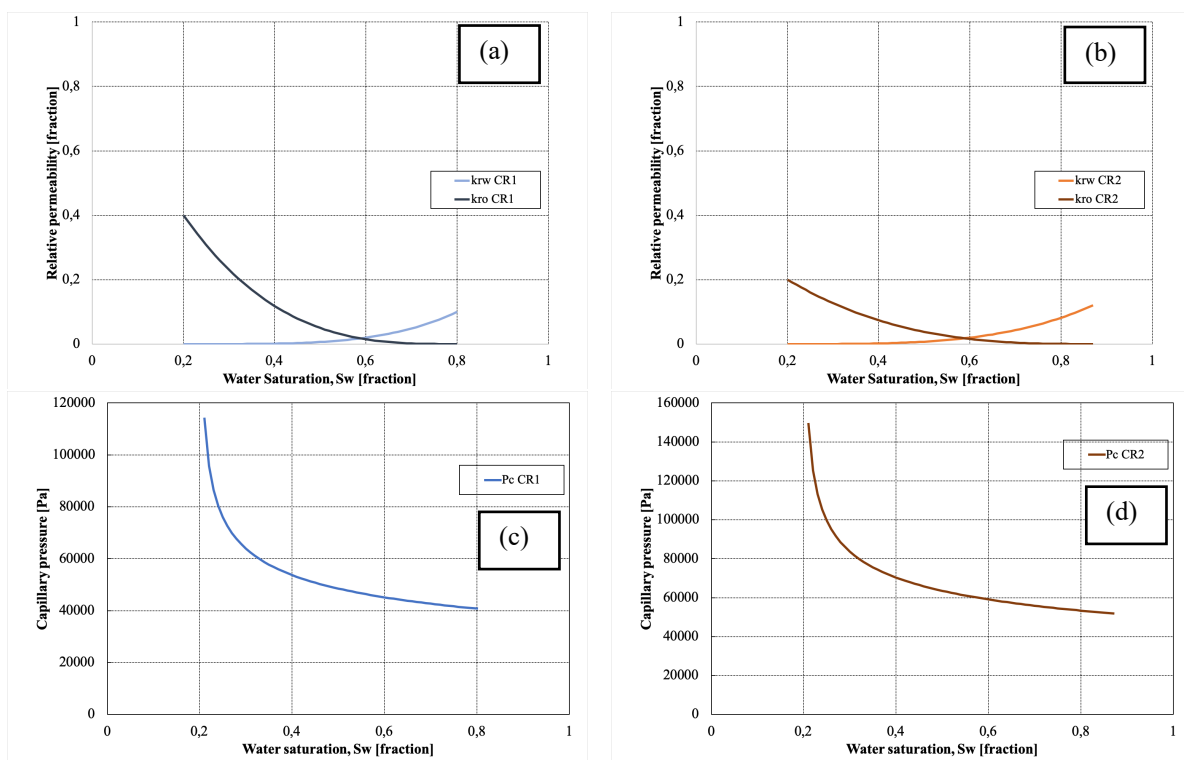


**Figure 8.24:** Relative permeability and capillary pressure curve for strongly water-wet cores based on manually history matching. (a) Relative permeability for CR1, (b) Relative permeability for CR2, (c) Capillary pressure for CR1 and (d) Capillary pressure for CR2.

Capillary pressure (Figure 8.24 c and d) can also dictate the core wettability. Positive capillary pressure indicates a water-wet systems, while negative capillary pressure indicates oil-wet systems (Anderson, W. G., 1987a). In the case for strongly water-wet cores, the capillary pressure is positive. This can be verified by spontaneous imbibition, where capillary forces act on the core imbibing water and produce oil.

For the fractionally-wet core C2, the relative permeability curve illustrated in figure 8.24 a are based on the automatic matching SENDRA made. The COS are 0.53, which indicates slightly water-wet. Endpoint relative permeabilites are almost the same, indicating that both oil and water has the same tendency to flow. These results are different from the calculated values (Table 7). The  $k_{rw}(S_{or})$  are higher than calculated and  $k_{ro}(S_{wi})$  are lower than calculated.

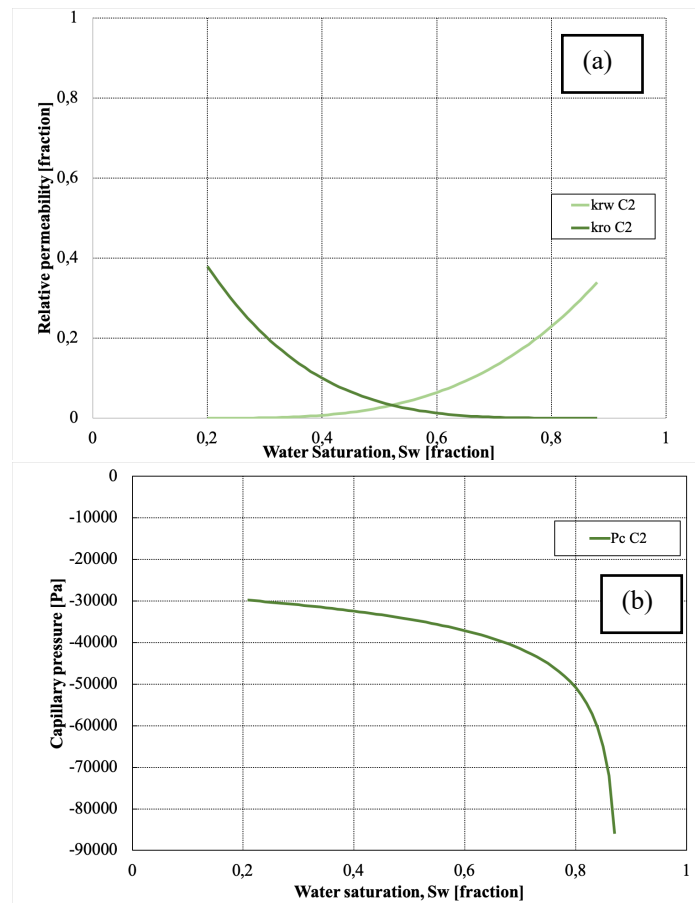


**Figure 8.25:** Relative permeability and capillary pressure curve for core C2 based on automatic history matching. (a) Relative permeability curve and (c) Capillary pressure curve.

For the capillary pressure curve it is interesting to observed that it is negative. In the experiment, it has been shown that there are capillary forces in core C2. During spontaneous imbibition, it has been observed that positive capillary forces assist water into the pores displacing oil. In this case modeled by SENDRA, negative capillary forces indicates a more oil-wet case. In an oil-wet case the capillary forces tend to prevent the imbibing of water. This is more discussed in section 8.6.5.

### 8.6.4.1 Fractional flow curves

Fractional flow curves were made based on relative permeabilities and is calculated using the Equation 4.10 in section 4.6. The curves in Figures 8.25 a and b shows the front saturation for each reference core and the average water breakthrough saturation. A tangent is drawn from  $S_{wi}$  to where it meets the fractional flow curve. At the crosspoint where these two meet, the front saturation is 0.64 for CR1 and CR2. This means that the water saturation behind the flood front has a minimum water saturation of 0.64. By extrapolating to  $f_w=1$ , the average water saturation can be found. The average water saturation is 0.68 for both CR1 and CR2.

At the flood front, no water moves a head of the front, while oil and water moves behind the front. Saturations before  $S_{wf}$  is unknown, and only saturations after flood front can be determined (Elraies & Hussin Yunan, 2019). In this case  $COS < S_{wf}$  for both core, so actually the crossover saturation is unknown.

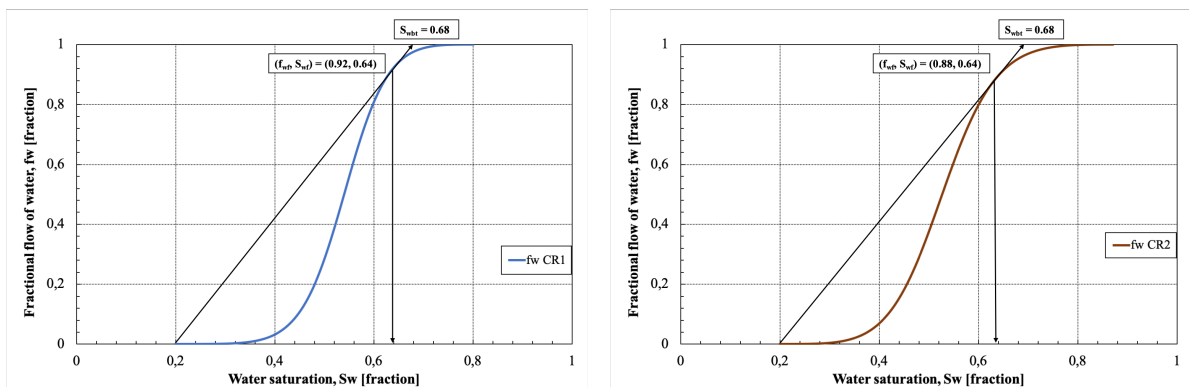


**Figure 8.26:** Fractional flow of water for cores CR1 and CR2 as a function of water saturation.

The recovery factor (RF) can be calculated based on the fractional flow data. At water breakthrough the RF can be calculated by using Equation 4.11.

$$RF_{CR1} = \frac{0.68 - 0.2}{1 - 0.2} = 0.6 \quad (8.7)$$

$$RF_{CR2} = \frac{0.68 - 0.2}{1 - 0.2} = 0.6 \quad (8.9)$$

In the fractionally-wet core (Figure 8.27), the front saturation is 0.56 and average water breakthrough saturation is 0.61. This indicates that the core produces water earlier in the process



compared to the reference cores. The shape of the fractional flow curves is the same for all three cores, with earlier water breakthrough for the fractionally-wet core. Also in this case  $COS < S_{wf}$ , which indicates that crossover saturation is unknown.

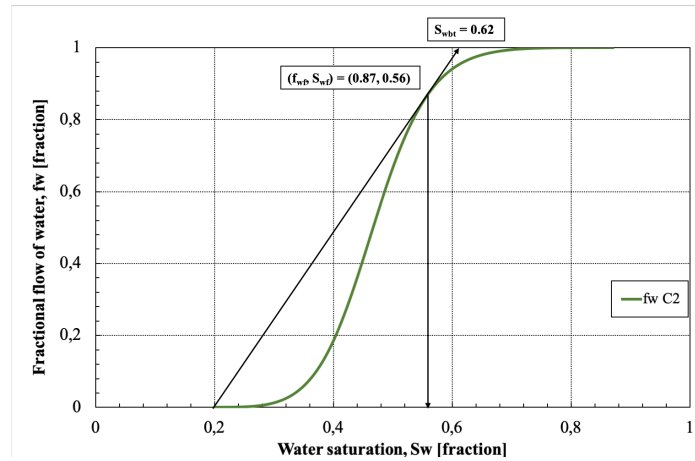


**Figure 8.27:** Fractional flow of water for core C2, as a function of water saturation.

The recovery factor (RF) at water breakthrough is calculated by using equation 4.11.

$$RF_{C2} = \frac{0.62-0.2}{1-0.2} = 0.53 \quad (8.10)$$

### 8.6.5 Comparing with other cores.

In this section a comparison of the other cores are done. From experimental work, core C1 with highest AN, should be the least water-wet core, while core C3 with lowest AN, should be the most water-wet core of the fractionally-wet cores. In Table 13 a comparing of the wetting properties are listed.

**Table 14:** Comparing crossover saturation, front saturation and water breakthrough saturation

Cores					
	CR1	CR2	C1	C2	C3
<b>COS</b>	0.59	0.59	0.57	0.53	0.59
<b>S<sub>wf</sub></b>	0.64	0.64	0.48	0.56	0.64
<b>S<sub>wbt</sub></b>	0.68	0.68	0.62	0.62	0.68
<b>RF at WBT[%]</b>	59	59	53	53	59

In Figure 8.28a, a comparison of relative permeabilities are done for all cores. All cores have crossover saturation (COS) around 0.53-0.59. This indicates water-wet system for all cores. In the right figure fractional flow are plotted for all cores. All cores have relatively low  $k_{ro}(S_{wi})$ , except from core C3 which has a  $k_{ro}(S_{wi})$  at 1. Core C3 is history matched automatic and has similar endpoint values to the automatic history matched reference cores, CR1 and CR2 (see Table 12).

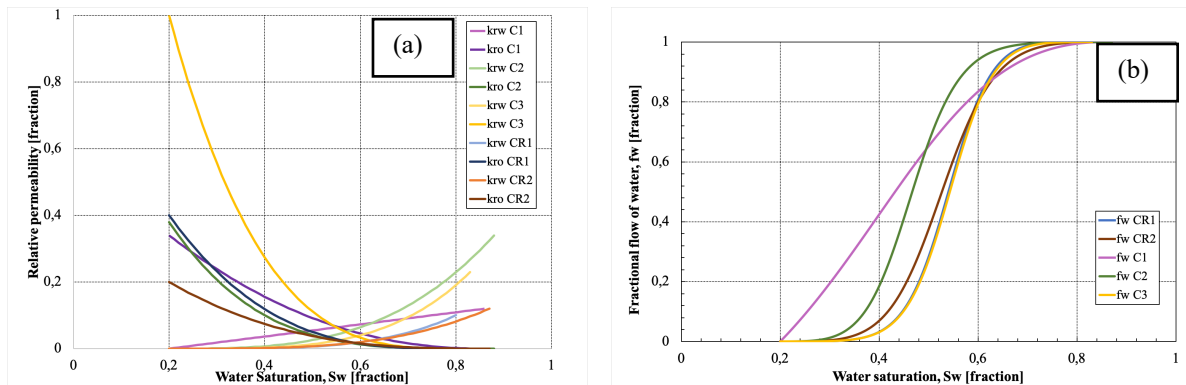


**Figure 8.28:** Comparison of relative permeability curves and fractional flow curves for cores with different initial wettability.

In figure 8.28b, a comparison of the fractional flow curves are done for all cores. All curves, besides C1, has the same shape but at slightly different values. The pink line, which is the least water-wet core is core C1. The blue line, which is the least water-wet core is core C1. Core C1 and C2 have different shapes and front saturation, but the same average water breakthrough. Core C3 and CR1 has the exact same shape and is overlying each other, and this gives the same values for  $S_{wf}$  and  $S_{wbt}$ . All cores, besides C1, has higher  $S_{wf}$  than COS, indicating that crossover saturation is actually unknown. For core C1,  $COS > S_{wf}$ , and one can say that the COS is known.

Figure 8.29 shows a comparison of the capillary pressure curves for all core, and a SI plot of the same cores. The strongly water-wet core are positive, which indicates the strong positive capillary forces imbibing water into the core. Fractionally-wet cores are negative, which is a bit strange since positive capillary forces has been proven in spontaneous imbibition (Figure 8.29 b). Another not observation in Figure 8.29a, is that core C2 (green curve) has highest negative capillary pressure. Compared to what has been observed earlier, core C1 (pink curve) should have the lowest capillary pressure. Compared with the spontaneous imbibition test, core C1 produced less indicating lower capillary forces imbibing water and displacing oil.

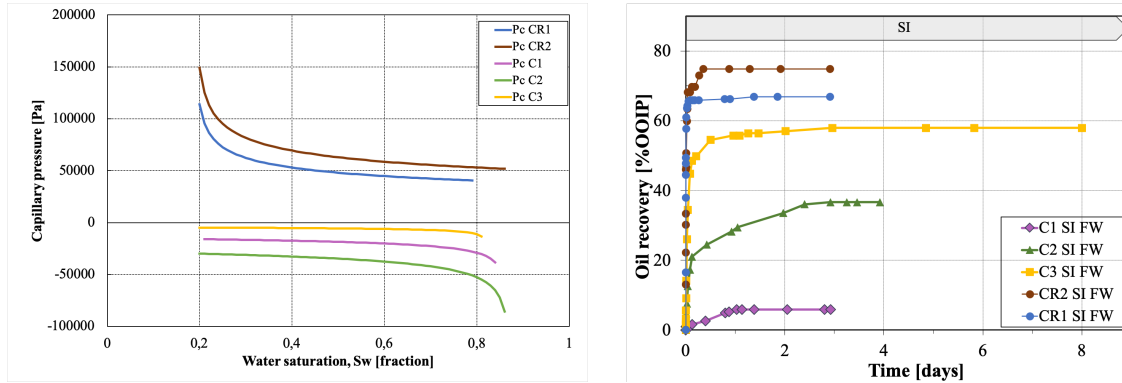


**Figure 8.29:** Comparison of capillary pressure curve for all cores with different initial wettability. Spontaneous imbibition of the same cores to compare capillary forces.

All capillary curves should be positive at some point, as capillary forces are observed in the cores. Core CR2 should have the strongest capillary forces, while core C1 should have the weakest capillary forces.

The results, especially for the capillary pressure curves are not true compared with experimental work. Positive capillary forces has been proven for all cores by spontaneous imbibition. Capillary forces cannot be proven by the simulator, and will not be the main driving force during oil production in the simulator. Wettability alteration in the simulator is represented by changed relative permeability curves. It was observed that the simulator gave small changes in relative permeability curves, and the results are not corresponding with the theory. Low mobility for water for all cores is the main force for later water breakthrough and increased oil recovery.

All experimental results are not taken care of in the modelling. Only 1 rate during waterflooding was used because low production (1-2%OOIP) after changing the rate. High front saturation, cannot distinguish between the different relative permeability curves and at saturations behind  $S_{wi}$  cannot be known. To get better matches for the relative permeability curves and  $S_{or}$ , the end values for production and pressure drop data should be matched instead of the peak. The peak seem to limit the end results. The history matches should not be done manually. The reference cores are matched manually, while the fractionally-wet cores are matched automatically. This can also affect and limits the results and comparison.

## 9 Conclusion and future work

The main object of this thesis was to observe the effect of wettability on waterflooding and relative permeability curves. In order to do so, two very water-wet reference outcrop chalk cores and two fractionally-wet outcrop chalk cores were compared with spontaneous and forced imbibition test, including simulation of experimental data to create relative permeability curves. To see the effect of wettability alteration, two sets of relative permeability curves were needed, one for initial wettability and one after smart water flooding. The experimental and simulated observations led to the following conclusions.

### 9.1 Conclusions

- Crude oil POC from pore surface lowered the IFT between water and M-OIL from 41 to 28 mN/m. IFT has a significant effect on capillary forces in the core, and these will be reduced when IFT is reduced.
- Higher AN reduces the IFT between the crude oil and water, which also reduces the capillary forces and reduces the water-wetness of the core. Higher AN gives lower recovery during spontaneous imbibition.
- Oil recovery by spontaneous imbibition indicated the wettability of the cores. The strongly water-wet cores produced 71± 4% OOIP, while the fractionally-wet cores C5 and C2 produced respectively 37 and 58 % OOIP. The difference in oil recovery is due to mild cleaning of core C2. Mild cleaning has a major effect on oil recovery during spontaneous imbibition. It reduces the effect of POC and increases the IFT.
- Core C5 describes the initial core wettability for both core C2 and C5.
- CWT confirmed that the wettability had changes from very water-wet to medium water-wet.
- Oil recovery by forced imbibition was high for all cores with different initial wetting, from slightly water-wet to very water-wet. The oil recovery was 70±5% OOIP.
- SENDRA did not confirm any effect of the wettability. The relative permeability curves were quite similar for all tested cores. The capillary pressure curve was not as expected or realistic.

### 9.2 Suggestions for future work

For future studies it can be convenient to use the JBN-method to calculate the relative permeability curves based on pressure drop data, at initial conditions and during the injection,

and volume of produced water and oil. The method was tried in this study, but did not work since water breakthrough was unknown. The water breakthrough happened during the night, and it would be convenient to have a camera to detect the water breakthrough at the right time.

Another suggestion is to use crude oil with lower IFT instead of the mineral oil with high IFT. This will lower the capillary forces, and the difference in cores with different wetting may be seen during forced imbibition. Recovery and capillary effects can be tested in a more oil-wet case, and this can be simulated in SENDRA to see if there is larger difference in relative permeability curves for a water-wet and an oil-wet case. Lower the injection rate for very water-wet cores, to observe oil recovery and capillary effects on the core. Will the recovery profile change? Last suggestion is to change oil viscosity and evaluate mobility ratio at different viscosity ratios.

## 10 References

- Abdelgawad, K. Z., & Mahmoud, M. A. (2014). *High-Performance EOR System in Carbonate Reservoirs*. Paper presented at the SPE Saudi Arabia Section Technical Symposium and Exhibition, Al-Khobar, Saudi Arabia. <https://doi.org/10.2118/172182-MS>
- Adamson, A. W., & Gast, A. P. (1997). *Physical chemistry of surfaces* (6th ed. ed.). New York: Wiley.
- Ahmed, T. (2010). *Reservoir engineering handbook* (4th ed. ed.). Amsterdam: Elsevier.
- Ahr, W. M. (2008a). *Geology of carbonate reservoirs : the identification, description, and characterization of hydrocarbon reservoirs in carbonate rocks*.
- Ahr, W. M. (2008b). Summary: Geology of Carbonate Reservoirs. In (pp. 200-254). Hoboken, NJ, USA: Hoboken, NJ, USA: John Wiley & Sons, Inc.
- Alagorni, A., Yaacob, Z., & Nour, A. (2015). *An Overview of Oil Production Stages: Enhanced Oil Recovery Techniques and Nitrogen Injection* (Vol. 6).
- Amott, E. (1959). Observations Relating to the Wettability of Porous Rock. In (pp. 7): Society of Petroleum Engineers.
- Anderson, W. G. (1986a). WETTABILITY LITERATURE SURVEY - PART 2: WETTABILITY MEASUREMENT. *JPT, Journal of Petroleum Technology*, 38(12), 1246-1262.
- Anderson, W. G. (1986b). Wettability Literature Survey- Part 1: Rock/Oil/Brine Interactions and the Effects of Core Handling on Wettability. *Journal of Petroleum Technology*, 38(10), 1125-1144. Retrieved from <https://doi.org/10.2118/13932-PA>. doi:10.2118/13932-PA
- Anderson, W. G. (1987). Wettability Literature Survey Part 5: The Effects of Wettability on Relative Permeability. *Journal of Petroleum Technology*, 39(11), 1453-1468. Retrieved from <https://doi.org/10.2118/16323-PA>. doi:10.2118/16323-PA
- Anderson, W. G. (1987a). Wettability Literature Survey- Part 4: Effects of Wettability on Capillary Pressure. *Journal of Petroleum Technology*, 39(10), 1283-1300. Retrieved from <https://doi.org/10.2118/15271-PA>. doi:10.2118/15271-PA
- Anderson, W. G. (1987b). Wettability Literature Survey-Part 6: The Effects of Wettability on Waterflooding. *Journal of Petroleum Technology*, 39(12), 1605-1622. Retrieved from <https://doi.org/10.2118/16471-PA>. doi:10.2118/16471-PA
- Apostolos, K., Bryan, J., & Taheri, S. (2016). *Fundamentals of fluid flow in porous media* Alberta: University of Calgary.
- Austad, T. (2013). *Water-Based EOR in Carbonates and Sandstones-Chapter 13:New Chemical Understanding of the EOR Potential Using "Smart Water"*: Elsevier Inc.
- Bavière, M. (1991). *Basic concepts in enhanced oil recovery processes* (Vol. 33). London: Published for SCI by Elsevier Applied Science.
- Brooks, R. H., & Corey, A. T. (1964). *Hydraulic properties of porous media*. Fort Collins: Colorado State University, [Hydrology and Water Resources Program].
- Brown, R. J. S., & Fatt, I. (1956). *Measurements Of Fractional Wettability Of Oil Fields' Rocks By The Nuclear Magnetic Relaxation Method*. Paper presented at the Fall Meeting of the Petroleum Branch of AIME, Los Angeles, California. <https://doi.org/10.2118/743-G>
- Buckley, J. S., & Fan, T. (2007). Crude Oil/Brine Interfacial Tensions1. *Petrophysics*, 48(03), 11. Retrieved from <https://doi.org/>.
- Chukwudeme, E. A., Fjelde, I., Abeyasinghe, K. P., & Lohne, A. (2014). Effect of Interfacial Tension on Water/Oil Relative Permeability on the Basis of History Matching to

- Coreflood Data. *SPE Reservoir Evaluation & Engineering*, 17(01), 37-48. Retrieved from <https://doi.org/10.2118/143028-PA>. doi:10.2118/143028-PA
- Craig, F. F. (1971). *The reservoir engineering aspects of waterflooding* (Vol. vol. 3). New York: Henry L. Doherty Memorial Fund of AIME.
- Cuiec, L. (1984). *Rock/Crude-Oil Interactions and Wettability: An Attempt To Understand Their Interrelation*. Paper presented at the SPE Annual Technical Conference and Exhibition, Houston, Texas. <https://doi.org/10.2118/13211-MS>
- Donaldson, E. C., & Alam, W. (2008). *Wettability*. Houston, Tex: Gulf Publ. Co.
- Donaldson, E. C., Thomas, R. D., & Lorenz, P. B. (1969). Wettability Determination and Its Effect on Recovery Efficiency. *Society of Petroleum Engineers Journal*, 9(01), 13-20. Retrieved from <https://doi.org/10.2118/2338-PA>. doi:10.2118/2338-PA
- Drummond, C., & Israelachvili, J. (2002). Surface forces and wettability. *Journal of Petroleum Science and Engineering*, 33(1), 123-133. doi:10.1016/S0920-4105(01)00180-2
- Ehrenberg, S., & Nadeau, P. H. (2005). *Sandstone vs. carbonate petroleum reservoirs: A global perspective on porosity-depth and porosity-permeability relationships* (Vol. 89).
- Elraies, K., & Hussin Yunan, M. (2019). *INVESTIGATION OF WATER BREAKTHROUGH TIME IN NON COMMUNICATING LAYERED RESERVOIR*.
- Fan, T., & Buckley, J. S. (2007). Acid Number Measurements Revisited. *SPE Journal*, 12(04), 496-500. Retrieved from <https://doi.org/10.2118/99884-PA>. doi:10.2118/99884-PA
- Fanchi, J. R. (2010). *Integrated reservoir asset management : principles and best practices*. Amsterdam,Burlington, Mass: Elsevier GPP.
- Fanchi, J. R. (2018). *Principles of applied reservoir simulation*.
- Fathi, S. J. (2012). *Water-Based Enhanced Oil Recovery (EOR) in Carbonate Reservoir*. (Philosophiae Doctor Doctoral), University of Stavanger, Norway,
- Fathi, S. J., Austad, T., & Strand, S. (2010). "Smart Water" as a Wettability Modifier in Chalk: The Effect of Salinity and Ionic Composition. *Energy & Fuels*, 24(4), 2514-2519. Retrieved from <https://doi.org/10.1021/ef901304m>. doi:10.1021/ef901304m
- Fathi, S. J., Austad, T., & Strand, S. (2011). Water-Based Enhanced Oil Recovery (EOR) by "Smart Water": Optimal Ionic Composition for EOR in Carbonates. *Energy & Fuels*, 25(11), 5173-5179. Retrieved from <https://doi.org/10.1021/ef201019k>. doi:10.1021/ef201019k
- Fathi, S. J., Austad, T., & Strand, S. (2012). *Water-Based Enhanced Oil recovery (EOR) by "Smart Water" in Carbonate Reservoirs*. Paper presented at the SPE EOR Conference at Oil and Gas West Asia, Muscat, Oman. <https://doi.org/10.2118/154570-MS>
- Frykman, P. (2001). Spatial variability in petrophysical properties in Upper Maastrichtian chalk outcrops at Stevns Klint, Denmark. *Marine and Petroleum Geology*, 18(10), 1041-1062. Retrieved from <http://www.sciencedirect.com/science/article/pii/S0264817201000435>. doi:[https://doi.org/10.1016/S0264-8172\(01\)00043-5](https://doi.org/10.1016/S0264-8172(01)00043-5)
- Green, D. W., & Willhite, G. P. (1998). *Enhanced oil recovery* (Vol. vol. 6). Richardson, Tex: Henry L. Doherty Memorial Fund of AIME, Society of Petroleum Engineers.
- Herrera, I., & Pinder, G. F. (2012). Enhanced Oil Recovery. In (pp. 149-164). Hoboken, NJ, USA: Hoboken, NJ, USA: John Wiley & Sons, Inc.
- Hopkins, P. A. (2016). *Water-based EOR and initial wettability in carbonates*. (Philosophiae Doctor Doctoral), University of Stavanger, University of Stavanger, Norway.

- Høgnesen, E. J., Strand, S., & Austad, T. (2005). *Waterflooding of preferential oil-wet carbonates: Oil recovery related to reservoir temperature and brine composition*. Paper presented at the SPE Europe/EAGE Annual Conference, Madrid, Spain. <https://doi.org/10.2118/94166-MS>
- Jadhunandan, P. P., & Morrow, N. R. (1995). Effect of Wettability on Waterflood Recovery for Crude-Oil/Brine/Rock Systems. *SPE Reservoir Engineering*, 10(01), 40-46. Retrieved from <https://doi.org/10.2118/22597-PA>. doi:10.2118/22597-PA
- Jardine, D., & Wilshart, J. W. (1982). *Carbonate Reservoir Description*. Paper presented at the International Petroleum Exhibition and Technical Symposium, Beijing, China. <https://doi.org/10.2118/10010-MS>
- Johnson, E. F., Bossler, D. P., & Bossler, V. O. N. (1959). Calculation of Relative Permeability from Displacement Experiments. In (pp. 3): Society of Petroleum Engineers.
- Kootiani, R. C., & Samsuri, A. B. (2012). Analysis Fraction Flow of Water versus Cumulative Oil Recoveries Using Buckley Leverett Method. *World Academy of Science, Engineering and Technology*, 72.
- Lake, L. W. (1989). *Enhanced oil recovery*. Englewood Cliffs, N.J: Prentice Hall.
- Lee, C.-H. (2010). *Experimental Investigation of Spontaneous Imbibition in Fractured Reservoirs*. Paper presented at the SPE Annual Technical Conference and Exhibition, Florence, Italy. <https://doi.org/10.2118/141243-STU>
- Lenormand, R., Lorentzen, K., Maas, J. G., & Ruth, D. (2017). Comparison of Four Numerical Simulators for SCAL Experiments. *Petrophysics*, 58(01), 48-56. Retrieved from <https://doi.org/>.
- Leverett, M. C. (1941). Capillary Behavior in Porous Solids. *Transactions of the AIME*, 142(01), 152-169. Retrieved from <https://doi.org/10.2118/941152-G>. doi:10.2118/941152-G
- Lucia, F. J. (1999). *Carbonate reservoir characterization*. Berlin: Springer.
- Ma, S. M., Zhang, X., Morrow, N. R., & Zhou, X. (1999). Characterization of Wettability From Spontaneous Imbibition Measurements. *Journal of Canadian Petroleum Technology*, 38(13), 8. Retrieved from <https://doi.org/10.2118/99-13-49>. doi:10.2118/99-13-49
- Mazzullo, S. J., Rieke, H. H., & Chilingarian, G. V. (1996). *Carbonate Reservoir Characterization: A Geologic-Engineering Analysis, Part II* (Vol. 44): Elsevier Science.
- Milner, J. (1996). Improved oil recovery in chalk: spontaneous imbibition affected by wettability, rock framework and interfacial tension. *Doctoral, Department of Chemistry, University of Bergen, Norway*.
- Mohammed, M., & Babadagli, T. (2015). Wettability alteration: A comprehensive review of materials/methods and testing the selected ones on heavy-oil containing oil-wet systems. *Advances in Colloid and Interface Science*, 220, 54-77. Retrieved from <http://www.sciencedirect.com/science/article/pii/S0001868615000421>. doi:<https://doi.org/10.1016/j.cis.2015.02.006>
- Moradi, B., Pourafshary, P., Jalali Farahani, F., Mohammadi, M., & Emadi, M. A. (2015). *Application of SiO<sub>2</sub> Nano Particles to Improve the Performance of Water Alternating Gas EOR Process*.
- Morrow, N., & Buckley, J. (2011). Improved Oil Recovery by Low-Salinity Waterflooding. *Journal of Petroleum Technology*, 63(05), 106-112. Retrieved from <https://doi.org/10.2118/129421-JPT>. doi:10.2118/129421-JPT



- Morrow, N. R. (1979). Interplay of Capillary, Viscous And Buoyancy Forces In the Mobilization of Residual Oil. *Journal of Canadian Petroleum Technology*, 18(03), 13. Retrieved from <https://doi.org/10.2118/79-03-03>. doi:10.2118/79-03-03
- Morrow, N. R. (1990). Wettability and Its Effect on Oil Recovery. *Journal of Petroleum Technology*, 42(12), 1476-1484. Retrieved from <https://doi.org/10.2118/21621-PA>. doi:10.2118/21621-PA
- Morrow, N. R., & Mason, G. (2001). *Recovery of oil by spontaneous imbibition* (Vol. 6).
- Mousavi, M. A., Prodanovic, M., & Jacobi, D. (2012). New Classification of Carbonate Rocks for Process-Based Pore-Scale Modeling. *SPE Journal*, 18(02), 243-263. Retrieved from <https://doi.org/10.2118/163073-PA>. doi:10.2118/163073-PA
- Pierre, A., Lamarche, J. M., Mercier, R., Foissy, A., & Persello, J. (1990). CALCIUM AS POTENTIAL DETERMINING ION IN AQUEOUS CALCITE SUSPENSIONS. *Journal of Dispersion Science and Technology*, 11(6), 611-635. Retrieved from <https://doi.org/10.1080/01932699008943286>. doi:10.1080/01932699008943286
- Punternvold, T. (2008). *Waterflooding of Carbonate reservoirs: EOR by wettability alteration*. (Philosophiae Doctor Doctoral), University of Stavanger,
- Punternvold, T., & Austad, T. (2008). Injection of seawater and mixtures with produced water into North Sea chalk formation: Impact of fluid–rock interactions on wettability and scale formation. *Journal of Petroleum Science and Engineering*, 63(1), 23-33. Retrieved from <http://www.sciencedirect.com/science/article/pii/S0920410508000636>. doi:<https://doi.org/10.1016/j.petrol.2008.07.010>
- Punternvold, T., Strand, S., & Austad, T. (2007). New Method To Prepare Outcrop Chalk Cores for Wettability and Oil Recovery Studies at Low Initial Water Saturation. *Energy & Fuels*, 21(6), 3425-3430. Retrieved from <https://doi.org/10.1021/ef700323c>. doi:10.1021/ef700323c
- Radenkovic, K. (2019). *Effect of Wettability on Waterflooding and Relative permeability at quite Water-wet conditions*. (Master), University of Stavanger,
- Rao, D. N. (1999). Wettability Effects in Thermal Recovery Operations. *SPE Reservoir Evaluation & Engineering*, 2(05), 420-430. Retrieved from <https://doi.org/10.2118/57897-PA>. doi:10.2118/57897-PA
- Rapoport, L. A., & Leas, W. J. (1953). Properties of Linear Waterfloods. *Journal of Petroleum Technology*, 5(05), 139-148. Retrieved from <https://doi.org/10.2118/213-G>. doi:10.2118/213-G
- Raza, S. H., Treiber, L. E., & Archer, D. L. (1968). Wettability of reservoir rocks and its evaluation. *Prod. Mon.; (United States)*, Medium: X; Size: Pages: 2-4, 6-7.
- RezaeiDoust, A., Punternvold, T., Strand, S., & Austad, T. (2009). Smart Water as Wettability Modifier in Carbonate and Sandstone: A Discussion of Similarities/Differences in the Chemical Mechanisms. *Energy & Fuels*, 23(9), 4479-4485. Retrieved from <https://doi.org/10.1021/ef900185q>. doi:10.1021/ef900185q
- Salathiel, R. A. (1973). Oil Recovery by Surface Film Drainage In Mixed-Wettability Rocks. *Journal of Petroleum Technology*, 25(10), 1216-1224. Retrieved from <https://doi.org/10.2118/4104-PA>. doi:10.2118/4104-PA
- Shariatpanahi, S. F., Hopkins, P., Aksulu, H., Strand, S., Punternvold, T., & Austad, T. (2016). Water Based EOR by Wettability Alteration in Dolomite. *Energy & Fuels*, 30(1), 180-187. Retrieved from <https://doi.org/10.1021/acs.energyfuels.5b02239>. doi:10.1021/acs.energyfuels.5b02239

- Shariatpanahi, S. F., Strand, S., & Austad, T. (2011). Initial Wetting Properties of Carbonate Oil Reservoirs: Effect of the Temperature and Presence of Sulfate in Formation Water. *Energy & Fuels*, 25(7), 3021-3028. Retrieved from <https://doi.org/10.1021/ef200033h>. doi:10.1021/ef200033h
- Shimoyama, A., & Johns, W. D. (1972). Formation of alkanes from fatty acids in the presence of CaCO<sub>3</sub>. *Geochimica et Cosmochimica Acta*, 36(1), 87-91. Retrieved from <http://www.sciencedirect.com/science/article/pii/0016703772901226>. doi:[https://doi.org/10.1016/0016-7037\(72\)90122-6](https://doi.org/10.1016/0016-7037(72)90122-6)
- Skjæveland, S. M., Siqueland, L. M., Kjosavik, A., Thomas, W. L. H., & Virnovsky, G. A. (2000). Capillary Pressure Correlation for Mixed-Wet Reservoirs. *SPE Reservoir Evaluation & Engineering*, 3(01), 60-67. Retrieved from <https://doi.org/10.2118/60900-PA>. doi:10.2118/60900-PA
- Speight, J. G. (2017). Carbonate Reservoir. In *Rules of Thumb for Petroleum Engineers* (pp. 115-115). Hoboken, NJ, USA: Hoboken, NJ, USA: John Wiley & Sons, Inc.
- Springer, N., Korsbech, U., & Aage, H. K. (2003). Resistivity index measurement without the porous plate: A desaturation technique based on evaporation produces uniform water saturation profiles and more reliable results for tight North Sea chalk. *Paper presented at the International Symposium of the Society of Core Analysts Pau, France*.
- Standnes, D. C., & Austad, T. (2000). Wettability alteration in chalk: 1. Preparation of core material and oil properties. *Journal of Petroleum Science and Engineering*, 28(3), 111-121. Retrieved from <http://www.sciencedirect.com/science/article/pii/S0920410500000838>. doi:[https://doi.org/10.1016/S0920-4105\(00\)00083-8](https://doi.org/10.1016/S0920-4105(00)00083-8)
- Strand, S., J. Høgnesen, E., & Austad, T. (2006). *Wettability alteration of carbonates—Effects of potential determining ions (Ca<sup>2+</sup> and SO<sub>4</sub><sup>2-</sup>) and temperature* (Vol. 275).
- Strand, S., Standnes, D. C., & Austad, T. (2006). New wettability test for chalk based on chromatographic separation of SCN<sup>-</sup> and SO<sub>4</sub><sup>2-</sup>. *Journal of Petroleum Science and Engineering*, 52(1), 187-197. Retrieved from <http://www.sciencedirect.com/science/article/pii/S0920410506000660>. doi:<https://doi.org/10.1016/j.petrol.2006.03.021>
- Taber, J. J., Martin, F. D., & Seright, R. S. (1997). EOR Screening Criteria Revisited - Part 1: Introduction to Screening Criteria and Enhanced Recovery Field Projects. *SPE Reservoir Engineering*, 12(03), 189-198. Retrieved from <https://doi.org/10.2118/35385-PA>. doi:10.2118/35385-PA
- Torrijos, I. D. P., Sæby, K. G., Strand, S., & Puntervold, T. (2019). Impact of Temperature on Wettability Alteration by Smart Water in Chalk. *EAGE*.
- Torsaeter, O. (1984). *An Experimental Study of Water Imbibition in Chalk From the Ekofisk Field*. Paper presented at the SPE Enhanced Oil Recovery Symposium, Tulsa, Oklahoma. <https://doi.org/10.2118/12688-MS>
- Treiber, L. E., Archer, D. L., & Owens, W. W. (1972). A Laboratory Evaluation of the Wettability of Fifty Oil-Producing Reservoirs. *Society of Petroleum Engineers Journal*, 12(06), 531-540. Retrieved from <https://doi.org/10.2118/3526-PA>. doi:10.2118/3526-PA
- Wade, J. E. (1971). *Some Practical Aspects of Waterflooding*. Paper presented at the 8th World Petroleum Congress, Moscow, USSR. <https://doi.org/>
- Wathne, A. K. (2019). *Effect of Wettability on Waterflooding and Relative permeability at Slightly water-wet conditions*. (Master thesis), University of Stavanger,

- Webb, K. J., Black, C. J. J., & Tjetland, G. (2005). *A Laboratory Study Investigating Methods for Improving Oil Recovery in Carbonates*. Paper presented at the International Petroleum Technology Conference, Doha, Qatar. <https://doi.org/10.2523/IPTC-10506-MS>
- Zhang, P., Tweheyo, M. T., & Austad, T. (2007). Wettability alteration and improved oil recovery by spontaneous imbibition of seawater into chalk: Impact of the potential determining ions Ca<sup>2+</sup>, Mg<sup>2+</sup>, and SO<sub>4</sub><sup>2-</sup>. *Colloids and Surfaces A: Physicochemical and Engineering Aspects*, 301(1), 199-208. Retrieved from <http://www.sciencedirect.com/science/article/pii/S0927775706009915>. doi:<https://doi.org/10.1016/j.colsurfa.2006.12.058>
- Zolotukhin, A. B., & Ursin, J.-R. (2000). *Introduction to petroleum reservoir engineering*. Kristiansand: Høyskoleforl.

## Appendix A: Chemicals

### A.1 Acid number solutions

**Table 15:** Chemicals for AN measurements

<b>Solution</b>	<b>Chemicals</b>	<b>Formula</b>	<b>Description</b>
<b>Titrant</b>	KOH (>85%) 2-propanol	KOH CH <sub>3</sub> CHOHCH <sub>3</sub>	2.8 g KOH (>85%) dilute to 1000 ml with 2-propanol (CH <sub>3</sub> CHOHCH <sub>3</sub> )
<b>Spiking solution</b>	Stearic acid Acid titration solvent	CH <sub>3</sub> (CH <sub>2</sub> ) <sub>16</sub> COOH	0.5 g Stearic Acid – CH <sub>3</sub> (CH <sub>2</sub> ) <sub>16</sub> COOH dilute to 100 ml with Acid titration solvent
<b>Standard solution</b>	Potassium Hydrogen Phtalate, KHP DI water	HOOC C <sub>6</sub> H <sub>4</sub> COOK	0.2 g Potassium Hydrogen Phtalate, KHP diluted to 500 ml with DI water
<b>Titration solvent</b>	DI water 2-propanol Toulene	CH <sub>3</sub> CHOHCH <sub>3</sub> C <sub>6</sub> H <sub>5</sub> CH <sub>3</sub>	6 ml DI water dilute with 494 ml 2-propanol and with 500 ml Toulene
<b>Electrode/ Electrolyte</b>	Potassium chloride DI water	KCl	Mettler DG-114 Electrode 3 M KCl in DI water

### A.2 Base number solutions

**Table 16:** Chemicals for BN measurements

<b>Solution</b>	<b>Chemicals</b>	<b>Formula</b>	<b>Description</b>
<b>Titrant</b>	Perchloric Acid (70%) Acetic Anhydride Acetic Acid	HClO <sub>4</sub> (70%) (CH <sub>3</sub> CO) <sub>2</sub> O CH <sub>3</sub> COOH	5 ml 70% Perchloric Acid (HClO <sub>4</sub> ) 15 ml Acetic Anhydride ((CH <sub>3</sub> CO) <sub>2</sub> O) dilute to 1000 ml with Acetic Acid (CH <sub>3</sub> COOH)
<b>Spiking solution</b>	Quinoline Decane	C <sub>9</sub> H <sub>7</sub> N CH <sub>3</sub> (CH <sub>2</sub> ) <sub>8</sub> CH <sub>3</sub>	0.5 Quinoline (C <sub>9</sub> H <sub>7</sub> N) dilute to 100 ml with Decane (C <sub>10</sub> H <sub>22</sub> )
<b>Standard solution</b>	Potassium Hydrogen Phtalate, KHP Acetic Acid	HOOC C <sub>6</sub> H <sub>4</sub> COOK CH <sub>3</sub> COOH	0.2 g Potassium Hydrogen Phtalate, KHP diluted to 250 ml with Acetic Acid CH <sub>3</sub> COOH
<b>Titration solvent</b>	Methyl Isobutyl Ketone, MIKB	(CH <sub>3</sub> ) <sub>2</sub> CHCH <sub>2</sub> COCH <sub>3</sub>	Methyl Isobutyl Keton (MIBK) ((CH <sub>3</sub> ) <sub>2</sub> CHCH <sub>2</sub> COCH <sub>3</sub> )
<b>Electrode/ Electrolyte</b>	Sodium Perchlorate, (solid) 2-propanol	NaClO <sub>4</sub> (S) CH <sub>3</sub> CHOHCH <sub>3</sub>	Mettler DG-113 Electrode Electrolyte: Saturated Sodium Perchlorate, (NaClO <sub>4</sub> (s)), in 2-propanol

## Appendix B: Experimental data

### B.1 Spontaneous imbibition data

*Table 17:* SI data, reference core, CR1

Time (min)	Produced oil (ml)	OOIP%
0	0.0	0.00
1	5.0	16.47
2	11.5	37.88
3	13.5	44.47
4	14.5	47.76
5	15.0	49.41
10	17.5	57.64
15	18.5	60.94
30	19.3	63.57
45	19.5	64.23
75	19.9	65.55
135	20.0	65.88
195	20.0	65.88
255	20.0	65.88
375	20.0	65.88
1125	20.1	66.21
1281	20.1	66.21
1981	20.3	66.86
2663	20.3	66.86
4200	20.3	66.86

*Table 18:* SI data, reference core, CR2

Time (min)	Produced oil (ml)	OOIP%
0	0.0	0.00
1	4.1	13.00
2	7.0	22.19
3	9.5	30.12
4	10.5	33.29
5	14.5	45.97
10	14.7	46.60
15	16.0	50.72
30	18.9	59.92
45	20.0	63.40
60	21.5	68.16
120	21.5	68.16
180	22.0	69.74
268	22.0	69.74
388	23.0	72.91
508	23.6	74.82
1258	23.6	74.82
1858	23.6	74.82
2760	23.6	74.82
4200	23.6	74.82

**Table 19:** SI data, core C2

<b>Time (min)</b>	<b>Produced oil (ml)</b>	<b>OOIP%</b>
0	0.0	0.00
1	1.0	3.1
2	1.8	5.6
3	2.9	9.1
4	3.6	11.3
5	4.0	12.5
10	8.6	26.9
15	10.0	31.3
30	11.5	36.0
60	14.5	45.4
120	15.6	48.9
180	16.2	50.7
412	16.8	52.6
605	17.1	53.5
1532	17.6	55.1
1672	17.6	55.1
1792	17.6	55.1
2917	17.7	55.4
3452	17.9	56.1
4250	17.9	56.1
4524	18.1	56.7
5934	18.4	57.6
7199	18.4	57.6
8639	18.4	57.6

**Table 20:** SI data, core C5

<b>Time (min)</b>	<b>Produced oil (ml)</b>	<b>OOIP%</b>
0	0.0	0.0
1	0.2	0.6
2	0.2	0.6
3	0.3	0.9
4	0.4	1.3
5	0.5	1.6
10	1.0	3.1
15	1.5	4.7
30	2.4	7.5
60	4.0	12.5
120	5.5	17.2
180	6.7	21.0
605	7.8	24.4
1330	9.0	28.2
1503	9.4	29.5
2830	10.7	33.5
3456	11.5	36.0
4210	11.7	36.7
4680	11.7	36.7
4980	11.7	36.7
5640	11.7	36.7

## B.2 Forced imbibition data

Table 21: FI, reference core CR1

Time	Time (PV)	Produced oil (ml)	OOIP%	$\Delta P$ (mbar)	Time	Time (PV)	Produced oil (ml)	OOIP%	$\Delta P$ (mbar)
13:20	0.00	0.00	0.0	142	17:08	2.15	20.40	67.9	1028
13:36	0.01	0.10	0.3	135	20:04	2.28	20.40	67.9	1014
13:54	0.02	0.60	2.0	138	22:06	2.36	20.40	67.9	1008
14:15	0.04	1.20	4.0	133	10:04	2.86	20.40	67.9	959
14:32	0.05	1.50	5.0	134	13:57	3.02	20.40	67.9	947
14:43	0.06	1.80	6.0	131	18:08	3.19	20.50	68.3	929
15:00	0.07	2.10	7.0	130	22:00	3.35	20.50	68.3	916
15:30	0.09	3.00	10.0	129	08:29	3.79	20.50	68.3	875
15:58	0.11	3.60	12.0	134	12:05	3.94	20.50	68.3	863
16:29	0.13	4.40	14.7	137	15:30	4.08	20.50	68.3	848
16:58	0.15	5.20	17.3	141	09:13	4.82	20.50	68.3	777
17:27	0.17	6.00	20.0	149	12:06	4.94	20.50	68.3	776
18:00	0.19	6.60	22.0	156	15:31	5.08	20.50	68.3	766
18:36	0.22	7.60	25.3	173	08:59	5.80	20.50	68.3	712
18:55	0.23	8.00	26.6	185	13:40	6.00	20.50	68.3	714
19:24	0.25	8.80	29.3	205	15:41	6.08	20.50	68.3	692
19:54	0.27	9.60	32.0	239	18:23	6.20	20.50	68.3	668
20:25	0.29	10.40	34.6	282	20:10	6.27	20.50	68.3	662
20:59	0.32	11.20	37.3	352	06:25	6.70	20.50	68.3	662
21:20	0.33	11.80	39.3	413	06:59	6.72	20.50	68.3	660
21:54	0.36	12.70	42.3	677	08:26	6.78	20.50	68.3	650
22:15	0.37	13.20	44.0	1350	08:31	6.78	20.50	68.3	651
08:24	0.79	18.60	62.0	1252	08:45	6.79	20.50	68.3	658
09:15	0.83	18.60	62.0	1232	09:09	6.81	20.50	68.3	659
10:10	0.87	18.80	62.6	1227	09:59*	6.84	20.55	68.4	1312
11:02	0.90	18.80	62.6	1209	10:32	6.87	20.60	68.6	1288
12:10	0.95	19.00	63.3	1194	11:06	6.89	20.60	68.6	1258
13:00	0.98	19.20	63.9	1180	11:32	6.91	20.60	68.6	1257
13:37	1.01	19.30	64.3	1178	11:57	6.93	20.60	68.6	1269
14:05	1.03	19.30	64.3	1177	13:15	6.98	20.60	68.6	1223
14:55	1.06	19.40	64.6	1167	14:33	7.03	20.60	68.6	1219
17:09	1.16	19.50	64.9	1151	15:17	7.06	20.60	68.6	1208
19:00	1.23	19.60	65.3	1150	15:58	7.09	20.60	68.6	1187
20:30	1.30	19.60	65.3	1132	17:59	7.18	20.60	68.6	1172
22:30	1.38	19.70	65.6	1116	19:08	7.22	20.60	68.6	1170
07:59	1.77	19.90	66.3	1060	19:49	7.25	20.60	68.6	1171
10:53	1.89	19.95	66.4	1056	20:43	7.29	20.60	68.6	1170
14:10	2.03	20.00	66.6	1042					

\* Changed rate, 4 PV/day

**Table 22:** FI, reference core CR2

Time	Time (PV)	Produced oil (ml)	OOIP%	$\Delta P$ (mbar)	Time	Time (PV)	Produced oil (ml)	OOIP%	$\Delta P$ (mbar)
13:26	0.00	0.00	0.0	148	20:22	2.27	22.50	71.8	985
13:39	0.01	0.20	0.6	150	20:47	2.29	22.50	71.8	979
14:15	0.03	1.00	3.2	144	08:37	2.78	22.50	71.8	945
14:33	0.05	1.60	5.1	140	09:02	2.80	22.50	71.8	944
14:55	0.06	2.20	7.0	139	10:45	2.87	22.50	71.8	932
15:30	0.09	3.00	9.6	136	13:37	2.99	22.50	71.8	932
16:16	0.12	4.30	13.7	133	15:35	3.07	22.50	71.8	922
17:37	0.17	6.40	20.4	127	19:00	3.21	22.50	71.8	920
18:10	0.20	7.20	23.0	133	22:10	3.34	22.50	71.8	911
18:36	0.21	7.80	24.9	139	00:00	3.41	22.50	71.8	909
18:59	0.23	8.50	27.1	148	08:00	3.75	22.50	71.8	893
19:30	0.25	9.30	29.7	167	10:00	3.83	22.50	71.8	889
20:00	0.27	10.10	32.2	190	12:00	3.91	22.50	71.8	884
20:42	0.30	11.10	35.4	242	13:22	3.97	22.50	71.8	868
21:10	0.32	11.90	38.0	295	09:53	4.82	22.50	71.8	830
21:45	0.34	12.70	40.5	388	08:18	5.74	22.50	71.8	828
08:10	0.77	20.00	63.8	1186	08:44	5.76	22.50	71.8	828
08:59	0.81	20.60	65.7	1177	09:27*	5.79	22.50	71.8	1342
10:02	0.85	20.80	66.4	1169	10:56	5.85	22.50	71.8	1297
10:57	0.89	20.90	66.7	1154	13:43	5.97	22.50	71.8	1258
12:00	0.93	21.00	67.0	1143	15:20	6.03	22.60	72.1	1256
13:28	0.99	21.20	67.7	1137	15:38	6.05	22.60	72.1	1250
15:11	1.06	21.60	68.9	1115	08:25	6.74	22.60	72.1	1202
17:35	1.16	21.60	68.9	1101	09:46	6.80	22.60	72.1	1208
19:00	1.22	21.60	68.9	1094	10:10	6.81	22.60	72.1	1202
20:21	1.28	21.60	68.9	1086	12:39	6.92	22.60	72.1	1202
09:14	1.81	22.20	70.9	1023	15:22	7.03	22.60	72.1	1195
11:00	1.88	22.20	70.9	1018	17:21	7.11	22.60	72.1	1194
13:18	1.98	22.20	70.9	1011	19:15	7.19	22.60	72.1	1195
14:58	2.05	22.20	70.9	1001	21:45	7.29	22.60	72.1	1195
15:58	2.09	22.20	70.9	999	01:55	7.46	22.60	72.1	1194

\* Changed rate, 4PV/day



**Table 23:** FI core C2

<b>Time</b>	<b>Time (PV)</b>	<b>Produced oil (ml)</b>	<b>OOIP%</b>	<b>ΔP (mBar)</b>	<b>Time</b>	<b>Time (PV)</b>	<b>Produced oil (ml)</b>	<b>OOIP%</b>	<b>ΔP (mBar)</b>
12:15	0.00	0.00	0.0	662	12:30	2.04	21.00	66.0	769
12:30	0.01	0.30	0.9	659	13:47	2.09	21.00	66.0	753
12:46	0.02	0.60	1.9	652	14:42	2.13	21.00	66.0	763
13:00	0.03	1.10	3.5	647	16:13	2.19	21.00	66.0	749
13:41	0.06	2.10	6.6	647	18:02	2.27	21.00	66.0	743
14:33	0.10	3.40	10.7	659	19:15	2.32	21.00	66.0	742
14:47	0.11	3.90	12.2	661	20:50	2.39	21.10	66.3	740
15:16	0.13	4.80	15.1	671	08:43	2.89	21.40	67.2	736
15:41	0.14	5.60	17.6	682	09:56	2.94	21.40	67.2	724
16:07	0.16	6.10	19.2	692	11:15	3.00	21.40	67.2	723
16:32	0.18	6.80	21.4	706	13:28	3.09	21.40	67.2	723
17:00	0.20	7.50	23.6	724	14:54	3.15	21.50	67.5	712
18:06	0.25	9.30	29.2	785	15:35	3.18	21.50	67.5	712
18:29	0.26	10.00	31.4	802	18:09	3.29	21.60	67.8	703
19:00	0.28	10.80	33.9	831	21:54	3.45	21.60	67.8	702
19:28	0.30	11.50	36.1	870	22:41	3.48	21.60	67.8	698
20:00	0.33	12.40	38.9	916	08:36	3.90	21.60	67.8	696
20:33	0.35	13.30	41.8	976	10:28	3.98	21.60	67.8	695
21:00	0.37	14.00	44.0	1014	11:00	4.00	21.60	67.8	695
21:30	0.39	14.90	46.8	1023	12:19	4.06	21.60	67.8	695
22:00	0.41	15.50	48.7	1029	12:30*	4.06	21.60	67.8	1155
08:30	0.85	19.20	60.3	838	13:36	4.11	21.80	68.5	1489
09:34	0.90	19.40	60.9	870	14:18	4.14	21.80	68.5	1441
10:08	0.92	19.50	61.2	864	15:00	4.17	21.90	68.8	1409
10:38	0.94	19.50	61.2	875	16:00	4.21	21.90	68.8	1362
11:15	0.97	19.50	61.2	876	19:48	4.37	22.00	69.1	1261
11:55	1.00	19.60	61.6	849	22:30	4.48	22.10	69.4	1227
13:03	1.05	19.60	61.6	842	02:00	4.63	22.10	69.4	1200
15:01	1.13	19.70	61.9	829	03:50	4.71	22.10	69.4	1195
16:58	1.21	19.90	62.5	831	05:12	4.77	22.10	69.4	1168
18:22	1.27	20.00	62.8	824	07:04	4.85	22.10	69.4	1162
19:08	1.30	20.20	63.4	823	09:19	4.94	22.10	69.4	1140
19:59	1.34	20.20	63.4	815	10:30	4.99	22.10	69.4	1140
20:51	1.38	20.20	63.4	829	12:50	5.09	22.10	69.4	1136
08:26	1.86	20.60	64.7	792	13:40	5.13	22.10	69.4	1136
10:58	1.97	20.90	65.6	775	14:30	5.16	22.10	69.4	1136

\* Changed rate, 4PV/day

**Table 24:** FI core C5

<b>Time</b>	<b>Time (PV)</b>	<b>Produced oil (ml)</b>	<b>OOIP%</b>	<b>ΔP (mBar)</b>	<b>Time</b>	<b>Time (PV)</b>	<b>Produced oil [ml]</b>	<b>OOIP%</b>	<b>ΔP (mBar)</b>
12:05	0.00	11.70	36.7	999	12:54	3.07	17.10	53.6	670
12:16	0.01	11.90	37.3	1003	09:11	3.92	17.20	53.9	642
12:40	0.02	12.20	38.2	968	13:39	4.11	17.30	54.2	641
12:57	0.04	12.50	39.2	974	19:27	4.35	17.30	54.2	638
13:32	0.06	12.80	40.1	956	06:06	4.80	17.30	54.2	637
14:02	0.08	13.30	41.7	925	09:16	4.93	17.30	54.2	637
14:30	0.10	13.50	42.3	920	10:24	4.98	17.30	54.2	637
15:00	0.12	13.90	43.5	916	10:25*	4.98	17.30	54.2	864
15:30	0.14	14.10	44.2	905	11:20	5.02	18.60	58.3	1909
16:00	0.16	14.30	44.8	880	12:08	5.05	18.90	59.2	1840
17:06	0.21	14.60	45.7	875	13:08	5.10	19.00	59.5	1779
17:30	0.23	14.70	46.1	848	13:55	5.13	19.10	59.8	1751
18:31	0.27	14.80	46.4	853	15:00	5.18	19.20	60.2	1745
19:24	0.31	15.00	47.0	838	16:04	5.22	19.30	60.5	1728
20:21	0.35	15.10	47.3	820	17:29	5.28	19.40	60.8	1702
21:29	0.40	15.30	47.9	805	22:08	5.48	19.70	61.7	1635
22:00	0.42	15.30	47.9	805	22:39	5.50	19.70	61.7	1628
08:02	0.84	15.60	48.9	772	06:09	5.81	20.80	65.2	1548
09:01	0.88	15.60	48.9	771	08:28	5.91	20.80	65.2	1528
11:02	0.97	15.80	49.5	775	10:47	6.01	20.80	65.2	1511
13:00	1.05	16.00	50.1	772	11:22	6.03	20.80	65.2	1500
16:05	1.18	16.20	50.8	755	14:09	6.15	20.80	65.2	1479
18:30	1.28	16.30	51.1	751	17:06	6.27	20.80	65.2	1444
21:35	1.41	16.40	51.4	740	20:07	6.40	20.80	65.2	1406
10:18	1.95	16.50	51.7	713	23:38	6.55	20.80	65.2	1396
19:13	2.32	16.70	52.3	693	02:38	6.68	20.80	65.2	1375
22:12	2.45	16.80	52.6	673	04:28	6.75	20.80	65.2	1355
08:23	2.88	16.90	52.9	678	06:41	6.85	20.80	65.2	1344
09:35	2.93	17.00	53.3	678	08:32	6.92	20.80	65.2	1344
11:11	2.99	17.00	53.3	674	09:30	6.96	20.80	65.2	1344

\* Changed rate, 4PV/day

### B.3 pH measurements

*Table 25:* pH measurements from reference core, CR1

<b>PV corrected</b>	<b>pH of effluent</b>
1.06	7.98
1.30	8.02
2.28	8.01
3.19	7.83
4.94	7.76

*Table 26:* pH measurements from reference core, CR2

<b>PV corrected</b>	<b>pH of effluent</b>
0.34	7.43
1.28	7.82
2.27	7.69
2.80	7.73
3.97	7.75
5.76	7.76
6.05	8.28
6.81	8.24

*Table 27:* pH measurements from core C2

<b>PV corrected</b>	<b>pH of effluent</b>
0.85	7.34
1.30	7.56
1.86	7.55
2.39	7.56
2.89	7.57
3.98	7.41

*Table 28:* pH measurements from core C5

<b>PV corrected</b>	<b>pH of effluent</b>
0.84	7.74
1.41	7.68
1.95	7.55
2.32	7.85
2.88	7.75
3.92	7.75
4.93	7.61

### B.3 Chromatography data

**Table 29:** Chromatography data for reference core, CR1

Thiocyanade			Sulfate		
PV	C/C <sub>0</sub>	Area under curve	PV	C/C <sub>0</sub>	Area under curve
0,63	0,00000	0,00000	0,71	0,00000	0,00000
0,71	0,37838	0,01526	0,79	0,02218	0,00089
0,79	0,59846	0,03940	0,87	0,11290	0,00547
0,87	0,78378	0,05593	0,95	0,33871	0,01815
0,95	0,89189	0,06736	1,04	0,43347	0,03135
1,04	0,92664	0,07383	1,12	0,62500	0,04241
1,12	0,97683	0,07626	1,20	0,71976	0,05442
1,20	0,98649	0,07945	1,28	0,80444	0,06147
1,28	0,98842	0,07965	1,36	0,92944	0,07016
1,36	0,99421	0,08023	1,44	0,87298	0,07245
1,44	0,99614	0,08001	1,52	0,92540	0,07205
1,52	0,99228	0,07966	1,60	0,98185	0,07743
1,60	0,98263	0,08018			

Total area thiocyanade	Total area sulfate	Area in between two curves
<b>0,80721</b>	<b>0,50625</b>	<b>0,301</b>

**Table 30:** Chromatography data for reference core, CR2

Thiocyanade			Sulfate		
PV	C/C <sub>0</sub>	Area under curve	PV	C/C <sub>0</sub>	Area under curve
0,60	0.00000	0.00000	0,76	0.00000	0.00000
0,68	0,15909	0,00607	0,83	0,04320	0,00167
0,76	0,43409	0,02285	0,91	0,15335	0,00754
0,83	0,69545	0,04379	0,99	0,34557	0,01922
0,91	0,85455	0,05950	1,06	0,54644	0,03458
0,99	0,91136	0,06801	1,14	0,74946	0,04975
1,06	0,93409	0,07155	1,22	0,79050	0,05951
1,14	0,96364	0,07285	1,30	0,88985	0,06493
1,22	0,97727	0,07500	1,37	0,99784	0,07295
1,30	0,98864	0,07597			
1,37	1,02273	0,07772			

Total area thiocyanade	Total area sulfate	Area in between two curves
<b>0,57331</b>	<b>0,31015</b>	<b>0,263</b>

**Table 31:** Chromatography data for core C2

Thiocyanade		
PV	C/C0	Area under curve
0,50	0.00000	0.00000
0,57	0,03138	0,00116
0,65	0,12134	0,00565
0,72	0,32636	0,01646
0,80	0,60669	0,03454
0,87	0,80544	0,05210
0,94	0,89331	0,06268
1,02	0,93724	0,06777
1,09	0,98536	0,07118
1,17	0,99163	0,07344
1,24	0,98536	0,07320
1,31	0,99372	0,07352

Sulfate		
PV	C/C0	Area under curve
0,80	0.00000	0.00000
0,87	0,32759	0,01209
0,94	0,45690	0,02895
1,02	0,68319	0,04221
1,09	0,74353	0,05282
1,17	0,83190	0,05853
1,24	0,84052	0,06192
1,31	1.00000	0,06837

Total area thiocyanade	Total area sulfate	Area in between two curves
<b>0,53172</b>	<b>0,32488</b>	<b>0,207</b>

**Table 32:** Chromatography data for core C5

Thiocyanade		
PV	C/C0	Area under curve
0,56	0,00000	0,00000
0,64	0,27148	0,01036
0,71	0,47070	0,02841
0,79	0,71289	0,04531
0,87	0,88086	0,06121
0,94	0,94141	0,06999
1,02	0,93555	0,07162
1,10	0,93359	0,07109
1,17	0,96289	0,07308
1,25	0,98828	0,07543
1,33	0,98047	0,07463
1,40	1,00000	0,07682
1,48	0,98047	0,07706

Sulfate		
PV	C/C0	Area under curve
0,64	0,00000	0,00000
0,71	0,05226	0,00200
0,79	0,12114	0,00664
0,87	0,27316	0,01514
0,94	0,47506	0,02874
1,02	0,72447	0,04577
1,10	0,73872	0,05565
1,17	0,80285	0,05940
1,25	0,79335	0,06171
1,33	0,90261	0,06429
1,40	0,95249	0,07195
1,48	0,98812	0,07551

Total area thiocyanade	Total area sulfate	Area in between two curves
<b>0,73501</b>	<b>0,48680</b>	<b>0,248</b>

## Appendix C: Input parameters in SENDRA

### C1: Reference cores

*Table 33:* Input data for all cores

<b>Core ID</b>	
<b>Fluid system</b>	Water-oil
<b>Process</b>	Imbibition
<b>Scenario</b>	Unsteady state – constant rate

*Table 34:* Input data for CR1

<b>Core ID</b>	CR1
<b>Length of core [cm]</b>	7.06
<b>Diameter of core [cm]</b>	3.78
<b>Porosity of core [fraction]</b>	0.47
<b>Base permeability of core [mD]</b>	4.0187
<b>Water viscosity [cP]</b>	0.851
<b>Oil viscosity [cP]</b>	2.69
<b>Water density [g/cm<sup>3</sup>]</b>	0.998
<b>Oil density [g/cm<sup>3</sup>]</b>	0.783
<b>Water Saturation [fraction]</b>	0.2
<b>Water injection rate [ml/min]</b>	0.026
<b>Total simulation time [days]</b>	7.00

*Table 35:* Input data for CR2

<b>Core ID</b>	CR2
<b>Length of core [cm]</b>	7.07
<b>Diameter of core [cm]</b>	3.79
<b>Porosity of core [fraction]</b>	0.49
<b>Base permeability of core [mD]</b>	4.0932
<b>Water viscosity [cP]</b>	0.851
<b>Oil viscosity [cP]</b>	2.69
<b>Water density [g/cm<sup>3</sup>]</b>	0.998
<b>Oil density [g/cm<sup>3</sup>]</b>	0.783
<b>Water Saturation [fraction]</b>	0.2
<b>Water injection rate [ml/min]</b>	0.027
<b>Total simulation time [days]</b>	6.00

### C2: Fractionally wet core

*Table 36:* Input data for C2

<b>Core ID</b>	C2
<b>Length of core [cm]</b>	7.12
<b>Diameter of core [cm]</b>	3.79
<b>Porosity of core [fraction]</b>	0.50
<b>Base permeability of core [mD]</b>	4.1596
<b>Water viscosity [cP]</b>	0.851
<b>Oil viscosity [cP]</b>	2.69
<b>Water density [g/cm<sup>3</sup>]</b>	0.998
<b>Oil density [g/cm<sup>3</sup>]</b>	0.783
<b>Water Saturation [fraction]</b>	0.2
<b>Water injection rate [ml/min]</b>	0.028
<b>Total simulation time [days]</b>	4.20